

**Large scale mass transportations on the Earth from
satellite gravimetry: Climate changes and earthquakes**

衛星重力観測でみる質量の大規模な移動：
気候変動と地震

Koji Matsuo

Department of Natural History Sciences, Graduate School of Science,
Hokkaido University

Submitted for the degree of Doctor of Philosophy

February 2013

Contents

Abstract	vi
概要	xi
Acknowledgment	xvi
謝辭	xviii
1 Introduction	1
1.1 Space geodesy	1
1.2 Geodetic measurement of the Earth's gravity field	2
1.3 Satellite gravity measurements of the Earth	3
1.4 Outline of this study	7
2 Data and processing	9
2.1 On GRACE data	9
2.2 Filtering process	14
2.2.1 Gaussian filter	15
2.2.2 De-stripping filter	17
2.3 Time-series analysis of GRACE data	19

3	Anomalous precipitation signatures of Arctic Oscillation in the time-variable gravity field by GRACE	25
3.1	Introduction	26
3.2	Data and Method	28
3.3	Result	31
3.3.1	GRACE and GLDAS	31
3.3.2	Microscopic view of the correlation between the GRACE/ GLDAS and AO	34
3.3.3	Macroscopic view of the correlation	35
3.3.4	Surface deformation by AO	38
3.3.5	Polar motion excitation by AO	40
3.4	Discussion	44
3.4.1	Contributions of various climatic modes to mass changes in NH winters	44
3.4.2	Influence of temperature anomaly by AO to terrestrial water storage	48
3.4.3	On detrending of GRACE mass-variation time-series to iso- late AO signature	48
3.5	Conclusion	53
4	Current ice loss in small glacier systems of the Arctic Islands (Iceland, Svalbard, and the Russian High Arctic) from satellite gravimetry	55
4.1	Introduction	56
4.2	GRACE observation	58
4.2.1	GRACE Data processing	58

4.2.2	Ice loss in small glacier systems of the Arctic Islands from GRACE	60
4.3	Estimation of ice loss	61
4.3.1	Method for estimation	61
4.3.2	Iceland	63
4.3.3	Svalbard	65
4.3.4	Russian High Arctic	68
4.4	Discussion	71
4.4.1	Sources of errors for the ice loss rate	71
4.4.2	AO and the temporal variability of the ice loss rates	75
4.5	Conclusion	78
5	Ice mass variations in Greenland from low-degree gravity field by Satellite Laser Ranging during 1991-2011	81
5.1	Introduction	82
5.2	Data and Method	85
5.3	Results	90
5.3.1	GRACE estimates of the GrIS mass balance in the period 2003-2011	90
5.3.2	SLR estimates of the GrIS mass balance in the period 1991-2002 and 2003-2011	92
5.3.3	Ice mass changes from GPS vertical displacement	98
5.4	Discussion	104
5.4.1	Relationship between the GrIS mass balance and climatic changes	104

5.4.2	EOF analysis of non-seasonal mass changes from GRACE	105
5.5	Conclusion	107
6	Coseismic gravity changes of the 2011 Tohoku-Oki great Earthquake from satellite gravimetry	109
6.1	Introduction	110
6.2	GRACE observation of gravity changes	111
6.3	Model calculation of gravity changes	115
6.4	Discussion	116
7	Conclusion	120
	Bibliography	124

Abstract

The dynamic Earth forms the large-scale mass circulation system. This system functions as a source of various geophysical phenomena constantly occurred on the Earth. Atmospheric circulation driven by solar heat brings rainfall and snow accumulation on the surface. Recent climate changes due to global warming cause large-scale swings of mass balance of continental ice sheets and mountain glaciers in the interannual-to-multidecadal period. Mantle convection within the Earth's interior induces volcanic activity and earthquakes. Because these geophysical phenomena accompany the movement of mass such as water/ice and crust/mantle materials, they also change the gravity field of the Earth. Therefore, observation of time-variable gravity field provides a key to understand the dynamics of the Earth's mass circulation system, and eventually leads to an insight into the physical process of various geophysical phenomena. Space geodetic techniques which have advanced in the last decade enable us to measure small gravity changes on the Earth with high temporal and spatial resolution. In this study, I study the time-variable gravity field observed by artificial satellites for the monitoring of mass redistributions caused by various geophysical events. The present thesis includes the following four topics; (1) Anomalous precipitation signatures of Arctic Oscillation in the time-variable by GRACE; (2) Current ice loss in small glacier systems of Arctic Islands from satel-

lite gravimetry; (3) Ice mass variations in Greenland from low-degree gravity field by Satellite Laser Ranging during 1991-2011; (4) Coseismic gravity changes of the 2011 Tohoku-Oki great earthquake from satellite gravimetry.

(1) Anomalous precipitation signatures of Arctic Oscillation in the time-variable by GRACE

The Arctic Oscillation (AO) controls winter climate in the Northern Hemisphere to a large extent. Positive AO brings higher (lower) surface temperature and higher (lower) precipitation in high (middle) latitude regions, and negative AO vice versa. In this study, we investigate signals of anomalous precipitation caused by AO using the data of the Gravity Recovery and Climate Experiment (GRACE) satellites. Wintertime mass deviations inferred from GRACE in the high and middle (boundary $\sim 55^\circ\text{N}$) latitude regions in Eurasia showed highly positive and negative correlations with AO index. This possibly reflects the northward (or southward) shift of the center of winter precipitation during the positive (or negative) phases of AO. Wintertime mass deviations also showed positive (or negative) correlation with AO index in the northern (or southern) parts of Greenland. In this case, the boundary was further to the north, say $\sim 55^\circ\text{N}$. AO redistributes the water mass as much as ~ 1000 Gt between high and middle latitude regions in the Northern Hemisphere. Such mass redistribution causes significant surface deformation due to water loading which is large enough to be observed by Global Positioning System. This also causes the shift of the Earth's rotation axis especially towards the Greenwich Meridian which is also large enough to be detected with space geodetic techniques. AO signatures are also derived from the empirical orthogonal function (EOF) analysis, which leads to the

first leading mode of EOF from GRACE data after excluding seasonal, linear and quadratic components. The EOF analysis also demonstrates that AO is a main contributor which gives rise to the anomalous winter precipitation in the Northern Hemisphere as a whole, although the influence of the El Niño and Southern Oscillation on the anomalous winter precipitation anomaly is larger than AO in North America.

(2) Current ice loss in small glacier systems of Arctic Islands from satellite gravimetry

Recent climate changes brought significant melting of ice sheets and glaciers in many parts of the world. Satellite gravimetry by GRACE revealed that such the ice melting also occurs in small glacier systems in the Arctic region, i.e. Iceland, Svalbard, and the Russian High Arctic. Using monthly gravity solutions from GRACE between February 2004 and January 2012, we obtained the average ice loss rates of 10.9 ± 2.1 , 3.6 ± 2.9 , and 6.9 ± 7.4 Gt/yr, for these three glacial systems, respectively. The total ice loss rate is 21.4 ± 12.4 Gt/yr, which is about two times as fast as the average rate over ~ 40 years interval before the above studied period. We found that the ice loss rates in Svalbard and Novaya Zemlya, in the Russian High Arctic, had significant temporal variability, showing decreasing trend before 2008 and increasing trend around the winter of 2009/2010. Due to such the variability, the total ice loss rate becomes as high as 32.9 ± 19.2 Gt/yr between February 2004 and January 2008. Such variability of the rate might reflect the strong negative Arctic Oscillation in the northern hemisphere in the winter of 2009/2010.

(3) Ice mass variations in Greenland from low-degree gravity field by Satellite

Laser Ranging during 1991-2011

Ice mass variations in Greenland since 1991 were studied using low-degree gravity field coefficients inferred from Satellite Laser Ranging (SLR). Here we determined gravity field spherical harmonic coefficients with degree and order up to 4 between January 1991 and December 2011 from tracking data of multiple SLR satellites. Between 2003 and 2011, the linear trend maps of mass variations from SLR showed significant negative patterns in Greenland, which is consistent with those from the GRACE satellite. On the other hands, the linear trend maps between 1991 and 2002 showed different behaviors: slightly increasing in Greenland prior to ~1999, near-balancing from 2000 to 2002, and shifting to decreasing afterwards. Such temporal variability was pronouncedly reflected in quadratic component of mass variations around Greenland. We confirmed that our SLR result agrees well with vertical displacement of the rocky margins of Greenland measured by Global Positioning System (GPS) which manifests ice mass variations in Greenland.

(4) Coseismic gravity changes of the 2011 Tohoku-Oki great Earthquake from satellite gravimetry

The great Tohoku-Oki earthquake of moment magnitude M_w of 9.0 occurred on 11 March 2011 off the Pacific coast of the Northeastern Japan. The mass redistribution in and around the focal region associated with this earthquake was studied using the gravity changes detected by GRACE satellite. After the 2004 Sumatra-Andaman and the 2010 Central Chile (Maule) earthquakes, we also observed the gravity changes. The present result presents the third case of the clear detection of coseismic gravity changes by GRACE. The observed gravity change was dominated

by decrease over the back-arc region of $\sim 7 \mu\text{Gal}$ or less. This reflects, to a large extent, coseismic crustal dilatation of the landward plate. This agrees well with the change calculated with the Green's function for the realistic earth using fault parameters inferred from coseismic crustal movements. The spatial pattern of the gravity changes of these earthquakes are similar to another because they are all shallow angle reverse faultings at convergent plate boundaries. We found linear relationship between the amount of gravity decreases and seismic moments.

概要

地球型惑星では大規模な物質循環システムが形成され、様々な自然現象が起きている。地球惑星内部で起こるマントル物質の湧昇は、表層に薄く硬いプレートを生成し、やがてプレート同士を移動・衝突させ、造山運動や地震/火山活動を引き起こす。太陽熱が駆動する大気の大気対流は、大陸に降雨/降雪をもたらす、表層で大規模な水の循環システムを構築させる。また、数万年もしくは数十年スケールで繰り返される気候変動は、氷床・氷河を消失/形成させ、さらには海水準面を上昇/下降させる。こうした一連の現象は、地殻/マントル、水/氷といった質量を持つ物質の移動によるものであり、そこには必ず重力場の変化が伴う。すなわち、重力場の時間変動観測はこれらのダイナミクスを解明する鍵なのである。近年目覚ましい進歩を遂げた宇宙測地技術は、地球上で起こるわずかな重力変化を高い精度と詳細な時空間分解能で計測することを可能とした。中でも、2002年にNASA/DLRが打ち上げた重力観測衛星GRACEは、その高い精度と応用性の広さから、地球惑星ダイナミクス研究に革命をもたらしつつある。GRACEは2つの衛星からなる双子型の人工衛星で、双子衛星間の距離を精密に測ることによって、地球表層や内部で起こる質量移動に起因した数 μGal (地球の標準重力の数億分の1)にも満たないわずかな重力時間変化を全球にわたって観測する。本研究では、GRACEを始めとする重力観測衛星を用いて、様々な地球物理現象によって生じる地球上の大規模質量変動について研究を行った。本論文は、以

下の4つの話題について記述する。(1) GRACEによる北極振動がもたらす半球規模の降水(降雪)量異常の検出(2) GRACEが捉える北極圏の小氷河帯(Iceland, Svalbard, Russian High Arctic)の氷消失(3) SLR(Satellite Laser Ranging)衛星による低次重力場観測から推定される1991-2011年のグリーンランド氷床の質量収支(4) GRACEが捉える2011年東北沖地震に伴う地震時重力変化。

(1) GRACEによる北極振動がもたらす半球規模の降水(降雪)量異常の検出

北極振動(AO: Arctic Oscillation)とは、北極域と中緯度域間で起こる大気圧のシーソー現象であり、北半球における主要な大気変動パターンの一つである。北極振動はとりわけ、北半球の冬季の気候に大きな影響を及ぼす。正の北極振動は高緯度地域に高い降水量と低い気温を、中緯度地域に低い降水量と高い気温をもたらす。一方、負の北極振動はこれらの状況を反転させる。本研究は、この北極振動がもたらす半球規模の降水量異常のシグナルを重力衛星GRACEから検出した。GRACEから推定されるユーラシア大陸における冬季の表層質量(土壌水分量・積雪量)偏差は、高緯度地域(北緯55度以北)で北極振動指数と高い正の相関、中緯度地域(北緯20度から55度)で高い負の相関を示した。すなわち、正の北極振動が発生した冬は高緯度地域で降水量異常が、負の北極振動が発生した冬は中緯度地域で降水量異常が生じていることを示唆する。グリーンランドでは北緯75度を境界として、北部で正の相関、南部で負の相関が見られた。北極振動はその位相に応じて、北半球の高緯度・中緯度地域間で約1000Gtにも及ぶ質量をシーソー的に移動させていることが空間的に明らかになった。GRACEデータの非季節・経年成分の統計的な主成分分析(EOF解析:Empirical Orthogonal Function Analysis)を行うと、北極振動は第一主成分として現れる。EOF解析から、ユーラシア大陸、グリーンランドでは北極振動が冬の降水量異

常に主要的な役割を果たすが、北米大陸ではエルニーニョ南方振動の影響のほうに顕著であることが明らかになった。

(2) GRACE が捉える北極圏の小氷河帯 (Iceland, Svalbard, Russian High Arctic) の氷消失

温暖化に代表される近年の気候変動は、世界各地の氷床・氷河を融解・消失させている。本研究は、重力衛星 GRACE から、Iceland, Svalbard, Russian High Arctic のような北極圏の小氷河帯においても同様の氷消失が起きていることを明らかにした。2004-2012 年までの GRACE の月毎の重力データから、氷河の損失率として、Iceland では 10.9 ± 2.1 Gt/yr、Svalbard では 3.6 ± 2.9 Gt/yr、Russian High Arctic では 6.9 ± 7.4 Gt/yr という結果を得た。その総量は 21.4 ± 12.4 Gt/yr であり、1961-2002 年に行われた現地調査の結果の約 2 倍の速度である。さらに我々は、Svalbard 氷河と Russian High Arctic の一部である Novaya Zemlya 氷河では、その損失率に、かなりの時間変動性があることを突き止めた。これらの氷河は、2008 年までは経年的な負の質量収支を示すが、2009/2010 年の冬で正の質量収支に転じている。このような時間変動性により、2004-2008 年の期間では、氷河の損失率は 32.9 ± 19.2 Gt/yr に上方修正される。2009/2010 年の冬は、観測史上最大の負の北極振動が発生した時期であり、北極振動による降水量異常を反映しているのかもしれない。

(3) SLR(Satellite Laser Ranging) 衛星による低次重力場観測から推定される 1991-2011 年のグリーンランド氷床の質量変動

グリーンランド氷床の質量収支は、この 20 年の間、宇宙測地的な手法による観測が盛んに行われてきた。その一つに、航空機搭載のレーザー測距計に

よる観測がある。1993年から2003年までの観測によると、グリーンランド氷床の質量収支は減少傾向にあり、その減少速度は -70 Gt/yr と見積もられた (e.g. Krabill et al. 2000)。また、航空機レーザー測量と並行して、人工衛星 ERS-1 搭載のレーダー高度計による計測も行われた。1992年から2002年までの観測によると、グリーンランド氷床の質量収支は増加傾向にあり、その増加速度は $+11 \text{ Gt/yr}$ と推定された (e.g. Zwally et al., 2005)。両者の観測は同時期に行われていたにも関わらず、その推定量に大きな食い違いが見られる。その後2003年以降に行われた ICESat によるレーザー測量や ERS-2, Envisat, ALOS による合成開口レーダー測量では、いずれの結果も約 -200 Gt/yr の負の質量収支で、同様の傾向が得られている。本研究は、このようなグリーンランド氷床の質量収支の推移を、人工衛星による重力観測から解析を試みる。中でも我々は、GRACE 衛星の打ち上げ以前から運用を続ける SLR 衛星による低次重力場解に着目した。ここでは、他の測地観測との比較のため、1991-2011年までの SLR 重力解を示す。SLR 重力解から、グリーンランド氷床では、1991-2002年までは約 $+20 \text{ Gt/yr}$ の正の質量収支、2003-2011年では約 -200 Gt/yr の負の質量収支を得た。2000年代の推定値は、他の測地観測と良く一致しており、1990年代は、ERS-1のレーダー高度計測と良く一致する。1990年代の氷床の拡大傾向は、同時期に始まった温暖化によるものであろう。気温の増加は氷床を融解させる一方で、水蒸気量の増加をもたらし、さらには降雨/降雪量を増加させる。1990年代は水の涵養量が流出量をわずかに上回っていたが、2000年代に入りそのバランスが崩れ、流出量が涵養量を大きくなくなったものと予想される。

(4) GRACE が捉える 2011 年東北沖地震に伴う地震時重力変化

2011年3月11日に東北地方太平洋沖にて、 $M_w 9.0$ の超巨大地震が発生し

た。本研究は、この東北沖地震によって生じた地球表層・内部の質量移動に起因した重力変化について記述する。重力衛星 GRACE は地震発生後に、プレート沈み込み帯の背弧側、東北地方を中心に最大で約 $7 \mu \text{Gal}$ の重力減少を検出した。重力衛星によって地震に起因する重力変動が検出されたのは、2004 年スマトラ地震 ($M_w 9.2$)、2010 年チリ中部地震 ($M_w 8.8$) に続き、本地震で 3 例目となる。陸域に展開される GPS 局と宮城沖に設置された海底基準局の地殻変動データから推測される断層のすべり分布を用いて、推定される地震時重力変化を数値シミュレーションしたところ、GRACE の観測と非常によく一致した結果が得られた。また、観測された重力変化は主に、断層運動に伴う断層上盤側の体積膨張を反映していることが明らかになった。

Acknowledgment

First and foremost, I would like to express my sincere gratitude to my supervisor, Prof. Kosuke Heki, for everything that he gave me throughout the course of my study. Words don't express my deepest gratitude to him. When I encountered difficulties in my study, he always listens sincerely to what I said, and gave me sound and valuable advices. He gave me a lot of opportunities to join academic meetings and interact with scientists there. His warm and patient guidance had me grow as a scientist and a person. Additionally, I would like to appreciate very much Prof. Benjamin Fong Chao at Institute of Earth Science, Academia Sinica in Taiwan. I have stayed there between February 2012 and October 2012 and received his guidance. He gave me a warm welcome and every supports in my stay in Taiwan. His advices to my research are extremely valuable particularly on SLR. He took me to many meetings and gave me chances to communicate with members in the geodetic group in Taiwan. These are the most satisfying experiences of my life. Also, I would like to thank Dr. Tadashi Usuki and Ms. Masako Usuki for kind help in my stay, Dr. Shogo Komori for nice talking, and the geodetic group at IES for heartwarming welcome. I would like to appreciate Prof. Junji Koyama, Prof. Kiyoshi Yomogida, Prof. Kazuhisa Chikita, Prof. Shoshiro, Minobe, Prof. Masato Furuya, Prof. Kazunori Yoshizawa, Prof. Masaru Inatsu, and Dr. Yuta Mitsui for their constructive comments. I would like

to thank Prof. Toshimichi Otsubo at Hitotsubashi University for the collaboration of the study in Chapter 5. I would like to thank Dr. Hisashi Suito at Geospatial Information Authority of Japan for the cooperation of the study in Chapter 6. I also express my gratitude to Dr. John Fasullo for evaluating a paper on Chapter 3, Prof. C.K. Shum and Prof. Cheinway Hwang for evaluating a paper on Chapter 4, Prof. Wenke Sun for evaluating a paper on Chapter 6. I would like to thank JSPS fellowship for a grant that makes it possible to complete this study. We are grateful to NCEP (NOAA), CSR (UT), JPL (NASA), GFZ, GSFC (NASA), SOPAC (UCSD), and OP, for providing the datasets of climatic indices, GRACE, GLDAS, GPS, and earth orientation parameters, respectively.

謝辞

本研究を遂行するにあたり、多くの方々よりご支援・ご協力を賜りました。ここに記してお礼申し上げます。

まず何より、指導教官である日置幸介教授に心より深く感謝申し上げます。日置先生には筆舌に尽くしがたい感謝の気持ちでいっぱいです。私が研究で困難に遭遇した際には、いつも真摯に相談に乗ってくださり、的確かつ有益な助言を与えてくださいました。国内外の学会に参加する機会を積極的に与えてくださったおかげで、多くの研究者の方々と交流し議論する貴重な機会にも恵まれました。また、日置先生が取り組まれる革新的で科学的意義の極めて高い研究は、私の研究意欲を幾度となく奮い立たせました。日置先生は私を研究者としてだけでなく、一人の人間としても成長へと導いてくださいました。日置先生の懇篤なるご指導をなくして、本研究を完遂させることはできなかったと思います。これまでの学部・修士・博士課程の6年間、本当にありがとうございました。日置先生から学びました全てを糧に、これからも研究活動に邁進し精進して参りたいと存じます。

また、台湾中央研究院・地球科学研究所の Benjamin Fong Chao 教授に心よりお礼申し上げます。私は2012年2月から2012年10月までの期間、台湾台北市にある中央研究院・地球科学研究所に客員研究生として滞在し、Chao 先生より研究指導を賜りました。Chao 先生は私の滞在を暖かく迎えてくださり、台湾

での生活のあらゆる面倒を見てくださいました。Chao 先生主催のグループミーティングでは、最新の研究成果を講義して下さり、また私の研究に関して有意義な助言を与えてくださいました。さらには、台湾国内での様々な会合に積極的に連れて行ってくださり、現地の研究者の方々との貴重な繋がりを作ることができました。私のこれまでの研究生活の中で最も思い出深く充実した経験をさせて頂きました。心より感謝申し上げます。また、初めての海外生活で右も左も分からない私を親切にも助けてくださった臼杵直博士・臼杵昌子さん、いつも楽しくお話してくださいました小森省吾博士、心温かくもてなして下さった台湾測地グループの皆さまに、心から感謝申し上げます。

本研究に関し、小山順二教授、蓬田清教授、知北和久准教授、見延庄士郎教授、古屋正人教授、吉澤和範准教授、稲津将准教授、三井雄太博士にコメントを賜りました。深くお礼申し上げます。小山先生、吉澤先生、稲津先生は、本論文をご丁寧に高閲して下さり、問題点等をご指摘くださいました。Chapter 5の研究は、一橋大学の大坪俊通教授のご協力のもと、共同研究として遂行して参りました。Chapter 6の研究にあたり、国土地理院の水藤尚博士よりご協力賜りました。皆さま本当にありがとうございました。

本研究は、日本学術振興会からの研究費助成のもと遂行して参りました。また、本研究で用いた重力データ、地殻変動データ、極移動データ、GLDAS データは、NCEP(NOAA)、CSR(UT)、GSFC(NASA)、SOPAC(UCSD)、パリ天文台より提供して頂きました。ここに記してお礼申し上げます。

Chapter 1

Introduction

1.1 Space geodesy

Geodesy is to study the shape and size, composition, and the rotation of the Earth. Now, positioning, Earth's rotation, and gravity field are the three major concerns of modern geodesy. Geodetic surveys of the Earth have mainly been done on the ground for years. However, the introduction of artificial geodetic satellites enables us to look at the Earth from space. Such space-based geodetic surveys are referred to as "Space geodesy" in general. The space geodesy would have started in 1957 with the launch of the Sputnik 1, a first artificial satellite, by the former Soviet Union. After that, many artificial satellites for geodesic surveys were launched, and collected a lot of invaluable information on the Earth and other planets. In recent years, space geodetic techniques made drastic progresses in accuracy and spatio-

temporal resolution by the aid of the development of observational instruments and improvement of data processing methods. Owing to these progresses, Space geodesy allowed global measurements of positions, changes in the rotation, and in the gravity field of the Earth with the accuracy of several centimeters (*cm*), milli (*m*) second, and micro (μ) Gal. Moreover, space-based measurement has an advantage to obtain temporally continuous data as long as the satellite keeps observation of the Earth. Various kinds of geophysical phenomena occur on the Earth, and change the Earth. It is no doubt that space geodetic data plays an important role to reveal its physical process and to deepen the understanding of the changing Earth.

1.2 Geodetic measurement of the Earth's gravity field

The magnitude of the Earth's gravity on the ground is about 9.8 m/s^2 . This gravitational acceleration is expressed 980 Gal. Basically, we have three ways to measure the Earth's gravity field: surface gravity measurements, satellite altimetry measurements, and satellite tracking measurements.

Speaking about surface gravity measurements, there are two types of gravimeters: absolute gravimeter and relative gravimeter. The principle of absolute gravimeter is straight forward. It measures the velocity of a falling object in vacuum. Relative gravimeter uses precise spring (or floating ball) and measures the Earth's gravitational force through the elongation of spring (the changes in position of floating ball). The absolute gravity can be measured as precise as μGal or nGal order at specific points on land.

Satellite altimetry using laser or radar distance meter measures the geopotential

height (geoid) referring to the shape of ocean. Because sea water is mobile, the shape of ocean reflects the geoid. If the mean dynamic topography of sea surface could be constrained, satellite altimetry provides gravity and geoid anomalies over the ocean.

Satellite tracking measurements yield the global gravity field of the Earth including land and ocean. They can be made by tracing the trajectory or measuring the velocity of the orbiting artificial satellite. The motion of a satellite orbiting the Earth obeys the law of mechanical energy conservation. Therefore, velocity of an orbiting satellite is large where the gravitational potential is low. On the other hand, velocity becomes small where the gravitational potential is high. Then, the gravitational potential of the Earth can be recovered by monitoring the motion of an orbiting satellite.

1.3 Satellite gravity measurements of the Earth

The first result of satellite gravity was made by the Vanguard I launched by the United States in 1958. They determined the flattening of the Earth precisely expressed in the spherical harmonics of J_2 ($= -\sqrt{5} C_{20}$), suggesting that the flattening of the Earth was significantly smaller than that had been derived from surface gravity measurements beforehand. After that, early in 1959, Yoshihide Kozai (1959) found the pear-shaped component of the Earth's gravity field expressed by the spherical harmonics of J_3 from several satellites. This was the first evidence that the Earth's gravity field is irregular and asymmetric. He showed that the Northern Hemisphere of the Earth contains slightly more mass than the Southern Hemisphere.

In the late of 1960s, Satellite Laser Ranging (SLR) was used to derive the

global gravity field of the Earth. SLR is a technique to measure the distance from the ground-based station to an orbiting satellite with corner reflectors (SLR satellite) by using laser distance meter. SLR tracking data provide information on the change in satellite's orbital parameters, and yield temporal variations in the low-degree spherical harmonic components of the Earth's gravity field. Yoder et al. (1983) found the decreasing trend of the J_2 term due to the viscous rebound of the solid Earth by Glacial Isostatic Adjustment (GIA) and the Earth's secular spin-down by the friction of external tidal forces (tidal braking). Nerem et al. (1993) estimated monthly values of the J_2 and J_3 term and detected seasonal changes of them caused by the change in water storage on land by precipitation. Cox and Chao (2002) found a sudden shift in the J_2 trend from decrease to increase around 1998. The cause of this sudden change still remains unclear even today. Cheng and Tapley (1999) confirmed secular and annual changes in higher degrees of spherical harmonics from J_2 to J_8 . SLR gravity measurement was a breakthrough technique allowing us to derive temporal variations of the Earth's gravity field, although limited in spatial resolution due to the high orbital altitude (1000-5000 km) and the sparse distribution of SLR laser tracking stations.

In the 2000s, low-orbiting satellites dedicated to the measurement of the Earth's gravity field were launched. The first one is the CHAMP (CHALLENGING Minisatellite Payload), launched in July 2000 [Reigber et al., 2002]. The CHAMP satellite operated in the polar circular orbit with an altitude of ~ 500 km. In addition, it is notable that the CHAMP satellite is equipped with a Global Positioning System (GPS) receiver, which enabled to derive the satellite orbit with high accuracy. The method of gravity measurement adopted is to trace a low-orbiting satellite at ~ 500 km al-

titude from high-orbiting satellites at $\sim 20,000$ km altitude, and is called High-Low Satellite-to-Satellite Tracking (H-L SST). Because H-L SST data are sensitive to the change in the gravity field of long and medium wavelength components, the CHAMP satellite provided an improved gravity solution of the Earth at these wavelengths.

The next is the GRACE (Gravity Recovery And Climate Experiment) satellites, launched in March 2002 [Adam, 2002]. The GRACE satellites are originally designed to operate for five years, but the mission has now been extended and marked the 10th years in 2012. The GRACE is composed of twin satellites. The two satellites, separated by ~ 200 km, are in the same polar circular orbit at an altitude of ~ 500 km. They precisely measure the change of the inter-satellite distance and recover the gravity field of the Earth from the change of the distance. This method of measurement tracing a low-orbiting satellite at ~ 500 km altitude from another low-orbiting satellite at the same altitude is called Low-Low Satellite-to-Satellite Tracking (L-L SST). The GRACE satellites are equipped with K-band Ranging (KBR) system allowing to track the inter-satellite distance with a precision of a few micron meter. They are also equipped with GPS receiver to determine the accurate satellites' orbits. In addition, on-board accelerometers measure non-gravitational satellite accelerations by external forces (solar radiation pressure, atmospheric drag, and so on), and contribute to directly correct the change in the satellites' orbit by the forces. Thanks to these equipments, the GRACE satellites achieve higher accuracy than the CHAMP satellite and can detect the gravity changes as precise as several μGal .

The latest gravity satellite for now is the Gravity Field and steady-state Ocean Circulation Explorer (GOCE) satellite, launched in March 2009. The satellite is orbiting into polar and circular orbits at 300 km altitude. The GOCE satellite carries

a highly gravity gradiometer which can model the Earth's static gravity field with extremely high accuracy and spatial resolution. This measurement method is called Satellite Gravity Gradiometry (SGG). The SGG system consists of three pairs of ultra-sensitive accelerometers arranged in three dimensions that can precisely detect the difference of gravitational accelerations in all three spatial directions. The GOCE satellite is also equipped with an accelerometer to correct non-gravitational forces and a GPS receiver to determine its orbit, and achieves to higher accuracy and spatial resolution than GRACE as for static gravity field.

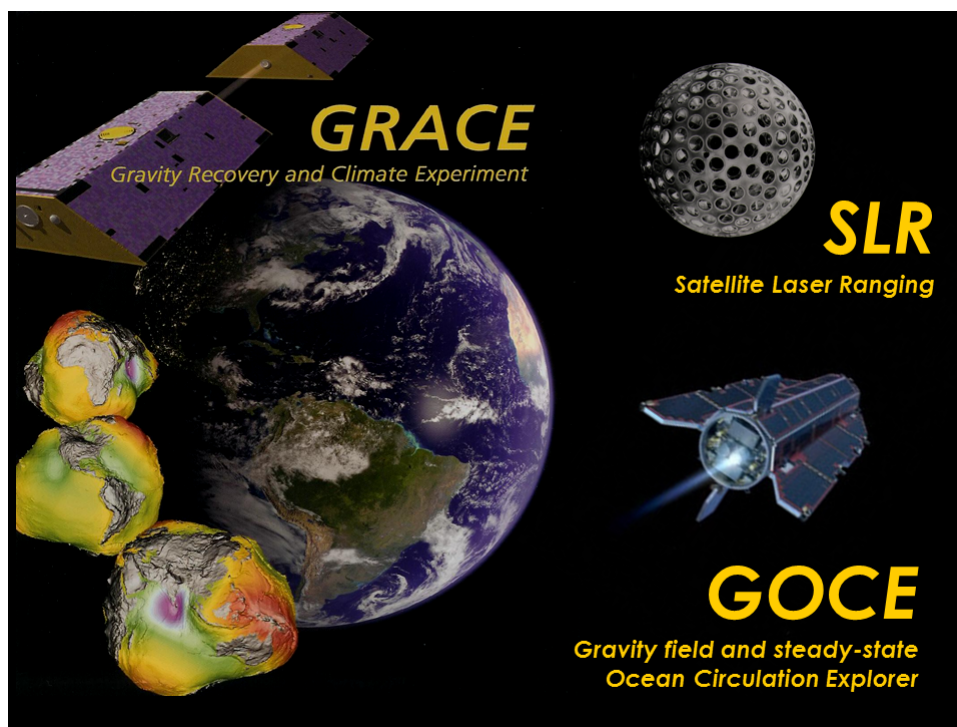


Figure 1.1: Satellites to measure the global gravity field of the Earth.

1.4 Outline of this study

This thesis is devoted to the geophysical application of satellite gravity data for Earth sciences. In particular, I utilize the time-variable gravity data obtained by GRACE and SLR. The objective of this study is to monitor the large scale mass redistribution caused by various geophysical phenomena and reveal the characteristics and mechanism quantitatively. Chapter 2 gives a brief overview of techniques of data processing of GRACE data. GRACE data has been contaminated by short-wavelength noises and striping noises. In order to apply GRACE data for geophysical studies, we need to correct these noises appropriately. There are two representative filtering methods to remove GRACE noises: Gaussian filter and de-striping filter. I will describe these filterings in detail in this Chapter. Chapters 3-6 describes actual applications of satellite gravity data for various geophysical phenomena. Chapter 7 presents a conclusion of this study. They are summarized as follows;

Chapter 3: Anomalous precipitation signature of AO detected by GRACE. AO is one of the main climatic modes that influences to wintertime climate on Northern Hemisphere. AO causes the mass transportation in a hemispheric scale through precipitation anomaly. The spatial distribution of anomalous precipitation by AO was studied in detail using the data from meteorological stations. However, concerning polar and mountainous regions where *in situ* observations are limited or unavailable, a definitive explanation on the link between AO and precipitation anomaly has been remained elusive. Here I delineate the global mass anomaly fields using GRACE data and discussed the relationship between the observed mass anomaly and AO.

Chapter 4: Current ice loss in small glacier systems of Arctic Islands is studied.

Data accumulation of GRACE over 10 years allowed the detection of small scale mass transportation in such the glacier systems of Arctic Islands, i.e. Iceland, Svalbard, and the Russian High Arctic. These glaciers are also experiencing significant ice loss in accordance with global tendency. In addition, their mass balances have large temporal variation and might be influenced by some climatic modes like AO.

Chapter 5: Ice mass variations in the Greenland Ice Sheet are inferred from low-degree gravity field by SLR during 1991-2011. The Greenland Ice Sheet (GrIS) is the second largest reservoir of fresh water on the Earth next to the Antarctic ice sheet, which means that the GrIS has a high potential for the contribution to the global sea-level-rise. Intense measurements of the GrIS mass balance have been performed through field works and satellite observations including GRACE, suggesting that substantial amount of ice has been losing in this century. Here I use the low-degree gravity field coefficient estimated from SLR tracking data in order to monitor the mass change in GrIS during 1991-2011. This is a first attempt to estimate the GrIS mass balance in 1990s from satellite gravimetry.

Chapter 6: Coseismic gravity change is studied concerning on the 2011 Tohoku-Oki Earthquake. The M_w 9.0 great earthquake hit offshore Tohoku region, eastern Japan, on March 11 2011, causing widespread destruction and catastrophic damages. This is the largest earthquake in Japan recorded by modern scientific instruments. Earthquakes accompanied by fault dislocation cause intense and large-scale mass redistribution, resulting in the gravitational adjustment around the hypocenter. Here I study the gravity change associated with this Tohoku-Oki Earthquake and investigated the cause of the observed gravity change quantitatively.

Chapter 7: I will conclude this study.

Chapter 2

Data and processing

2.1 On GRACE data

The GRACE data are divided into three levels: Level-1B, Level-2, and Level-3. They are distributed to public via Physical Oceanography Distributed Active Archive Center (PO.DAAC: <http://podaac.jpl.nasa.gov/>) and Information Systems and Data Center (ISDC: <http://isdc.gfz-potsdam.de/>). The Level 1B products include the inter-satellite range, range-rate, range-acceleration, the non-gravitational accelerations from each satellite, the pointing estimates, the orbits, etc. The Level-2 products which are constructed by the Level-1B products are provided as the monthly gravity field estimates in a form of spherical harmonic coefficients (the Stokes' coefficients). Occasionally, several months of data are combined to produce an estimate of the static gravity field. The Level-3 products present gravity anomalies (or mass anomalies expressed in equivalent water depth) at each grid point. They are de-

rived from the Level-2 products after applying the appropriate spatial filters to reduce short-wavelength noises. The GRACE data products are processed by several data analysis centers. The representative data centers are the University of Texas Center for Space Research (UTCSR), the Jet Propulsion Laboratory (JPL), United States, and the GeoForschungsZentrum Potsdam (GFZ), Germany. Because the methods for data processing vary by each institute, there are slight differences in the gravity data from these centers. In this thesis, I used the Level-2 GRACE data (the Stokes' coefficients) because the size and type of spatial filters can be adjusted depending on a case-by-case basis.

Figure 2.1 shows the each component of the Stokes' coefficients projected to the sphere. C_{nm} and S_{nm} are the Stokes' coefficients. Their suffix n and m denote the degree and order of the Stokes' coefficients. The components with order zero ($m=0$) are called " zonal ", those with the same degree and order ($n=m$) are " sectorial ", and the other ($n \neq m$) are " tesseral ".

The static gravity field (g) of the Earth can be derived from the Stokes' coefficients of GRACE using the equation (2.1) [Kaula, 1966; Heiskanen and Moritz, 1967].

$$g(\theta, \phi) = \frac{GM}{R^2} \sum_{n=2}^{n_{max}} (n-1) \sum_{m=0}^n (C_{nm} \cos m\phi + S_{nm} \sin m\phi) \bar{P}_{nm}(\sin \theta), \quad (2.1)$$

where G is the universal gravity constant, and M is the mass of the Earth. R is the equatorial radius. $\bar{P}_{nm}(\sin \theta)$ is the n -th degree and m -th order fully-normalized associated Legendre function. As for static gravity solution of GRACE, we can use

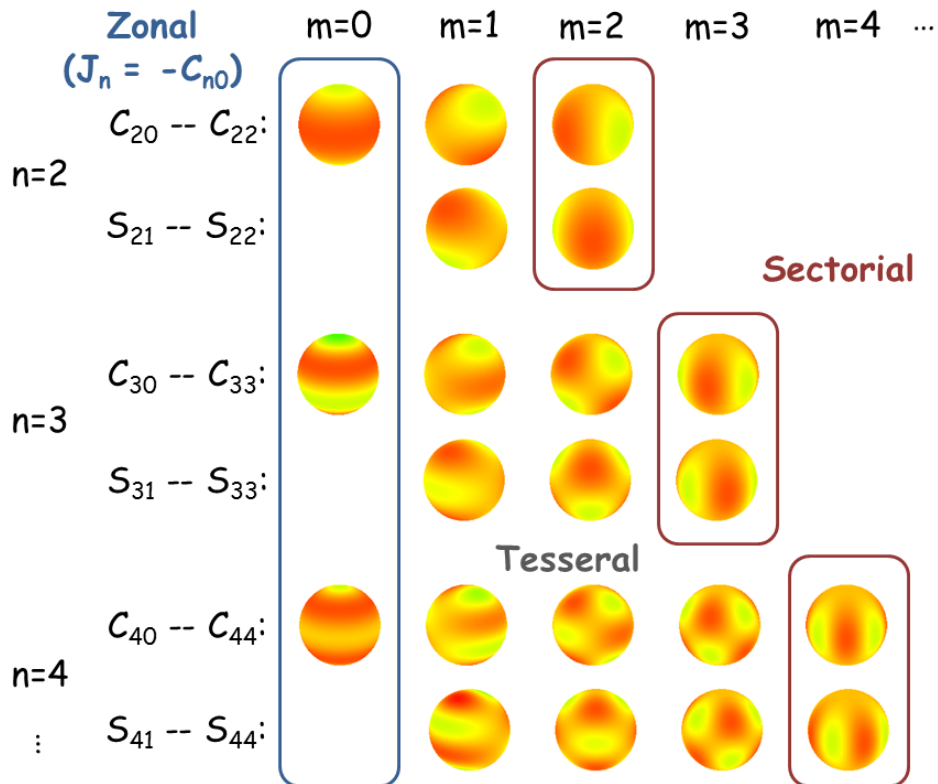


Figure 2.1: The shape of each component of the Stokes' coefficients.

the Stokes' coefficients with degrees and orders up to 360, equivalent to the spatial resolution of ~ 50 km. Figure 2.2 and 2.3 show the static gravity field of the Earth measured by GRACE.

In order to see the gravity anomaly field (Δg), we should use the deviations of the Stokes' coefficient from the reference value.

$$\Delta g(\theta, \phi) = \frac{GM}{R^2} \sum_{n=2}^{n_{max}} (n-1) \sum_{m=0}^n (\Delta C_{nm} \cos m\phi + \Delta S_{nm} \sin m\phi) \bar{P}_{nm}(\sin \theta), \quad (2.2)$$

where Δ indicates the deviation from the reference value. ΔC_{nm} and ΔS_{nm} mean the deviations from the static Stokes' coefficients. Monthly gravity solutions are

Gravity field of the Earth

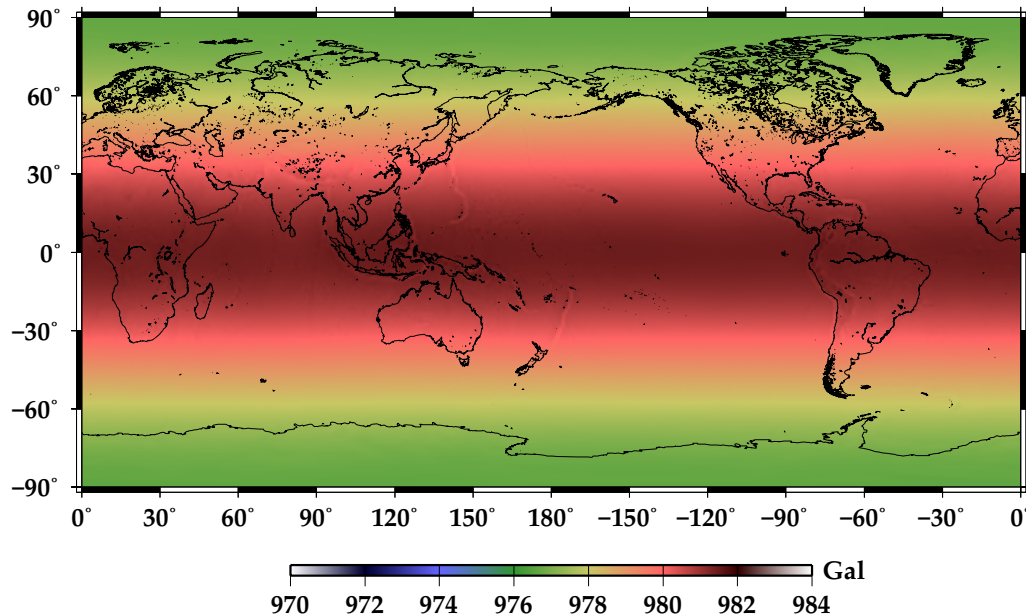


Figure 2.2: Static gravity field of the Earth measured by GRACE. Degree and order up to 360 of the Stokes' coefficients are expanded.

available complete to degree and order 60, equivalent to the spatial resolution of ~ 300 km. Conventionally, the Earth's dynamic oblateness, expressed in the Stokes' coefficient $J_2 (= -\sqrt{5} C_{20})$, from GRACE is replaced with those from SLR because GRACE system is insensitive to the changes in long-wavelength components. In addition, satellite gravimetry itself cannot measure the geocenter motion of the Earth (ΔC_{10} , ΔC_{11} , ΔS_{11} terms).

Figure 2.4 shows the gravity anomaly field of the Earth observed by GRACE. As shown in this figure, the obtained gravity anomaly map is dominated by north-south striping. GRACE data are known to suffer from short-wavelength noises. The cause of GRACE noise can be attributed to aliasing error in sampling theory. The GRACE satellites operate in the polar circular orbit at an altitude of ~ 500 km and

Gravity field of the Earth (C_{00} and C_{20} are removed)

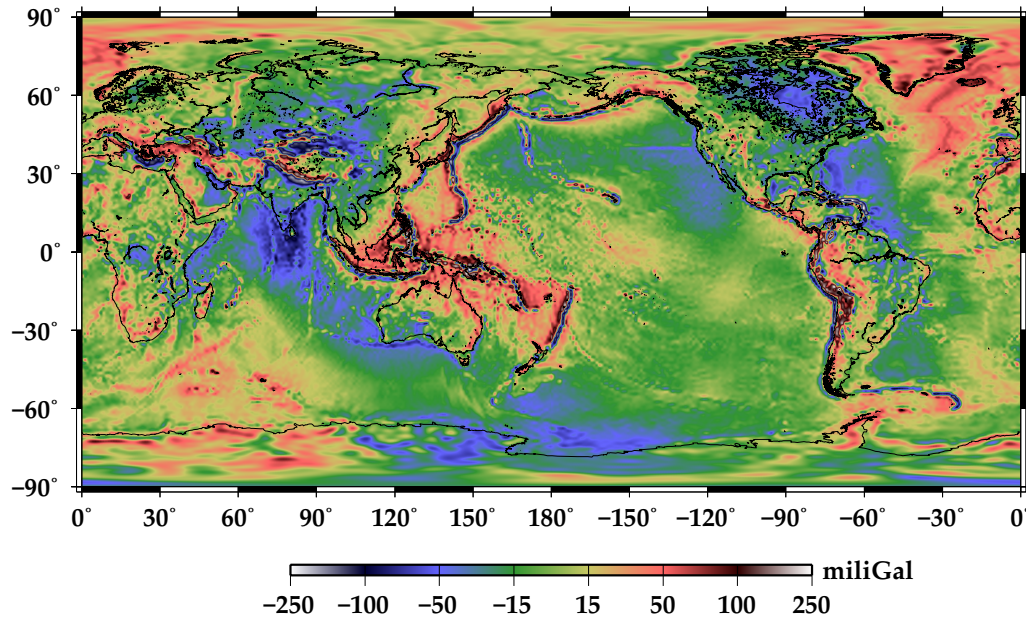


Figure 2.3: Static gravity field of the Earth measured by GRACE. Degree and order up to 360 of the Stokes' coefficients are expanded. The nominal average gravity at the surface, known as the standard gravity (J_0 term), is removed. The Earth's dynamic oblateness (J_2 term) is also removed.

make one trip around the Earth in 90 minutes. It takes about a month to return to the same path, making about 550 circuits of the globe. The data sampling are mainly along ground tracks of the orbit, but mass variations occur over entire Earth. Especially, the atmospheric and oceanic mass move fast with periods of hours to days in every direction, which significantly contaminates the monthly solutions of GRACE data with aliasing error. So, each GRACE data center make correction of these atmospheric and oceanic mass changes (including their tidal and non-tidal variabilities) using the European Centre For Medium-range Weather Forecasts (ECMWF) atmospheric model and a baroclinic or barotropic ocean model driven by this atmospheric model, called Atmospheric and Ocean De-aliasing Level-1B (AOD1B) prod-

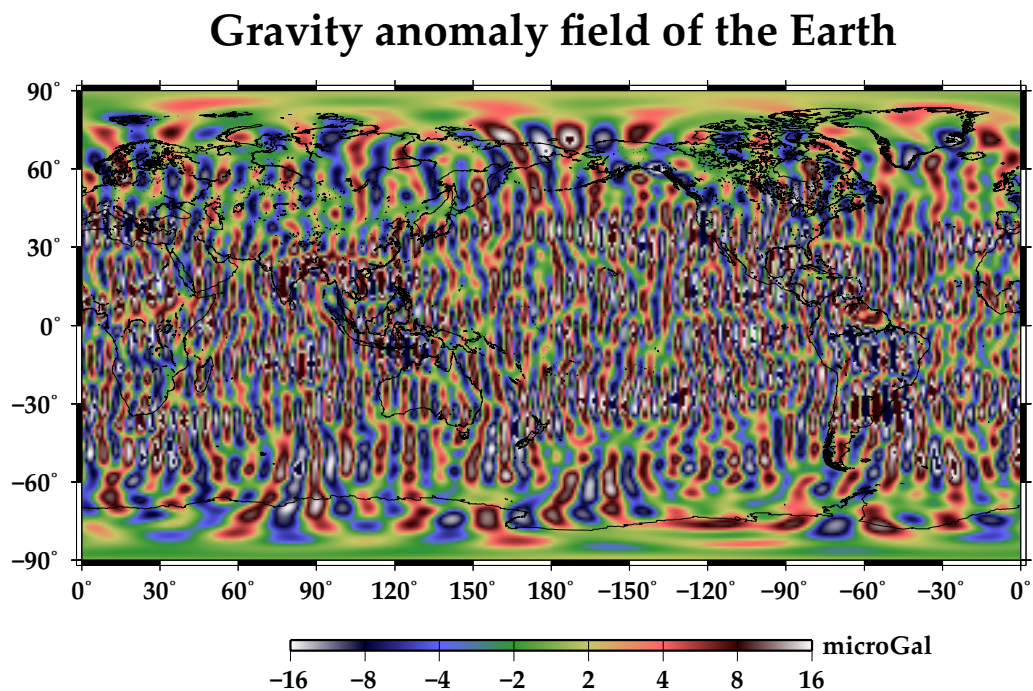


Figure 2.4: Gravity anomaly on July 2007 observed by GRACE, which any filtering processes for noise reduction are not applied.

ucts [Bettadpur, 2007]. However, these mass changes cannot be completely corrected because of errors in the model prediction. This problem remains as north-south striping noise as seen in Figure 2.3. North-south stripes increase as latitude becomes lower. This is because the data coverage of GRACE measurement decreases toward lower latitudes because of its polar orbit at operation. That is why the GRACE data has large uncertainties in low latitude regions (Figure 2.5).

2.2 Filtering process

In order to reduce the shortwave-length noises due to the aliasing as described above, spatial filtering processes are needed. Here I will introduce two widely used filters: Gaussian filter [Wahr et al., 1998; Zhang et al., 2009] and De-striping filter

Uncertainty in GRACE mass estimates

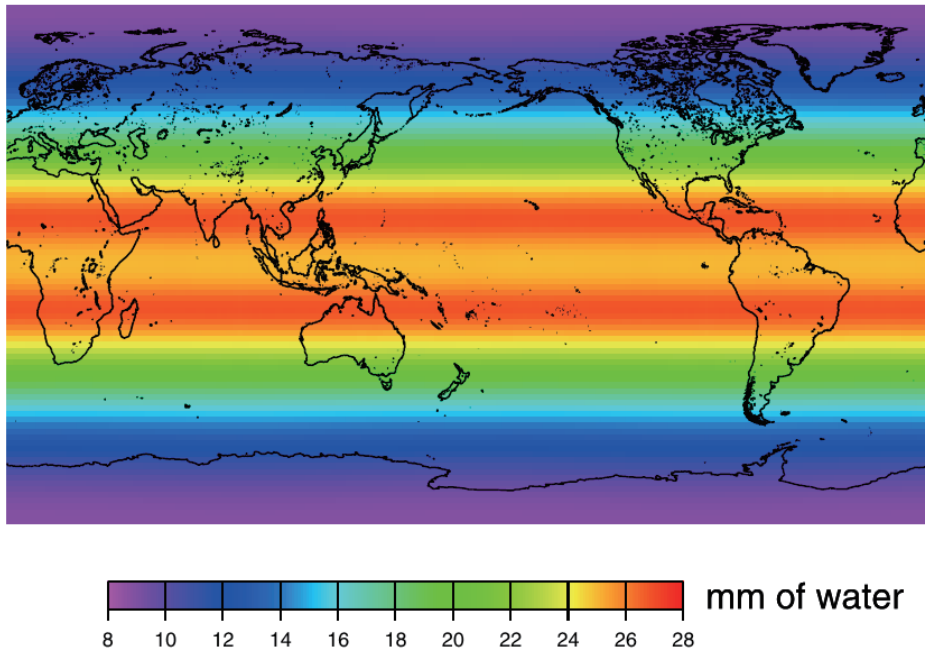


Figure 2.5: Uncertainties in the GRACE mass estimates, in mm of water thickness, for 750 km Gaussian averages and averaged over all 22 months estimated by Wahr et al. (2006).

[Swenson and Wahr, 2006].

2.2.1 Gaussian filter

The noise of GRACE data becomes large as the degree n of the Stokes' coefficient become higher. So, we reduce the contribution of the short-wavelength domain by applying a low-pass filter with Gaussian distribution function. The filter with the isotropic Gaussian distribution function is called Gaussian filter [Wahr et al., 1998]. This type of filter acts as spatial averaging of signal and noise. The weighting function with Gaussian distribution at degree n can be expressed in the following

recurrence formula,

$$W_0 = 1, \quad (2.3)$$

$$W_1 = \frac{1 + e^{-2b}}{1 - e^{-2b}} - \frac{1}{b}, \quad (2.4)$$

$$W_{n+1} = -\frac{2n+1}{b}W_n + W_{n-1}, \quad (2.5)$$

$$b = \frac{\ln(2)}{(1 - \cos(r/R))}, \quad (2.6)$$

where W_n is the weighting function with Gaussian distribution at degree n , and r is the averaging radius. The amplitude of Gaussian weight with different averaging radius is shown in Figure 2.6. The Gaussian filter can be applied by multiplying the weighting function W_n to the equation (2.2),

$$\Delta g(\theta, \phi) = \frac{GM}{R^2} \sum_{n=2}^{nmax} (n-1)W_n \sum_{m=0}^n (\Delta C_{nm} \cos m\phi + \Delta S_{nm} \sin m\phi) \bar{P}_{nm}(\sin \theta), \quad (2.7)$$

Figure 2.7 shows the global gravity anomaly map after applying Gaussian filter with different averaging radius.

Similarly, the noise of GRACE becomes large as the order m of the Stokes' coefficient becomes higher. So, we apply the same Gaussian filter for the order m together with the degree n . This anisotropic Gaussian filter is called Fan filter [Zhang et al., 2009]. The Fan filter can be applied as follows

$$\Delta g(\theta, \phi) = \frac{GM}{R^2} \sum_{n=2}^{nmax} (n-1)W_n \sum_{m=0}^n W_m (\Delta C_{nm} \cos m\phi + \Delta S_{nm} \sin m\phi) \bar{P}_{nm}(\sin \theta), \quad (2.8)$$

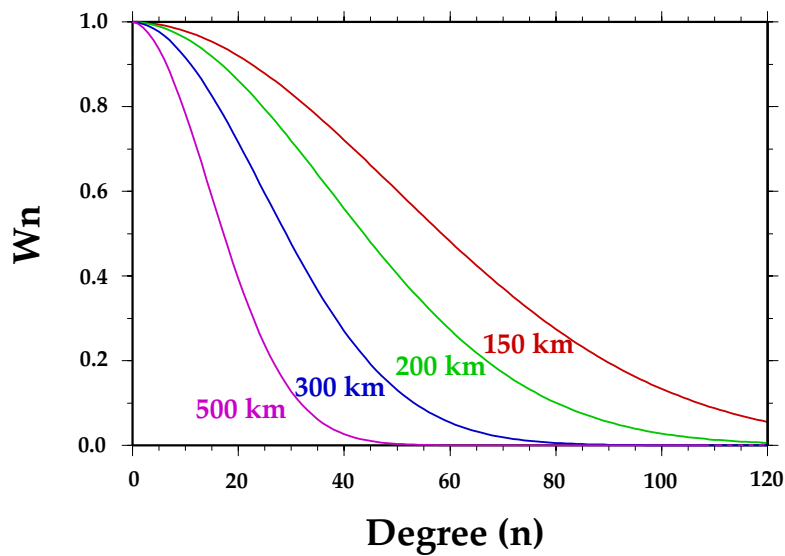


Figure 2.6: Spherical harmonic coefficients W_n of isotropic Gaussian filters with the averaging radius of 150 km, 200km, 300km, and 500km.

Figure 2.8 shows the global gravity anomaly map after applying Fan filter with different averaging radius. The north-south striping of the gravity anomaly map with Fan filter seems to be smaller than that with Gaussian filter in the same averaging radius.

2.2.2 De-striping filter

Swenson and Wahr (2006) found that the presence of north-south stripes indicates a high degree of spatial correlation in the GRACE error. An examination of Stokes' coefficients for a particular order gives us an insight into this problem. Figure 2.9 shows the Stokes' coefficients C_{nm} , as a function of degree n for orders $m=19$. Plotting the Stokes' coefficients with even degree and odd degree separately (Figure 2.9a), one can see obvious correlation between them. Such correlation is found especially in higher degrees and orders. This results in the intense spike of

Gravity anomaly of the Earth (Gaussian filter)

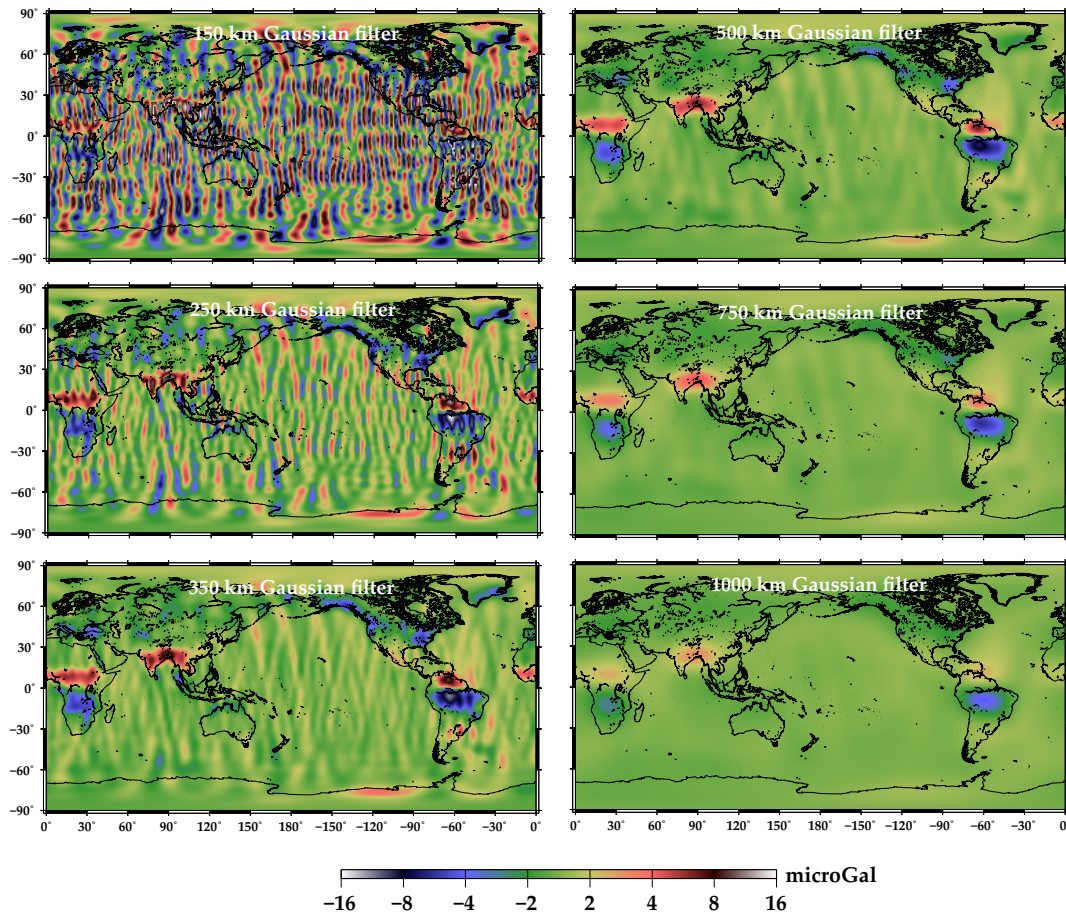


Figure 2.7: Gravity anomaly on July 2007 observed by GRACE, which Gaussian filter with different radius (150 km, 250 km, 350 km, 500 km, 750 km, 1000 km) is applied.

the Stokes' coefficient as a function of degree n , emerging as north-south stripes. To alleviate this correlated error, we modeled the even and odd coefficients with a polynomial of degree 5 by least-squares method, and subtracted the fitted curves from the original ones respectively (Figure 2.9b). Figure 2.10 shows the global gravity anomaly map after applying De-stripping filter, together with Fan filter. Here we applied the De-stripping filter for the Stokes' coefficients with order $m=6$ or higher using a polynomial of degree 5. This is referred to as P5M6 De-stripping filter.

Gravity anomaly of the Earth (Fan filter)

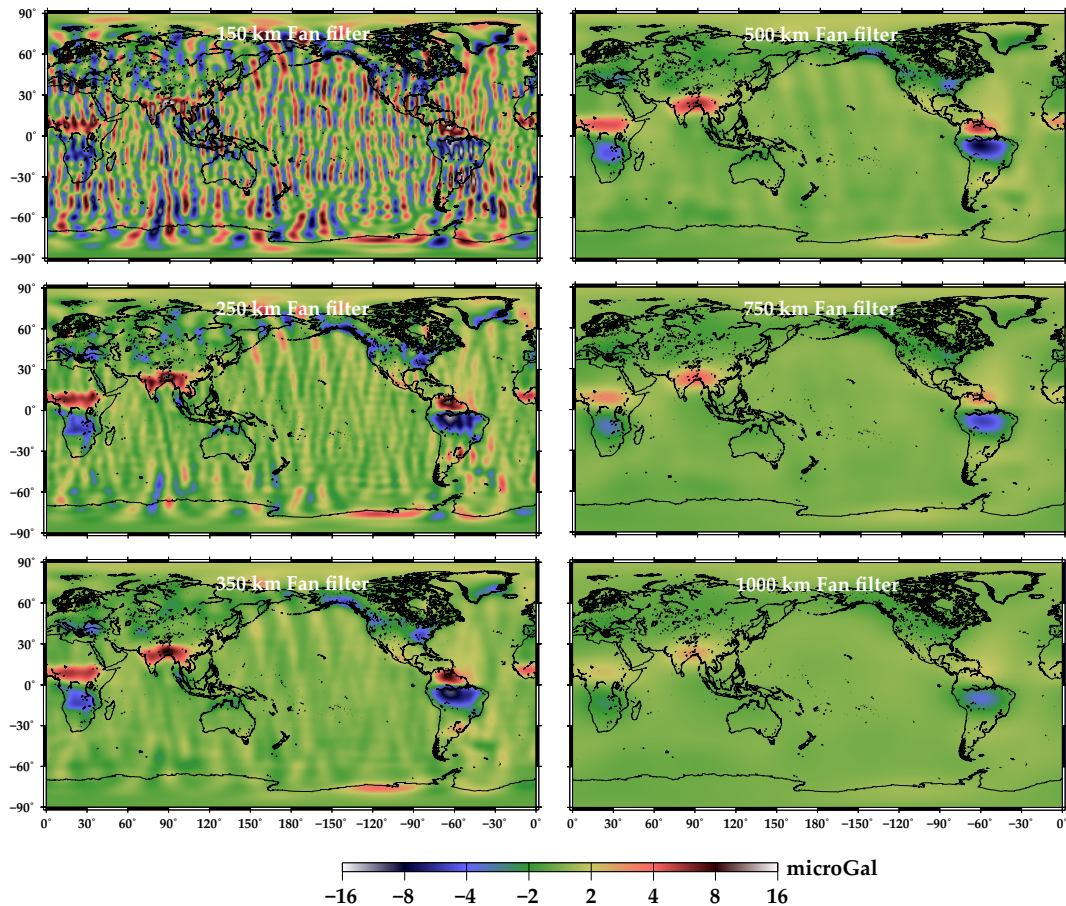


Figure 2.8: Gravity anomaly on July 2007 observed by GRACE, which Fan filter with different radius (150 km, 250 km, 350 km, 500 km, 750 km, 1000 km) is applied.

2.3 Time-series analysis of GRACE data

In many cases, there are temporal characteristics in the mass redistributions that occur on/in the Earth. For examples, hydrological mass changes due to rainfall and snowfall show strong seasonality in their temporal variation. Mass increase by GIA can be well expressed in linear function. Accelerated melting in mountain glaciers and polar ice sheets are expressed in quadratic function. Such *a priori* in-

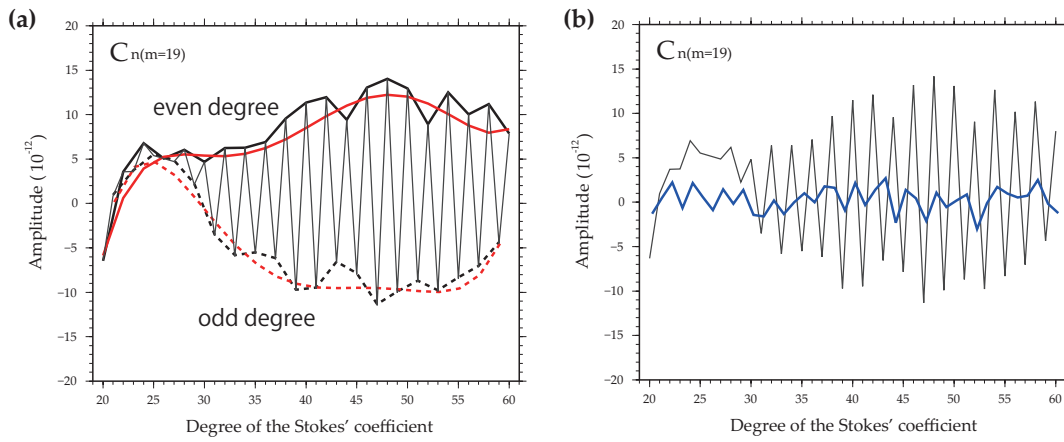


Figure 2.9: (a) The Stoke's coefficients C_{nm} plotted as a function of degree n for the order $m=19$. The solid black line is the Stoke's coefficients with even degrees, and the broken black line is those with odd degrees. The solid and broken red lines are their modeled curve with a polynomial degree 5. (b) The blue line is the residual between the black lines and the red lines, which mean the Stoke's coefficients after applying De-stripping filter.

formation is of great help to effectively extract their signatures from GRACE gravity data. We modeled the time-series of GRACE gravity change at each grid point with a polynomial of degree 2 and seasonal (annual + semi-annual) components by least-squares method as follow.

$$\Delta g(t) = a_1 t + a_2 t^2 + a_3 \cos(2\pi t) + a_4 \sin(2\pi t) + a_5 \cos(4\pi t) + a_6 \sin(4\pi t), \quad (2.9)$$

where a_1 is a regression coefficient of linear function, a_2 is a quadratic function, and a_3 - a_6 are seasonal components.

Figure 2.11 represents the seasonal component of the global gravity field in each month. Strong seasonal signals can be found in tropical region and high latitude region. They reflect changes in soil moisture and snowpack, respectively [Tapley et

Gravity anomaly of the Earth (De-stripping filter and Fan filter)

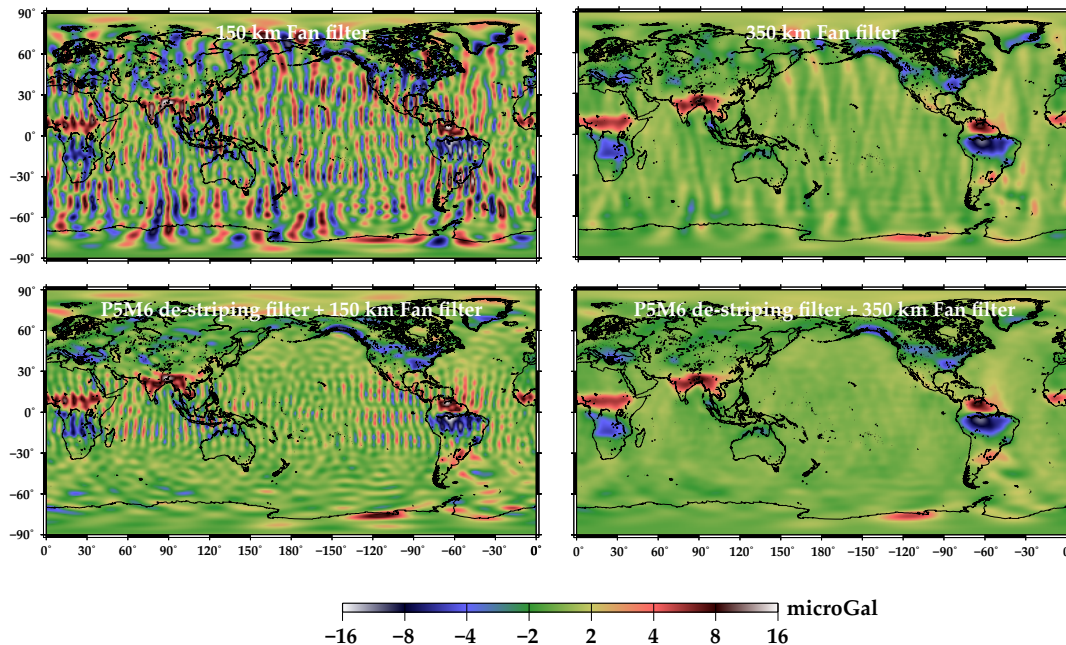


Figure 2.10: Gravity anomaly on July 2007 observed by GRACE, which (upper) Fan filter with 150 km and 350 km radius is applied, (lower) Fan filter and P5M6 De-stripping filter are applied.

al., 2004].

Figure 2.12 shows the linear component of the global gravity field during 2003-2011. The gravity increases seen in Scandinavia peninsula and North America are due to GIA [e.g. Tamisiea et al., 2007]. The gravity decreases seen in Greenland, East Antarctica, Alaska, Patagonia are caused by ice losses due to recent climatic changes like global warming [e.g. Veliconga and Wahr, 2006a,b; Luthcke et al., 2006]. Slight gravity decreases are found around northwestern India and Asian high mountain ranges such as Himalayan Mountains. They can be attributed to ground-water depletion by irrigation for crop and glacial melting [Rodell et al., 2009; Tiwari and Wahr, 2009; Matsuo and Heki, 2010]. The gravity changes in Sumatra

Gravity seasonal change (Jan. - Dec.)

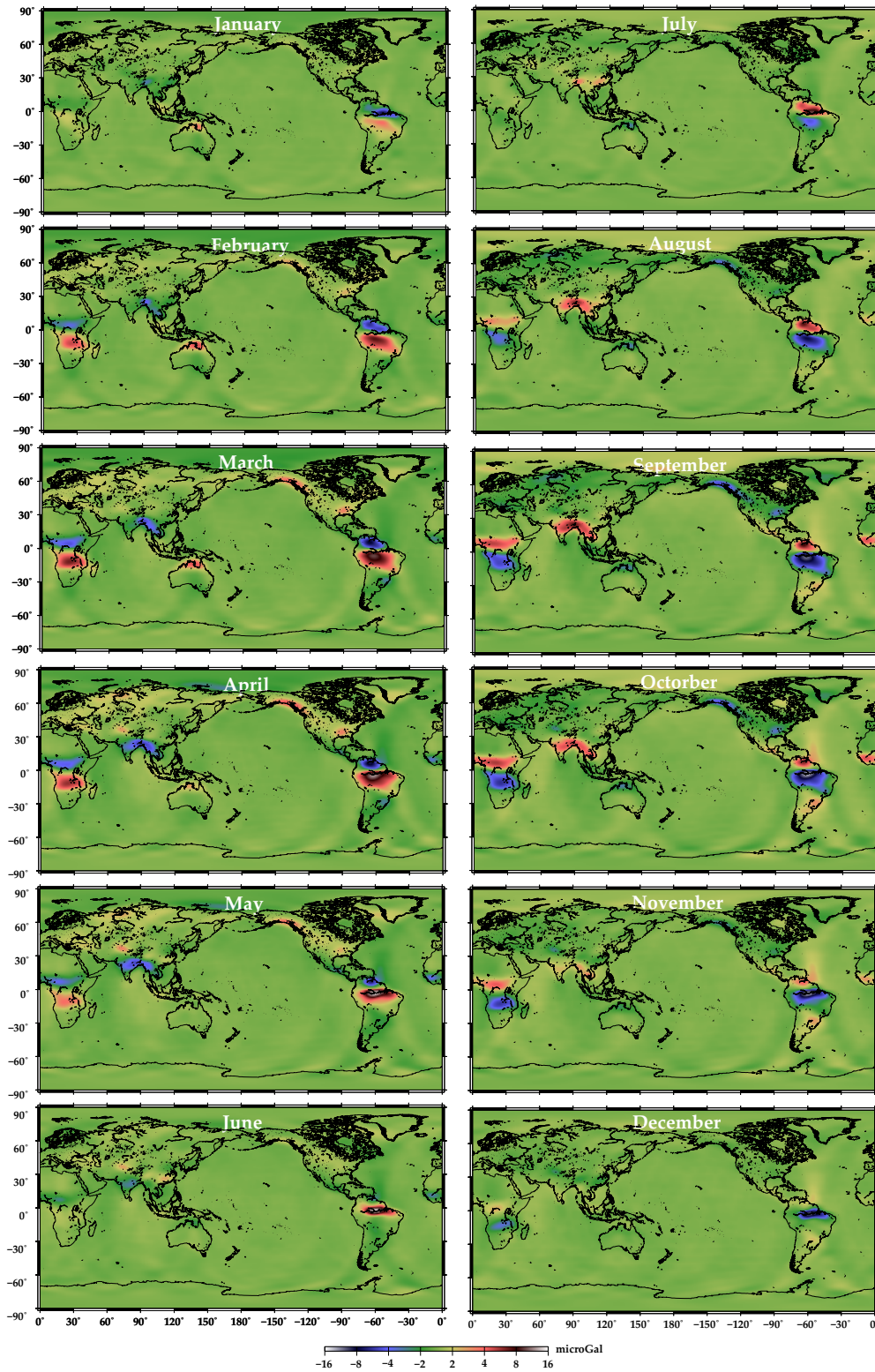


Figure 2.11: Gravity seasonal change from January to June observed by GRACE. Fan filter with 350 km radius and P5M6 De-stripping filter are applied.

Indonesia are the leakage of coseismic and postseismic gravity changes caused by the 2004 Sumatra-Andaman Earthquakes to the linear component [e.g. Han et al., 2006; Ogawa and Heki, 2007]. Same kind of signals are found in central Chile and northeastern Japan, which are caused by the 2010 Maule Earthquake and the 2011 Tohoku-Oki Earthquake [e.g. Heki and Matsuo, 2010; Matsuo and Heki, 2011].

Figure 2.13 shows the quadratic component of the global gravity field during 2003-2011. As GRACE data accumulates, the contribution of this component is becoming greater in GRACE time-series. Ogawa et al. (2011) showed that quadratic variation in continental areas can be often explained by inter-annual changes in precipitation. Gardner et al. (2011) also showed that ice loss in northwestern part of Greenland and its adjacent glacier systems are accelerating, which emerges as quadratic gravity changes. Same kind of quadratic change is also found in Antarctic ice sheet. The signal in Sumatra Indonesia is postseismic gravity changes of the 2004 Sumatra-Andaman Earthquake.

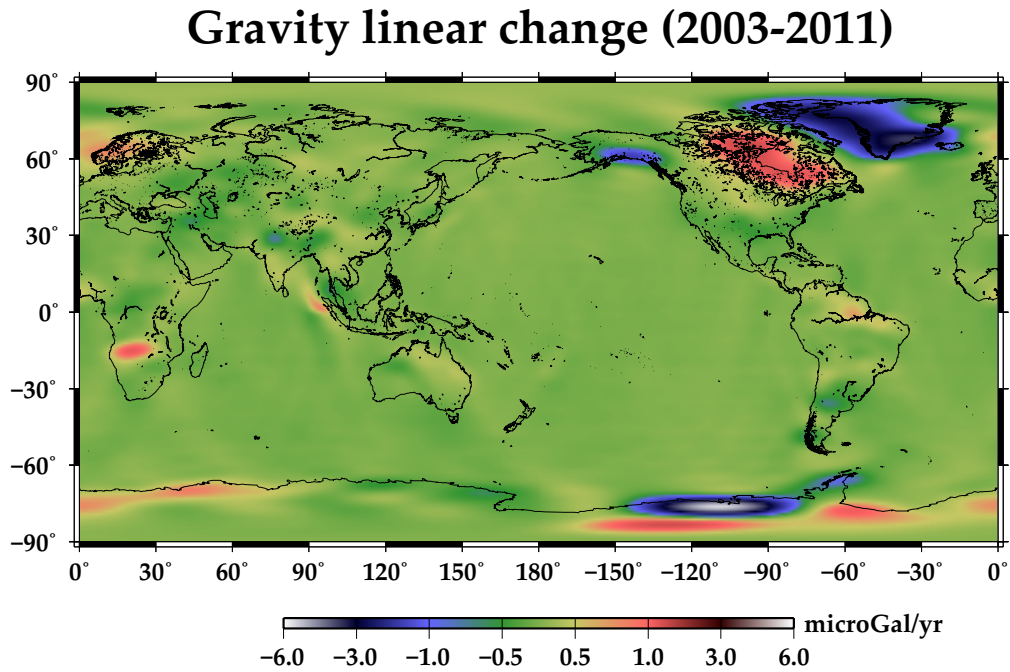


Figure 2.12: Gravity linear change during 2003-2011 observed by GRACE. Fan filter with 350 km radius and P5M6 De-stripping filter are applied.

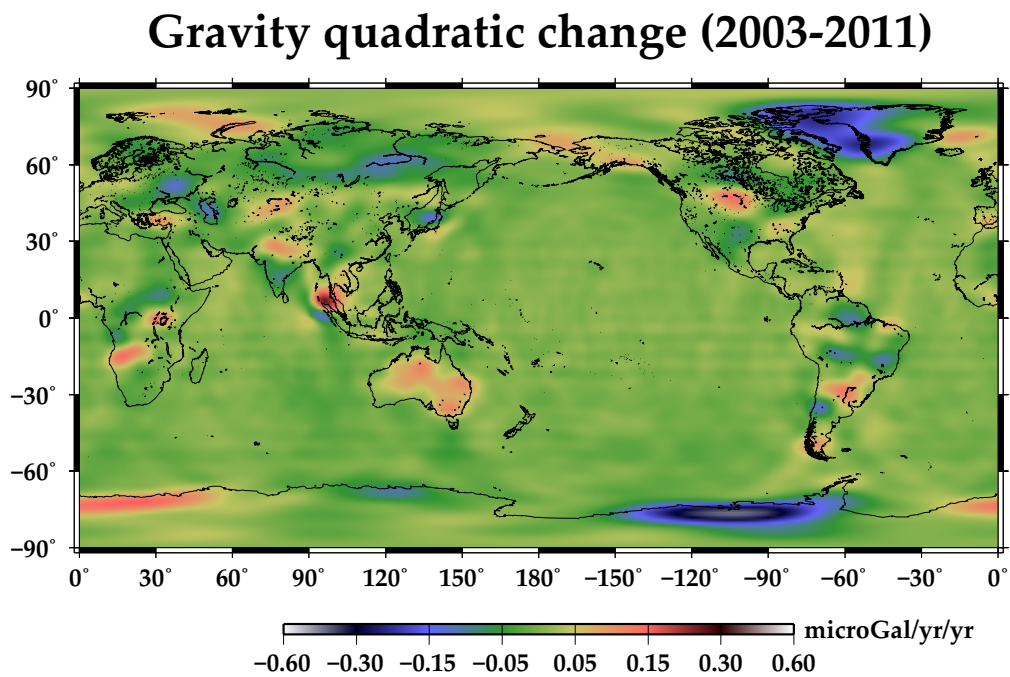


Figure 2.13: Gravity quadratic change during 2003-2011 observed by GRACE. Fan filter with 350 km radius and P5M6 De-stripping filter are applied.

Chapter 3

Anomalous precipitation signatures of Arctic Oscillation in the time-variable gravity field by GRACE

Paper was published in *Geophysical Journal International*

Matsuo, K. and K. Heki, 2012: Anomalous precipitation signatures of the Arctic Oscillation in the time-variable gravity field by GRACE, *Geophys. J. Int.*, 130, 1495-1506, doi:10.1111/j.1365-246X.2012.05588.x.

3.1 Introduction

Arctic Oscillation (AO) is a seesaw like fluctuation in the sea-level pressure (SLP) between polar and middle latitude regions of the northern hemisphere (NH), and its index characterizes the dominant pattern of atmospheric circulation in NH [Thompson and Wallace, 1998]. AO resembles to the North Atlantic Oscillation (NAO), a seesaw of SLP between the Icelandic low and the Azores high [Walker and Bliss, 1932], but AO represents the variability in the atmospheric circulation of the whole NH [Wallace, 2000]. Their indices are known to have high temporal correlation. There are some debates as to their differences [e.g. Ambaum et al., 2001], but here we consider NAO a part of AO.

AO exerts strong influences on wintertime climate in NH [Thompson and Wallace, 2000]. The intensity and phase of AO is represented by the AO index (AOI) derived as the first leading mode of Empirical Orthogonal Function (EOF) of monthly mean SLP anomaly field north of $\sim 20^\circ\text{N}$. AOI becomes positive when SLP around the North Pole is lower than the average. Positive AO brings the retention of arctic cold surge and enhancement of polar front jet (PFJ), the northern stream of the westerly jet, causing low temperature and high precipitation (mainly snowfall) in the high latitude regions [Hurrell, 1995; Thompson and Wallace, 2001]. The opposite occurs in the middle latitude regions. On the other hand, AOI becomes negative when SLP around the North Pole gets higher than the average. Negative AO is characterized by the southward advection of arctic cold wave and southward shift of PFJ, and it causes low temperature and high precipitation (rainfall and snowfall) in the middle latitude regions. The opposite occurs in the high latitude regions.

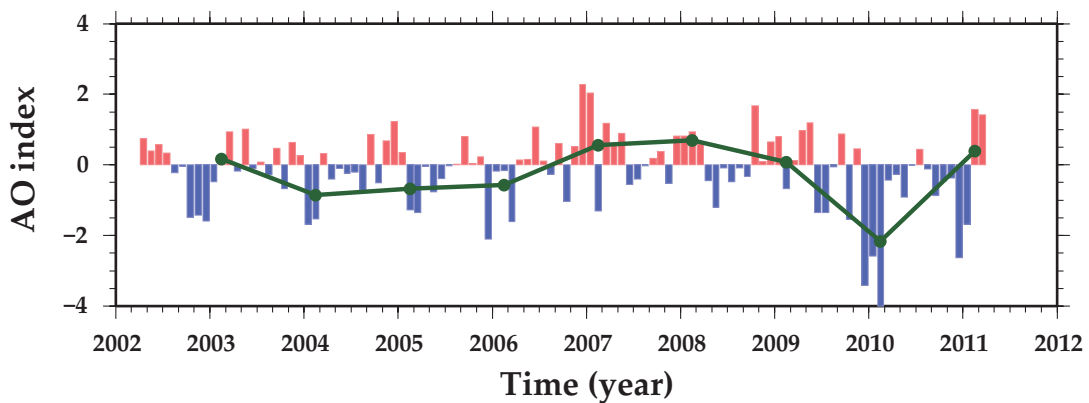


Figure 3.1: Time-series of the monthly AO index from National Oceanic and Atmospheric Administration ([http : //www.cpc.ncep.noaa.gov/products/precip/CWlink/daily_ao_index/ao.shtml](http://www.cpc.ncep.noaa.gov/products/precip/CWlink/daily_ao_index/ao.shtml)). Red and blue bars show positive and negative phases of AO, respectively. The green curve shows the time series of the three month (JFM) averages of AO indices in NH winters.

Figure 3.1 shows the time-series of AOI between April 2002 and March 2011. In the NH winter of 2009-2010, the record-breaking strong negative AO occurred, and brought about anomalous precipitation and temperature in various regions in middle latitude regions [Wang et al., 2010; L’Heureux et al., 2010; Cohen et al., 2010].

Precipitation changes the Earth’s gravity fields as it redistributes water on land and ocean. Such mass redistribution can be detected and measured by the GRACE satellite system, composed of twin satellites launched in 2002. The two satellites, separated by ~ 220 km, are in the same polar circular orbit at an altitude of ~ 500 km, and the change of the inter-satellite distances are measured precisely. The time-variable gravity fields of the earth are inverted from the changes of such distances. The gravity measured by GRACE is accurate to several μGal , and has spatial and temporal resolutions of ~ 300 km and ~ 1 month, respectively [Wahr et al., 1998].

Up to now, GRACE results have been utilized for various disciplines of earth

sciences, such as hydrology [e.g. Tapley et al., 2004; Morishita and Heki, 2008], glaciology [e.g. Tamisiea et al., 2005; Matsuo and Heki, 2010], physical oceanography [e.g. Chamber et al., 2004], seismology [e.g. Han et al., 2006; Matsuo and Heki, 2011], and geodynamics [e.g. Tamisiea et al., 2007]. The advantage of satellite gravimetry is the direct and quantitative measurement of mass changes, especially in regions where *in situ* observations are limited, e.g. polar and high mountain regions. In this paper, we discuss wintertime precipitation anomalies caused by AO in NH by analyzing the time-variable gravity data from GRACE. In order to further validate the GRACE results, we also analyzed the changes in terrestrial water (including snow) storage given by the Global Land Data Assimilation System (GLDAS) Noah model [Rodell et al., 2004].

3.2 Data and Method

We used the GRACE data (Level-2, Release 4) from the Center for Space Research (CSR), Univ. Texas, consisting of 103 monthly data sets from April 2002 to March 2011. This time span covers 9 winters in NH. A monthly GRACE data set includes a set of the coefficients of spherical harmonics (Stokes' coefficient) C_{nm} and S_{nm} with degree n and order m complete to 60. We replaced the coefficients indicating the Earth's oblateness (C_{20}) with those from Satellite Laser Ranging (SLR) [Cheng and Tapley, 2004] because of their poor accuracy. We used the degree-1 components (C_{10} , C_{11} , and S_{11}), which reflect the geocenter motion, estimated by combining GRACE and ocean model [Swenson et al., 2008] because GRACE alone cannot measure them. We also applied the Fan filter with averaging radius of 400

km to reduce short wavelength noises [Zhang et al., 2009], together with the De-correlation filter using polynomials of degree 5 for coefficients with orders 6 or higher to alleviate longitudinal stripes [Swenson and Wahr, 2006].

In order to interpret gravity changes in terms of surface mass variations, we need to calculate σ equivalent water thickness (EWT) using the relationship [Wahr et al., 1998]

$$\Delta\sigma(\theta, \phi) = \frac{R\rho_{ave}}{3} \sum_{n=2}^{nmax} \sum_{m=0}^n \frac{2n+1}{1+k_n} [\Delta C_{nm} \cos m\phi + \Delta S_{nm} \sin m\phi] P_{nm}(\sin \theta), \quad (3.1)$$

where R is the equatorial radius, ρ_{ave} is the mean density of the Earth, and the load Love numbers k_n is to account for the Earth's elastic yielding effect under the mass load in question. $P_{nm}(\sin \theta)$ is the n th degree and m th order fully-normalized associated Legendre function, and Δ indicates the deviation from the reference value. We assumed that the GRACE gravity changes reflect those of the surface load, and converted them into EWT. Chao (2005) showed that the inverse solution is unique in this case.

Temporal variations of EWT contain mass changes of various origins. Such changes usually include strong seasonal (annual and semiannual) and linear components. Seasonal changes mainly come from the variations in soil moisture and snow-pack [Frappart et al., 2006; Schmidt et al., 2008]. Linear changes reflect secular mass movements, such as glacial isostatic adjustment in North America and northern Europe [Tamisiea et al., 2007; Steffen et al., 2009], and ice melting in continental ice sheets [e.g. Velicogna and Wahr, 2006a,b] and mountains glaciers [e.g. Chen et al.,

2006].

In addition to these components, quadratic changes became evident as the GRACE data accumulated. Ogawa et al. (2011) showed that quadratic terms seen in the GRACE data are often explained by inter-annual changes in precipitation. Gardner et al. (2011) also showed that quadratic gravity changes are significant in the northwestern part of Greenland, and suggested that it reflects accelerating melting of ice sheet there over the last several years. In order to isolate AO signals from these mass changes, we remove seasonal, linear and quadratic components from the EWT time-series by least-squares method. Here we refer to the residual as equivalent water thickness deviation (EWD). Then we calculate averages of the three winter months (JFM; January, February, and March) to discuss mass changes in NH winters.

In addition to GRACE, we have also used monthly solutions of the changes in terrestrial water storage by the GLDAS Noah model [Rodell et al., 2004]. GLDAS provides soil moisture, canopy, and snow data at 1×1 degree grid points, except for Antarctica where hydrological models are not established and meteorological data are unavailable. GLDAS contains the values in Greenland, but their accuracy is dubitable due to the same reason as Antarctica. So we did not use the GLDAS model in the Greenland area. To compare GLDAS with GRACE, we applied the same spatial filters (Fan filter and De-stripping filter) for the GLDAS models, and removed seasonal, linear and quadratic components by the least-squares method (we will discuss this detrending in detail in Section 3.4). Then we also calculated their averages of months JFM.

3.3 Result

3.3.1 GRACE and GLDAS

Following the analysis methods in the previous section, we plot the EWD distributions in NH to the north of $\sim 25^{\circ}\text{N}$ in the winters from 2003 (“2003 winter” means the NH winter encompassing the 2002-2003 boundary) to 2011 in Figure 3.2 (GRACE) and Figure 3.3 (GLDAS). Their spatial patterns roughly agree well with each other, but small differences in magnitudes remain.

Syed et al. (2008) suggested that such difference in magnitudes may reflect model deficiencies in GLDAS, such as inadequate snow models in high mountain ranges and polar regions, missing surface and/or groundwater components, and so on. The difference might also reflect errors in GRACE data processing, aliasing, or instrumental noises. Moreover, GRACE data includes mass change signals from semi-closed ocean basins (or large lakes) such as the Mediterranean Sea [Fenoglio-Marc et al., 2006], Black Sea, Caspian Sea, and Red Sea, but GLDAS does not include them. Leakage from such signals might have enhanced the signals of terrestrial mass changes. From these reasons, the magnitudes of EWT or EWD in GLDAS are apt to become smaller than those in GRACE.

The largest positive (AOI = +0.8) and negative (AOI = -2.4) AO in the studied period occurred in the winters of 2008 and 2010, respectively. The EWD distributions in these two winters show characteristic spatial patterns (Figures 3.2 and 3.3). The polarity of EWD reverses across the latitude 55°N in Eurasia continent and North America and $\sim 75^{\circ}\text{N}$ in Greenland. It also reverses temporally between these two

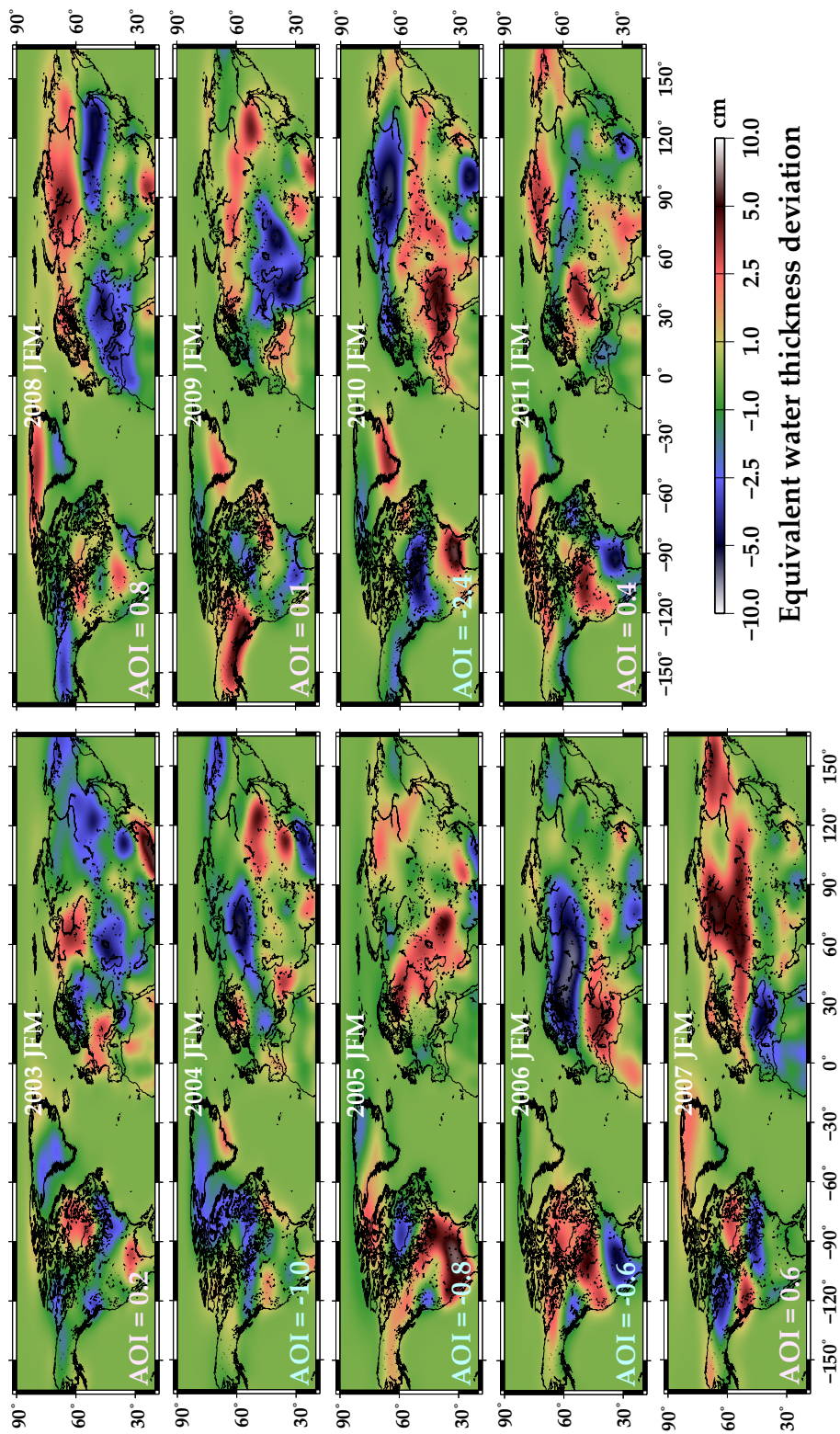


Figure 3.2: NH maps of wintertime (JFM) equivalent water thickness deviations observed by GRACE. In the lower left corners of the maps are shown AOI corresponding to the green curve in Figure 3.1

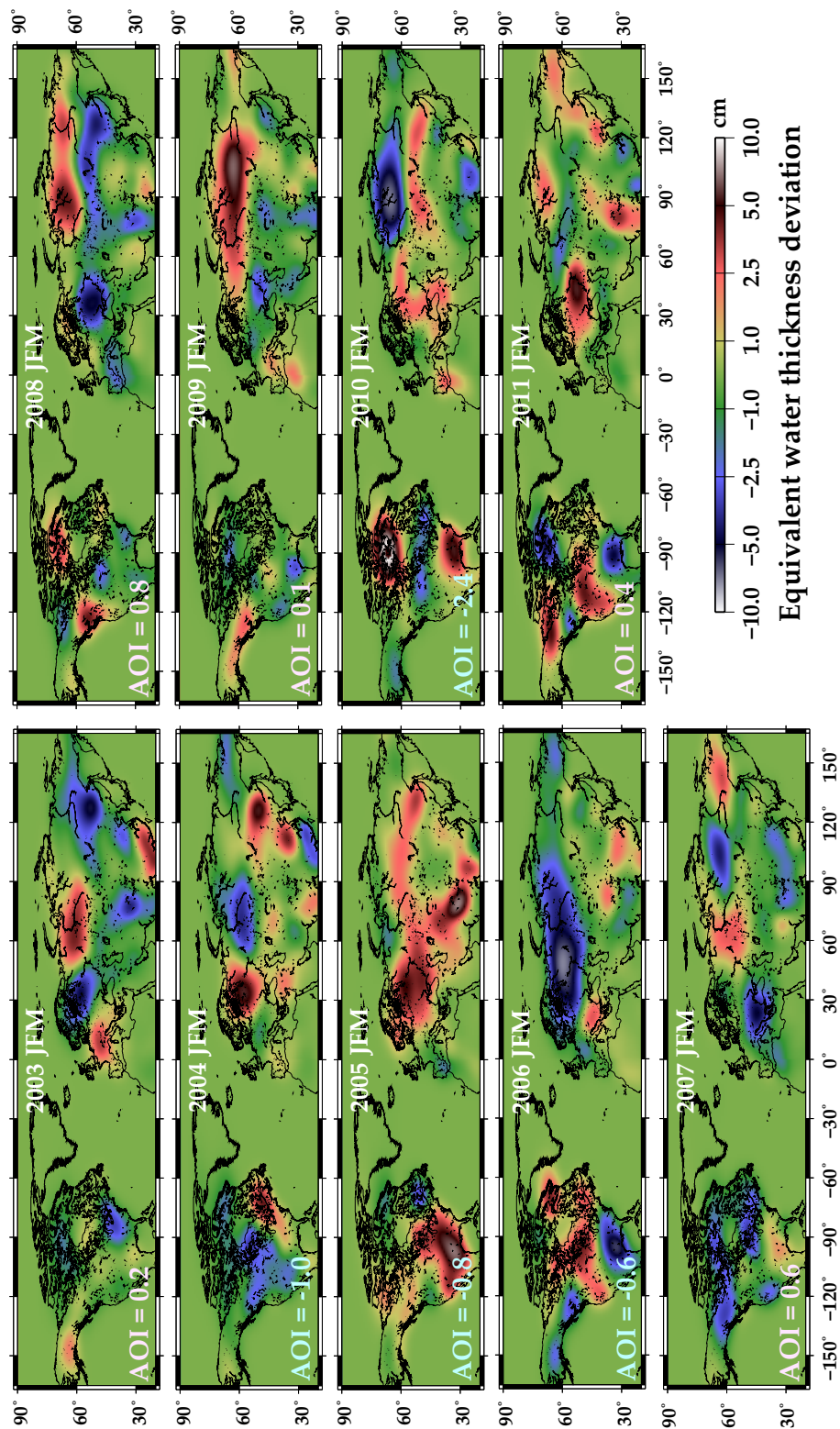


Figure 3.3: NH maps of wintertime (JFM) equivalent water thickness deviation from the GLDAS models. The same spatial filters as GRACE have been applied. We excluded Greenland (values are fixed to zero there) because of relatively poor reliability there (see text).

winters. Especially, the winter of 2010 witnessed the largest negative AO in the last 60-year record, causing record-breaking precipitations in many parts of the middle latitude regions of NH, such as the southern North America [Seager et al., 2010] and southern Europe [Ball, 2010].

3.3.2 Microscopic view of the correlation between the GRACE/GLDAS and AO

We plot the time-series of monthly and wintertime EWD obtained by GRACE and GLDAS at two points, i.e. the Western Siberia and Tien-Shan Mountain Range, representing the high and the middle latitude regions in Eurasia in Figures 3.4a and 3.4b, respectively. Figure 3.4 also shows the time-series of the wintertime AOI. Wintertime EWDs in the Western Siberia, inferred from GRACE and GLDAS, showed positive/negative deviations during periods of positive/negative AO indices. On the other hands, those in the Tien-Shan Mountain Range showed the opposite; negative/positive deviation occurred during AO of positive/negative indices. The wintertime EWD and AOI showed large positive correlation in Western Siberia, i.e. +0.95 (GRACE) and +0.84 (GLDAS). These positive correlations mean that the positive/negative AO increased/decreased the terrestrial water storages in these regions. By contrast, they showed significant negative correlation in the Tien-Shan Mountain Range, i.e. -0.68 (GRACE) and -0.70 (GLDAS). These negative correlations imply that the positive/negative AO decreased/increased the terrestrial water storages there.

Matsuo and Heki (2010) suggested that glacial mass in Asian high mountains surrounding the Tibetan Plateau shows significant decrease using the GRACE data 2002-2009. They also reported that glacial mass losses are fairly variable in time and

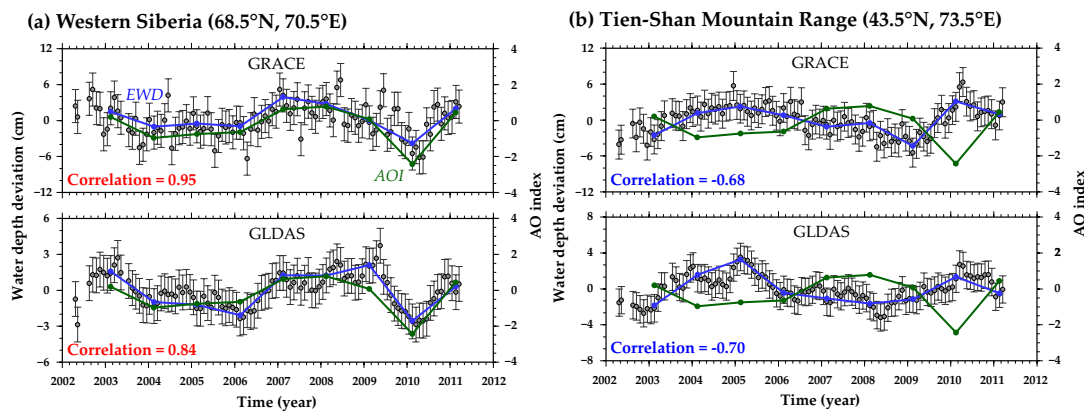


Figure 3.4: Time-series of EWD at points in (a) the Western Siberia (68.5°N , 70.5°E) and (b) the Tien-Shan Mountain Range (43.5°N , 73.5°E). The top and the bottom panels are derived from GRACE and GLDAS, respectively. Gray dots are monthly values of EWD. Error bars show one-sigma formal errors inferred *a posteriori* by bringing the chi-square of the post-fit residual to unity. Blue curves are the three month (JFM) averages of the EWDs. Green curves show winter AOI (Figure 3.1, green curve). The correlation coefficients between wintertime EWDs and AOI are given in the lower left corners (red and blue characters show positive and negative correlations, respectively).

space, especially in the glaciers fed by westerly winds from November to April such as those in the Karakorum, Pamir and Tien-Shan regions. AO is known to influence the strength and trajectory of the westerly wind [Thompson and Wallace, 2000]. The present study suggests that climatic fluctuations controlled by AO played a key role in the glacial mass changes in these regions.

3.3.3 Macroscopic view of the correlation

Next we computed correlation coefficients between the wintertime EWD and AOI at each grid points in NH, and show their distribution in Figure 3.5. We can find that high latitude region is dominated by positive correlation, and middle latitude region is dominated by negative correlation. This means that wintertime precipitation

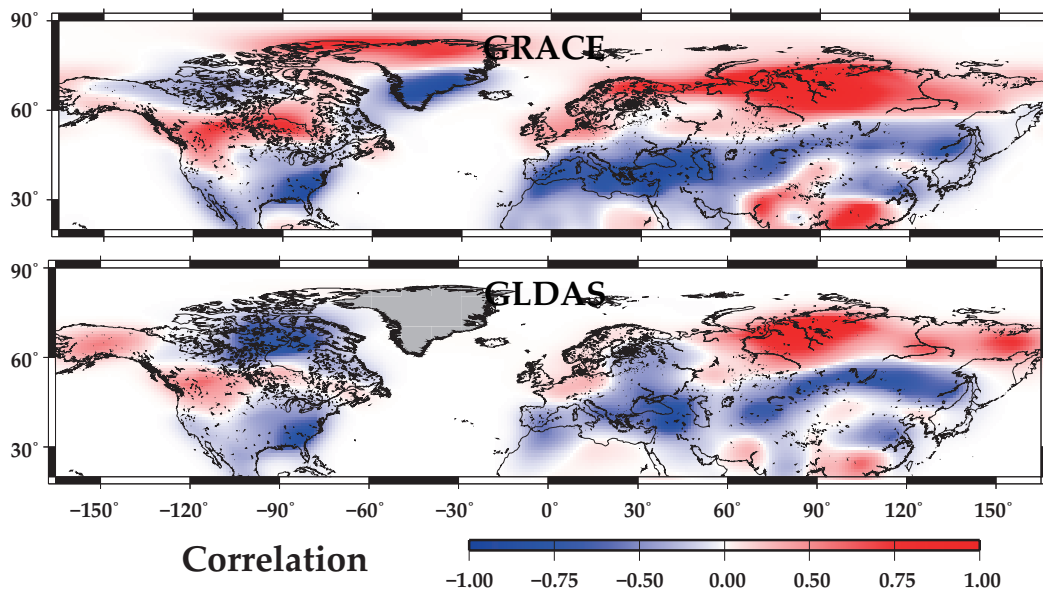


Figure 3.5: Distribution of the correlation coefficients between wintertime EWDs and AO indices for GRACE (top) and GLDAS (bottom) at grid points in NH. We excluded Greenland in the GLDAS models (pasted in gray). The boundary between the positive and negative correlations lies along $\sim 55^\circ\text{N}$ in Eurasia and North America for both GRACE and GLDAS, and $\sim 75^\circ\text{N}$ in Greenland for GRACE.

increases in the high latitude region during positive AO. On the other hand, such an increase in the middle latitude region occurs during negative AO. This agrees with climatological studies that a negative AO makes the southern and the northern Europe wetter and drier, respectively [Quadrelli et al., 2001; Hurrell et al., 2003]. It appears that the boundary of the polarity change lies $\sim 55^\circ\text{N}$ in Eurasia and North America, and $\sim 75^\circ\text{N}$ in Greenland.

Though the North American continent shows similar distribution of the correlation to Eurasia, climatic situation is somewhat more complex there. Wintertime precipitations in North America are highly influenced by El Niño and Southern Oscillation (ENSO) episodes as well as AO. According to Ropelewski and Halpert (1987), El Niño/La Niña episodes tend to cause more/less precipitation in southeastern U.S

and less/more precipitation in northwestern North America, respectively. Thus we need more sophisticated numerical studies there to separate contributions from AO and ENSO. We discuss the influences of ENSO and other climatic modes on the mass changes in NH in the Section 3.4.

AO also exerts strong influence on the total amount of precipitation and EWD changes in NH, especially in Eurasia. Here we integrate EWD in Eurasia from GRACE and GLDAS over high (55°N to 90°N , 15°W to 165°E) and middle (25°N to 55°N , 15°W to 165°E) latitude regions, and show their time-series in the top two panels in Figures 3.6a, b. The time-series of the sum of and the difference between these two regions are shown in the bottom two panels of the same figure. Total masses in the high latitude region is positively correlated with AO, i.e. $+0.69$ for GRACE and $+0.42$ for GLDAS. On the other hands, those in the middle latitude region are negatively correlated with AO, i.e. -0.81 for GRACE and -0.61 for GLDAS. In short, stronger positive/negative AOI brings more precipitations in the high/middle latitude regions, respectively.

The sum of mass deviations in the high and middle latitude regions does not show notable correlation with AO. They are only weakly correlated negatively, i.e. -0.35 for GRACE and -0.30 for GLDAS. In contrast, the difference between the high and middle latitude regions shows strong correlations with AO, i.e. $+0.89$ for GRACE and $+0.76$ for GLDAS. This suggests that the center of precipitation anomalies moves between high and middle latitude regions in response to the polarity of AO. The water mass that moves between these two latitudinal bands amounts up to ~ 1000 Gt in the studies period. However, the total mass over the entire region changes only a little. The slight increase of the total mass during periods of negative

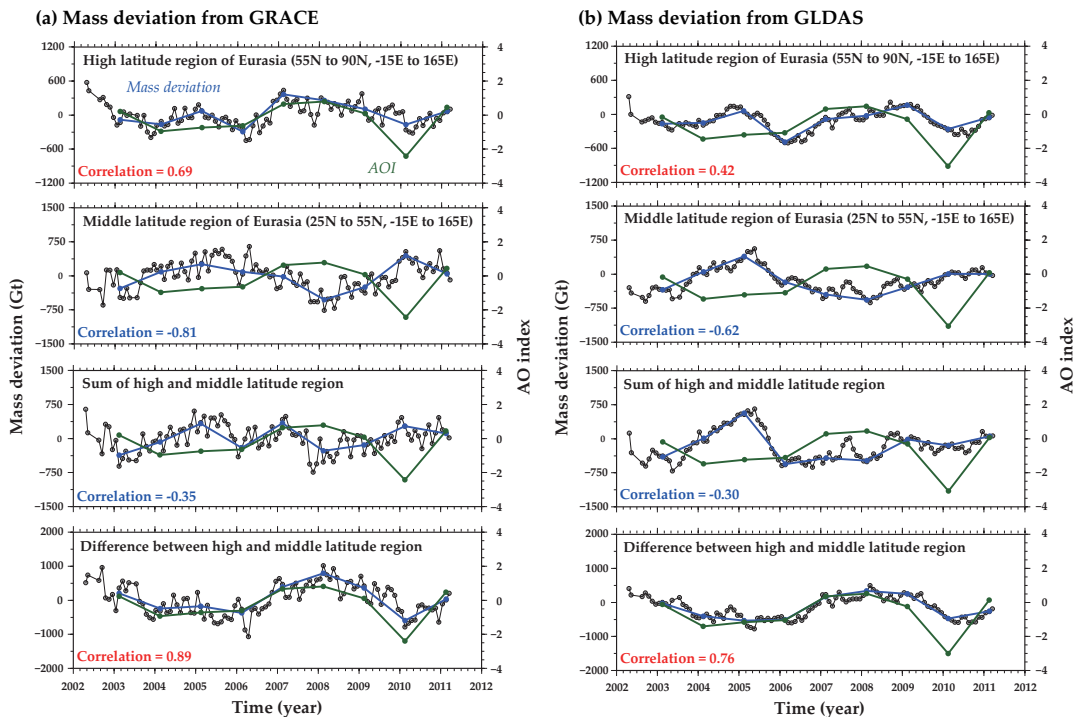


Figure 3.6: From top to bottom, time-series of mass deviation in high latitude region (55°N - 90°N), middle latitude region (25°N - 55°N), the sum of the two regions, the difference between the two regions, calculated from (a) the GRACE data and (b) the GLDAS models. Gray dots are monthly values of mass deviations. Blue and green curves are the three month (JFM) averages of mass deviations and AOI. The correlation coefficients between wintertime mass deviations and AOI are shown in the lower left corners. Red and blue characters show positive and negative correlations, respectively.

AO may partly reflect the difference in land area between the middle and high latitude regions (the former has continental area twice as large as the latter, and so its hydrological capacity is also larger).

3.3.4 Surface deformation by AO

Mass redistribution by AO leaves non-gravity signatures in the solid earth detectable with other geodetic techniques. Anomalous precipitation by AO brings

surface loads and causes crustal deformation which can be directly measured with Global Positioning System (GPS). We can also infer such deformation from the GRACE data through elastic loading theory on the spherical earth using the load Love numbers [Farrell, 1972; van Dam et al., 2007].

We compared the vertical movements observed by GPS with those calculated from the GRACE data. Here, we used the data at 83 continuous GPS stations deployed by the International GNSS Service (IGS). All GPS data are processed by SOPAC (Univ. California San Diego) and available at <ftp://garner.ucsd.edu/pub/time-series/>. In each GPS time-series, we eliminated the outliers deviating by more than three-sigma formal errors from models (composed of seasonal, linear, and quadratic components). One-sigma formal errors are inferred *a posteriori* by bringing the chi-square of the post-fit residuals to unity. Deformations due to atmospheric loads are also removed from the GPS data using the ECMWF (European Centre for Medium-Range Weather Forecasts) atmospheric model. In the same manner as GRACE and GLDAS analysis, we computed the average residuals over the three winter months (JFM) of the GPS vertical coordinates to infer AO signatures.

Vertical movement induced by AO was found to be up to ~ 5 mm, large enough to be detected by GPS. The correlation coefficients between wintertime vertical position residuals at GPS stations and AOI are shown in Figure 3.7. Positive correlations mean that the surface is uplifted/depressed by positive/negative AO, and negative correlations imply the opposite. Positive correlations are mostly found in middle latitude stations of Eurasia, North America, and southern Greenland. On the other hands, negative correlations are dominant in high latitude stations of Eurasia, North America, and northern Greenland. This result is just consistent with the correlation pattern

between wintertime EWD and AOI (Figure 3.5). We can summarize the relationship among GPS, EWD, and AO as follows. In the high latitude region and northern Greenland, GPS stations are displaced downward/upward by positive/negative EWD brought about by positive/negative AO. In the middle latitude region and southern Greenland, GPS stations move upward/downward by negative/positive EWD caused by positive/negative AO.

Figure 3.7 also shows the time-series of vertical movements at 6 continuous GPS stations, (a) Vancouver (49.3°N, 235.9°E), Canada, (b) Washington, D.C. (38.9°N, 282.9°E), the United States, (c) Cornwallis Island (82.5°N, 297.7°), near Northern Greenland, (d) Qaqortoq (60.7°N, 314.0°E), Southern Greenland, (e) Norilsk (69.4°N, 88.4°E), near the West Siberian Plain of Russia, and (f) Selezaschita (43.2°N, 77.0°E), near the Tien-Shan Mountain Ranges of Kazakhstan. We confirmed that the behaviors of GPS, GRACE, and AOI are in good agreement. The correlation coefficients in the NH winters were (a) -0.59, (b) +0.78, (c) -0.56, (d) +0.72, (e) -0.81, (f) +0.63 for GPS-AOI, and (a) -0.45, (b) +0.93, (c) -0.67, (d) +0.74, (e) -0.95, (d) +0.71 for GRACE-AOI, respectively.

3.3.5 Polar motion excitation by AO

Large hydrological mass redistribution by AO would also excite the Earth's polar motion [Chao, 1988]. Its X (toward the Greenwich Meridian) and Y (toward 90°E) components can be inferred from ΔC_{21} and ΔS_{21} , respectively, the changes in the degree-2 tesseral components of the gravity changes observed by GRACE [e.g. Chen and Wilson, 2008].

The mass redistribution by AO occurs mainly in Eurasia, and it accounts for

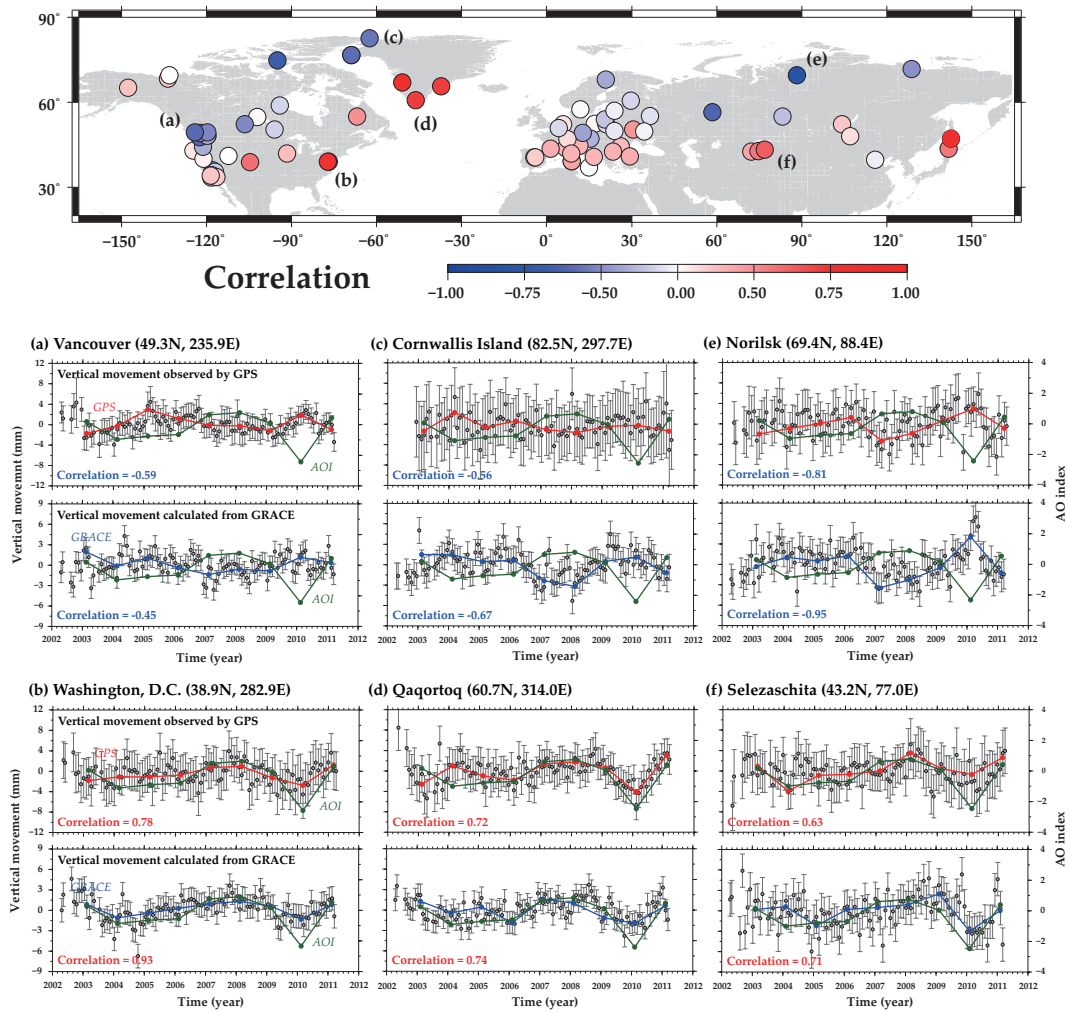


Figure 3.7: Upper map shows distribution of the correlation coefficients between vertical movement and AO indices at each continuous GPS station. Red dots mean positive correlation and blue dots mean negative correlation. Lower graphs show time-series of vertical movements at (a) Vancouver (49.3°N, 235.9°E), Canada, (b) Washington, D.C. (38.9°N, 282.9°E), United States, (c) Cornwallis Island (82.5°N, 297.7°E), near Northern Greenland, (d) Qaqortoq (60.7°N, 314.0°E), Southern Greenland, (e) Norilsk (69.4°N, 88.4°E), near the West Siberian Plain of Russia, and (f) Selezschita (43.2°N, 77.0°E), near the Tien-Shan Mountain Ranges of Kazakhstan, observed by GPS (upper) and inferred from the GRACE data (lower). Gray dots are monthly values of vertical movement after removing seasonal, linear, and quadratic components. The atmospheric loading contributions are removed from the GPS data using the ECMWF atmospheric model. Blue and red curves are the three month (JFM) averages of the vertical movements measured by GPS and inferred from GRACE, respectively. Green curves show AOI. Error bars in GPS are 1-standard deviation and those in GRACE are one-sigma formal errors inferred *a posteriori* by bringing the chi-square of the post-fit residuals to unity.

~80% of the total amount of mass changes in the NH winters. Hence, AO would excite the polar motion mainly through mass changes in Eurasia. Here we compare (1) the polar motion excitations in the X and Y axes observed by space geodetic techniques, such as the Very-Long-Baseline Interferometry (VLBI), with (2) NH wintertime mass changes inferred from the observed time-variable gravity changes in Eurasia. The polar motion excitations (1) are obtained from the Observatoire de Paris (OP) (<http://hpiers.obspm.fr/eop-pc>) after correcting for geophysical fluid (atmosphere and ocean, both mass and velocity terms) contributions using geophysical models (these corrections are also available from OP). Those from GRACE (2) are calculated by integrating the mass changes over the high and middle latitude regions in Eurasia (25°N to 90°N, 15°W to 165°E) and by converting them to the components ΔC_{21} and ΔS_{21} (i.e. we did not use these coefficients available as the direct outputs of GRACE level-2 data but isolated the Eurasian contribution in these coefficients).

We show the results in Figures 3.8a, b. The observed X and Y excitation (1) showed good agreement with the Eurasian mass changes inferred from GRACE (2), i.e. +0.51 for X and +0.58 for Y . This suggests that the NH wintertime polar motions are largely excited by mass changes there. The polar motion excitation in the X axis from OP (1) and GRACE (2) showed strong positive correlation (+0.57 and +0.63) with AOI while those in the Y axis showed much weaker correlation (+0.21 and +0.24).

This suggests that positive AO moves the excitation pole toward 0°E (negative AO reverses the situation). This may sound strange considering that the center of the Eurasian continent lies in the Y direction. As seen in Figure 3.7a, AO exchanges the terrestrial water mass between middle and high latitude regions in Eurasia in

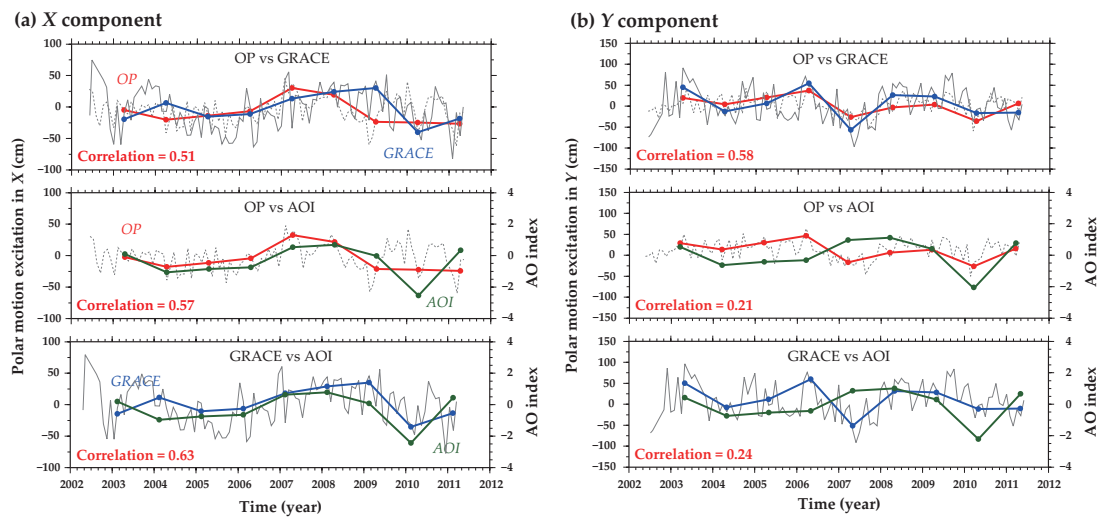


Figure 3.8: Time-series of the polar motion excitation in (a) X ($0^{\circ}E$) and (b) Y direction ($90^{\circ}E$) estimated from the observations of earth rotation parameters from the Observatoire de Paris (OP) and calculated from mass changes over Eurasia from the GRACE gravimetry. The polar motion observations are based on space geodetic techniques such as the Very-Long-Baseline Interferometry (VLBI). The upper, middle and lower panels compare pairs of OP-GRACE, OP-AOI, and GRACE- AOI, respectively. Dashed and solid curves in gray are monthly values of the polar motion excitation from OP (daily values are averaged to monthly values) and GRACE, respectively. Seasonal, linear, and quadratic components of these two time-series are removed using least-squares method. Polar motion excitation data are corrected for the geophysical fluid contributions (atmosphere and ocean) available from OP. Blue and red curves are the three months (JFM) averages of the polar motion excitations and GRACE, respectively. Green curves show those of AOI.

response to its polarity, and their centers of mass lie around ($40^{\circ}N$, $40^{\circ}E$) and ($60^{\circ}N$, $75^{\circ}E$), respectively. If a point mass of ~ 1000 Gt moved from ($40^{\circ}N$, $40^{\circ}E$) to ($60^{\circ}N$, $75^{\circ}E$), the excitation pole would move ~ 101 cm toward X and ~ 36 cm toward Y . The reverse movement would let the excitation pole move back to the original position. Thus, AO excites the polar motion more in the X direction than in Y through the terrestrial water mass redistribution in Eurasia. As a consequence, the polar motion excitation along the X axis is more strongly correlated with AOI.

3.4 Discussion

3.4.1 Contributions of various climatic modes to mass changes in NH winters

There are climatic modes other than AO that may influence continental water mass changes in NH winters. One such mode is the El Niño and Southern Oscillation (ENSO), an episodic change in sea surface temperature in the equatorial eastern Pacific Ocean for a half year or more. An ENSO episode causes climate changes such as precipitation anomaly not only in the equatorial Pacific area, but also in remote areas by teleconnection [e.g. Ropelewski and Halpert, 1987]. Another prominent mode in the NH winter would be the Pacific-North American (PNA) pattern [Wallace and Gutzler, 1981]. PNA is strongly linked to climate variations in the Pacific Ocean and North America and large scale atmospheric circulation across North America. The intensity and polarity of these modes are expressed with the Southern Oscillation Index (SOI) and the Pacific-North American Index (PNAI) for ENSO and PNA, respectively.

Here we compare contributions of AO, ENSO, and PNA, to wintertime EWD in NH by performing the EOF analysis following the method of Quadrelli et al. (2001). EOF analysis, also known as the Principal Component Analysis, enables us to extract principal changing mode in time-series of the dataset and to separate spatial variability (spatial function) from temporal variability (temporal function). EOFs can be derived as eigenvectors of the covariance matrix of the data set. We performed the EOF analysis of wintertime EWD time-series from GRACE for the

entire NH and three specific regions, i.e. Eurasia (25°N-90°N, 15°W-165°E), North America (25°N-75°N, 195°E-300°E), and Greenland (55°N-90°N, 285°E-345°E).

The spatial function of the first leading mode for NH (Figure 3.9a) shows the polarity reversals around 55°N in Eurasia and North America, and around 75°N in Greenland. Contribution of this first mode accounts for ~30% of all modes (Figure 3.9c). Such spatial patterns are in good agreement with those of the correlation coefficients between wintertime EWD and AOI (Figure 3.5). Similarly, the temporal functions are highly correlated (+0.90) with AOI (Figure 3.9b). These results suggest that the first leading mode of GRACE, after removing seasonal, linear and quadratic components, corresponds to the precipitation anomalies by AO. As for other climate modes, the correlations are +0.45 for SOI and -0.56 for PNAI, respectively, which is much smaller than AOI. The ENSO signature could be found as the third mode (the correlation coefficient of -0.68 between wintertime SOI and the temporal function).

Figure 3.10 shows the spatial and temporal functions of the first leading mode of regional GRACE data of Eurasia (a), North America (b), and Greenland (c). The results of Eurasia and Greenland agree well with those of the entire NH, as seen by the high correlation (+0.86 and +0.84, respectively) with AOI. North America, however, seems to behave somewhat differently from them; terrestrial water storage there is more influenced by ENSO (correlation: +0.80) than AO (correlation: +0.53). The spatial function also resembles to the precipitation anomaly pattern of ENSO [e.g. Ropelewski and Halpert, 1987]. After all, AO is the largest contributor to the wintertime terrestrial water storages of the entire NH, but ENSO also plays a dominant role regionally in North America.

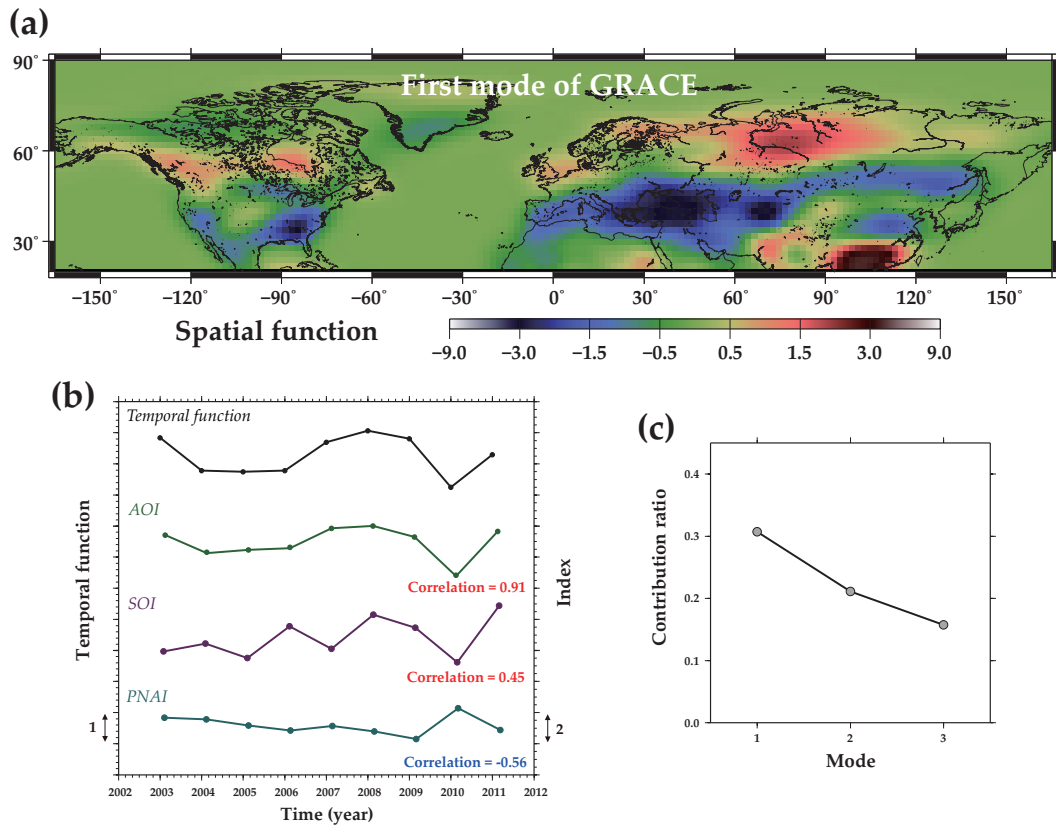
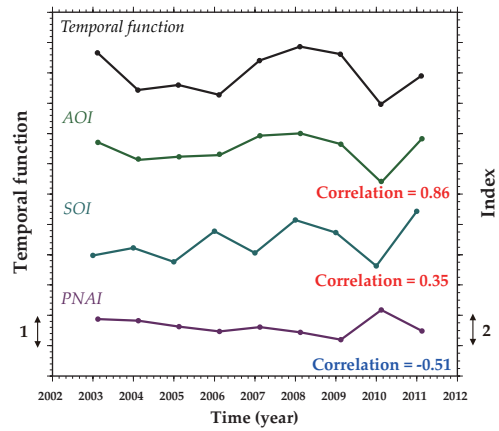
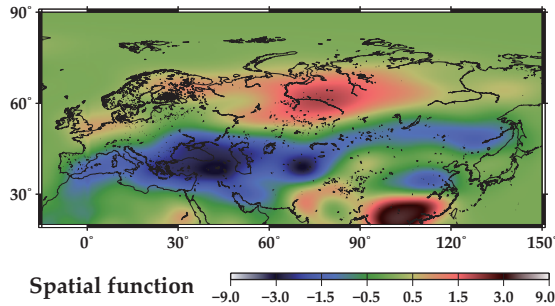
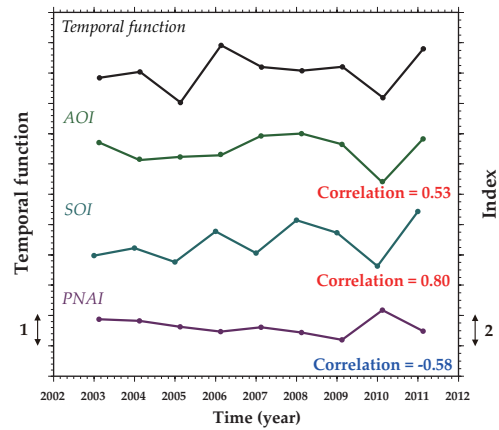
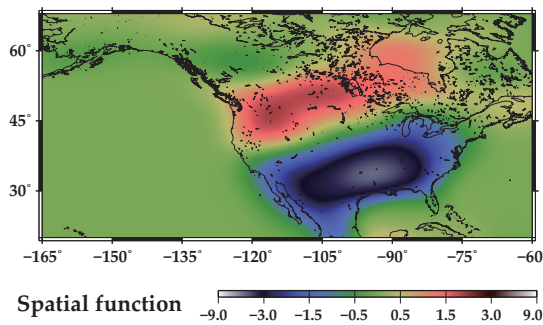


Figure 3.9: (a) Spatial and (b) temporal functions of the first leading mode derived by the EOF analysis of wintertime mass changes from GRACE after removal of seasonal, linear and quadratic components. Weight factor of the cosine of latitude was applied for the GRACE data. Black, green, purple, and light blue curves are the three month (JFM) averages of the time functions, AOI, SOI, and PNAI, respectively. SOI is obtained from <http://www.cpc.ncep.noaa.gov/data/indices/soi>, and PNAI is obtained from http://www.cpc.ncep.noaa.gov/products/precip/CWlink/pna/pna_index.html. Strong positive correlation can be found between the time functions and AOI. (c) Contributions of the largest 3 modes. The first mode contributes by ~30%.

(a) Eurasia (20N-90N, -15E-165E)



(b) North America (20N-75N, 195E-300E)



(c) Greenland (57N-90N, 285E-345E)

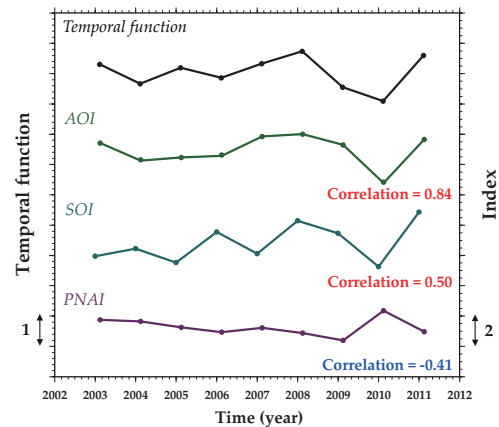
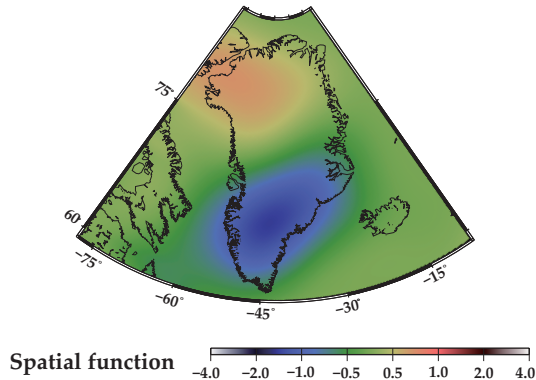


Figure 3.10: Spatial (left) and temporal (right) functions of the first leading mode derived by the EOF analysis of wintertime mass deviations from GRACE for the three regions, namely (a) Eurasia, (b) North America, and (c) Greenland. Black, green, purple, and light blue curves are the three month (JFM) averages of the indices AOI, SOI, and PNAI, respectively. Contribution of the first mode was 39% for Eurasia, 47% for America, and 44% for Greenland. Time functions in Eurasia and Greenland show high correlations with AOI while that in North America resembles more to SOI.

3.4.2 Influence of temperature anomaly by AO to terrestrial water storage

AO influences surface air temperature (SAT) over NH. Positive AO tends to increase/decrease SAT north/south of $\sim 45^\circ\text{N}$ in Eurasia, decrease/increase SAT north/south of $\sim 45^\circ\text{N}$ in North America, and decrease SAT in Greenland [Thompson and Wallace, 1998]. Negative AO reverses the situation. In the 2010 winter, a year of the record-breaking strong negative AO, SAT anomaly attains up to $\sim 2.5^\circ\text{C}$ in each continent [Cohen et al., 2010]. Such anomalous SAT would influence terrestrial water storage through evaporation, snow melting, and runoff (Increase/decrease of SAT enhances/reduces them).

The balance between precipitation-driven mass change and temperature-driven mass changes (evapo-transpiration, snow melting, and runoff) can be evaluated through the framework of GLDAS model. GLDAS suggests that total water budget has much more similar distribution in space and sense to precipitation than evapo-transpiration, snow melting, and runoff. Of course, temperature anomaly by AO must contribute to the changes in terrestrial water storage. However, in this case, temperature appears to play a lesser role in terrestrial water storage than precipitation.

3.4.3 On detrending of GRACE mass-variation time-series to isolate AO signature

It is known that GIA changes the Earth's gravity field secularly in long time span. Recent climate changes bring about inter-annual or multi-decadal variation in precipitation over the Earth or mass balance of the Earth's ice reservoirs. As de-

scribed in Section 3.4, we removed linear and quadratic components from GRACE mass-variation time-series to correct such mass changes. However, there is a possibility that this process could also remove AO-derived signature from GRACE.

In order to investigate this possibility, we performed EOF analysis for the time-series of non-detrended GRACE mass-variation in NH. Figures 3.11, 3.12 and 3.13 are the first mode, the second mode and the third mode, respectively. The temporal function of the first mode (Figure 3.11c) can be explained by linear trend. In fact, the spatial function (Figure 3.11a) shows very good agreement with the linear component of GRACE mass-variation time-series (Figure 3.11b). The temporal function of the second mode (Figure 3.12c) represents a function which is close to quadratic curve. The spatial function (Figure 3.12a) is quite similar to the quadratic component of GRACE mass-variation time-series (Figure 3.12b). Looking at the third mode (Figure 3.13), we can notice that the spatial function looks very similar to the correlation distribution between wintertime water thickness deviation and AOI (Figure 3.5). This third mode is also in accordance with the first mode of EOF analysis for detrended GRACE mass-variation time-series (Figure 3.9). Therefore, it can be said that detrending using regression functions with the linear and quadratic components adequately correct principal mass changes other than AO from GRACE data.

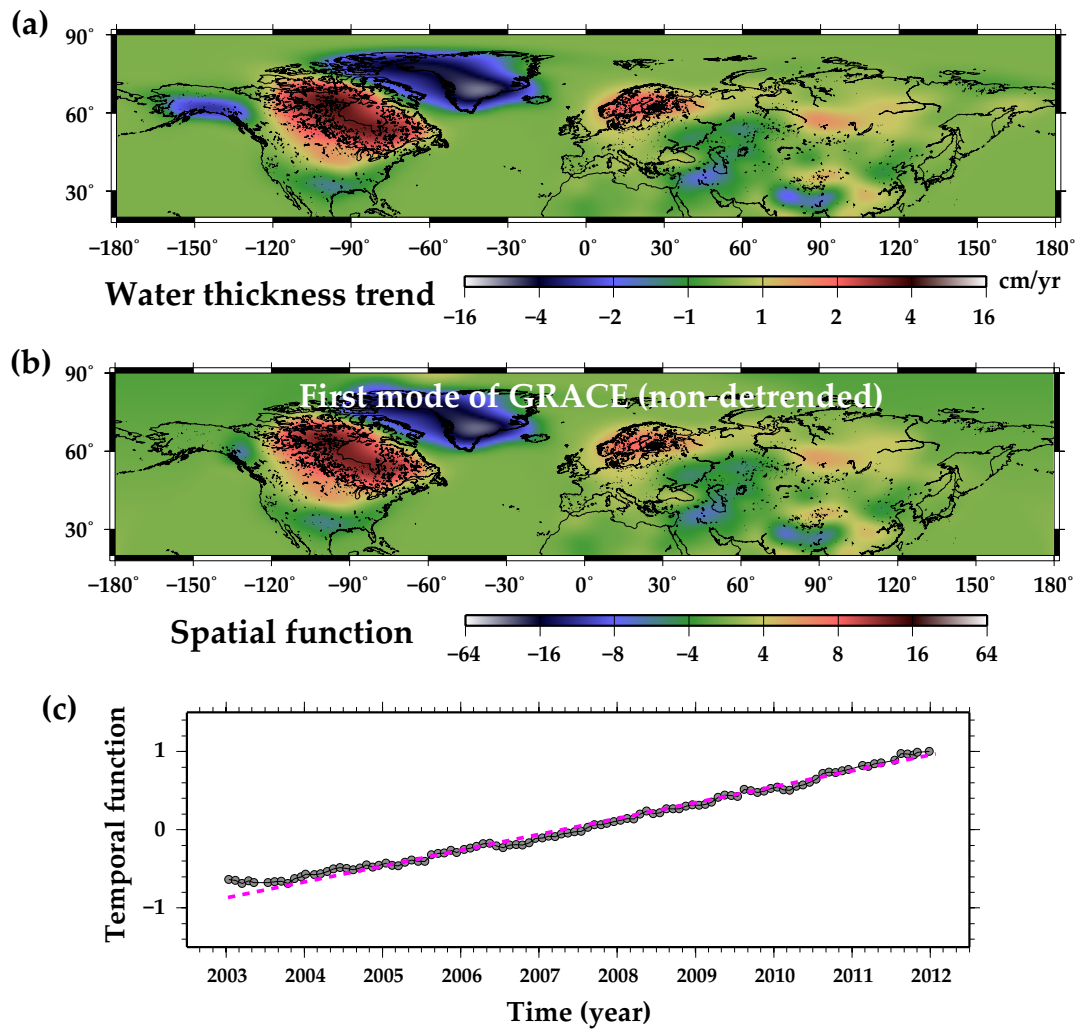


Figure 3.11: (a) Linear mass trend map in NH obtained by least-squares method. (b) (c) Spatial and temporal functions of the first leading mode derived by the EOF analysis of non-detrended mass changes from GRACE in NH. Contribution of the first mode was 84%.

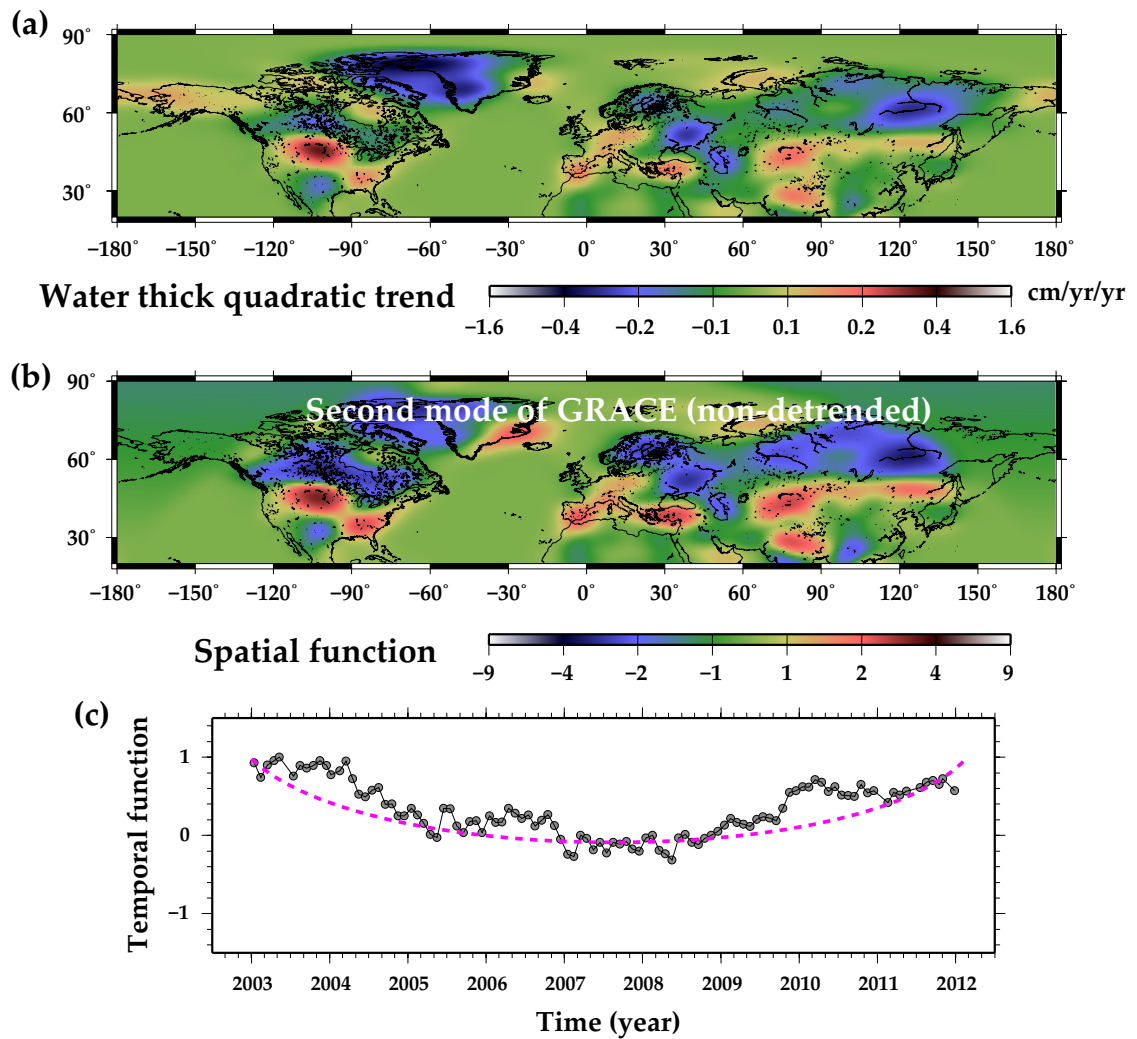


Figure 3.12: (a) Quadratic mass trend map in NH obtained by least-squares method. (b) (c) Spatial and temporal functions of the second mode derived by the EOF analysis of non-detrended mass changes from GRACE in NH. Contribution of the second mode was 7%.

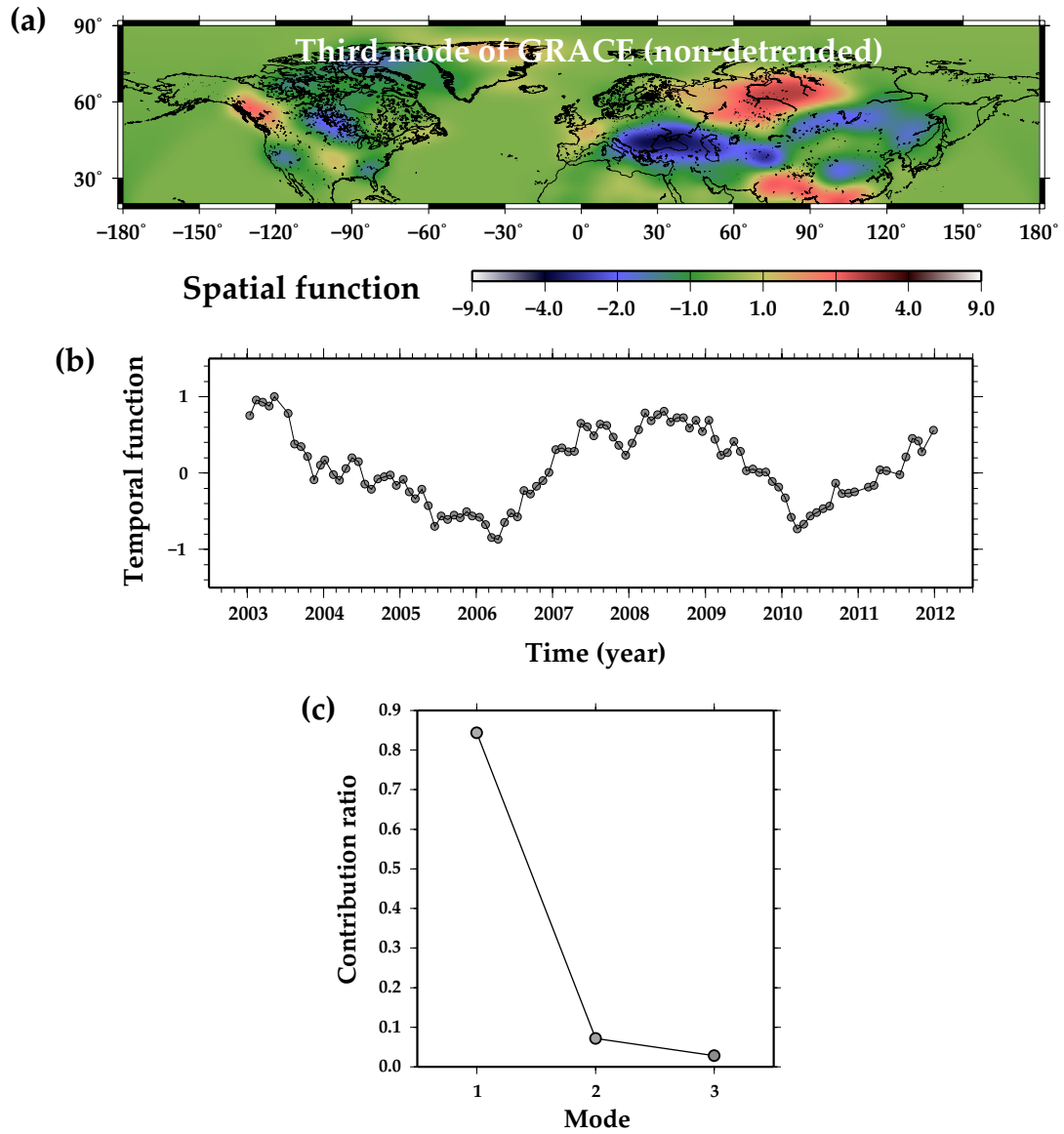


Figure 3.13: (a) (b) Spatial and temporal functions of the second mode derived by the EOF analysis of non-detrended mass changes from GRACE in NH. Contribution of the second mode was 3%. (c) Contributions of the largest 3 modes.

3.5 Conclusion

We have analyzed 9 years of time-variable gravity data by the GRACE satellites, and the GLDAS land hydrological models to investigate signatures of precipitation anomalies in NH winters caused by AO. Our study is summarized as follows.

- (1) Positive and negative AO are considered to enhance wintertime precipitations in the high and middle latitude regions in NH, respectively, and such mass redistributions can be seen in the GRACE data.
- (2) The distribution of the correlation coefficients between precipitation anomalies and AOI shows characteristic patterns; i.e. boundary of the positive and negative correlations lie along the latitude of $\sim 55^\circ\text{N}$ in Eurasia and North America, and along $\sim 75^\circ\text{N}$ in Greenland.
- (3) AO moves the center of precipitation depending on its polarity. AO could move mass as large as ~ 1000 Gt over the distance of ~ 2000 km like a seesaw between these two regions in response to its polarity.
- (4) The mass movements by AO are also observed as the surface deformation using GPS. The surface deformation shows similar correlation pattern with AOI to the GRACE data.
- (5) The mass movements by AO excite the Earth's polar motion above the detection level of space geodetic techniques, such as VLBI. The excitation pole was found to move mainly along the X axis

-
- (6) EOF analyses showed that the AO signature is the leading mode of the GRACE gravity data after removing seasonal, linear and quadratic components.
 - (7) Other climatic modes, ENSO and PNA, also influence wintertime terrestrial water storages, but their contributions to the whole NH are smaller than AO.

This study is the first attempt to explore the AO-driven mass redistribution signatures in the time-variable gravity field observed by GRACE. The implication of this research is threefold. At first, GRACE is a new tool, and we need to know how a known climatological phenomenon appear in GRACE data in order to identify unknown signals (such as co- and postseismic gravity changes). Secondly, GRACE is the only tool to directly measure global-scale mass redistributions. It would enable us to study mass balances in polar and high mountain regions where *in situ* observations are limited or unavailable. In fact, this study revealed characteristic links between AO and mass changes in Greenland and northwestern Asian High Mountains. As the third point, GRACE enables us to see precipitation anomalies through a filter of terrestrial water storage. Precipitation anomaly and the water storage anomaly are not equivalent; the latter reflects not only precipitation but also factors such as water storage capacity, run-off time constants, land-ocean distribution, etc. Scrutiny of their differences will enable us to further understand the link between changes in climate and water resources.

Chapter 4

Current ice loss in small glacier systems of the Arctic Islands (Iceland, Svalbard, and the Russian High Arctic) from satellite gravimetry

Paper was accepted in *Terrestrial, Atmospheric and Oceanic Sciences*

Matsuo, K. and K. Heki, 2013: Current ice loss in small glacier systems of the Arctic Islands (Iceland, Svalbard, and the Russian High Arctic) from satellite gravimetry, *in press*.

4.1 Introduction

Over 80% of the islands in the Arctic region (Arctic Islands) are covered with water ice (i.e. ice sheet, glacier, and ice cap), and form the largest store of water ice in the Northern Hemisphere (NH). The Arctic Islands consist of Greenland, the Canadian Arctic Archipelago, Iceland, Svalbard and the Russian High Arctic (Novaya Zemlya, Severnaya Zemlya, and Franz Josef Land). The total ice covered area in these islands is $\sim 2,000,000 \text{ km}^2$, in which the Greenland ice sheet is the largest ($\sim 1,750,000 \text{ km}^2$). About a half of the glaciers and ice caps are located in the Canadian Arctic Archipelago ($\sim 150,000 \text{ km}^2$). One quarter is found around the Greenland ice sheet ($\sim 76,000 \text{ km}^2$), and the other quarter is located in Iceland, Svalbard, and the Russian High Arctic ($\sim 100,000 \text{ km}^2$) [Dyrgerov and Meier, 2005]. The geographical location of these glacier systems are shown in Figure 4.1.

In recent years, rapid shrinking of polar ice sheets and mountain glaciers due to global warming has been reported in various regions of the world. The satellite system GRACE, launched in 2002, enables direct measurements of such mass losses. GRACE consists of two satellites. Since its launch in 2002, GRACE observations have revealed the losses of ice sheets in Antarctica and Greenland [e.g. Velicogna, 2009; Susgen, et al., 2012], and of mountain glaciers in Alaska [e.g. Luthcke et al., 2008], Patagonia [e.g. Chen et al., 2007], the Asian High Mountain Ranges [Matsuo and Heki, 2010], the Canadian Arctic Archipelago [Gardner et al., 2011], and so on. Recently, Jacob et al. (2012) has estimated the ice loss rates of all of these glaciers and polar ice sheets using the GRACE data between January 2003 and December 2010 to be $536 \pm 93 \text{ Gt/yr}$.

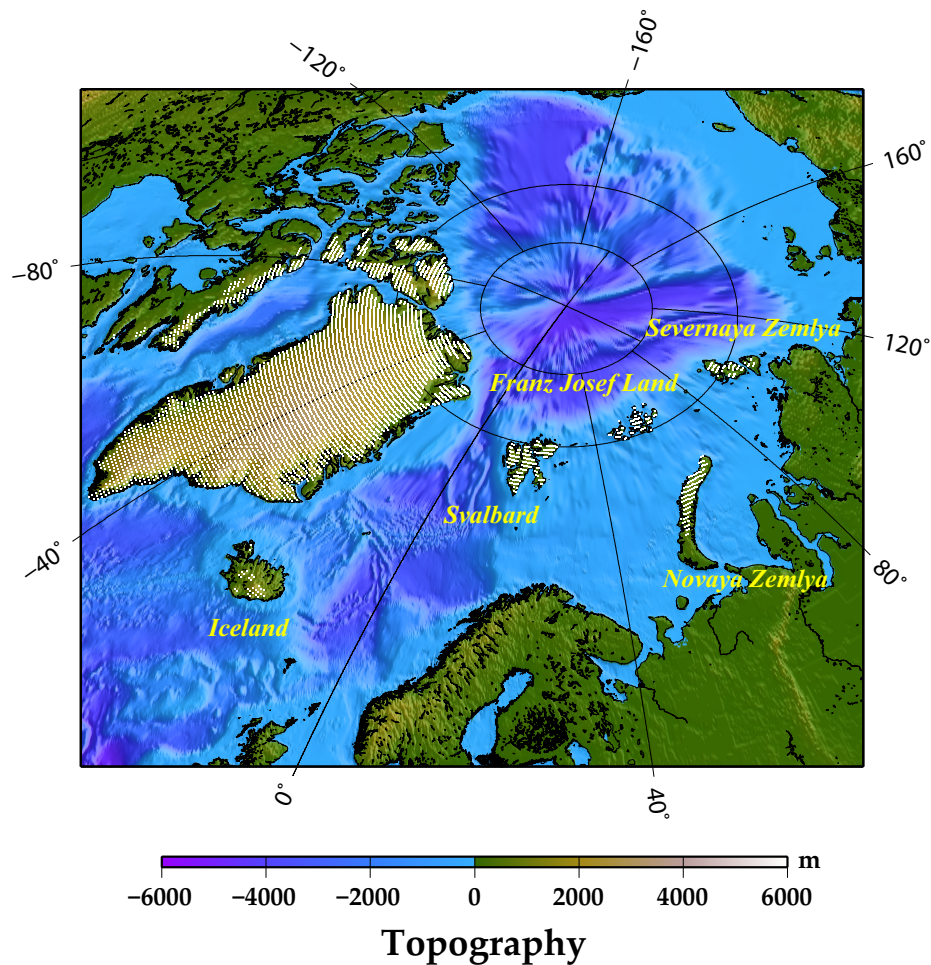


Figure 4.1: Geographical locations of the small glacier systems of Arctic Islands. White dots represent ice covered areas. The topographic and bathymetric data are from ETOPO1 global relief model [Amante, and Eakins, 2009].

Owing to the increasing time span covered by the GRACE data, we are able to discuss inter-annual variability of such ice losses [e.g. Chen et al., 2009; Matsuo and Heki, 2010, Gardner et al., 2011]. The increasing time span also enables us to investigate slight mass fluctuations of relatively small glacier systems that have been difficult to discuss because of low signal-to-noise ratio. In this paper, we investigate current ice loss and its temporal variability in the three small glacier systems of the Arctic Islands, i.e. Iceland, Svalbard, and the Russian High Arctic, using the

GRACE data. To enable precise assessments of their quantities, spatial localizations, and temporal variability, we employ the point-mass modeling approach by Baur and Sneeuw (2011), which is useful to discuss mass changes in small areas.

4.2 GRACE observation

4.2.1 GRACE Data processing

The GRACE inter-satellite ranging data are processed by several data analysis centers. Because the methods for data processing vary by each institute, we can see slight differences in the gravity data from these centers. To alleviate such a problem, we stacked the GRACE data provided by three centers, the University of Texas Center for Space Research (UTCSR), the Jet Propulsion Laboratory (JPL), USA, and the GeoForschungsZentrum Potsdam (GFZ), Germany. Here we used the Level-2 Release 05 GRACE data consisting of 94 monthly data sets from February 2004 to January 2012. The Earth's gravity field is modeled as a combination of spherical harmonics. A monthly GRACE data set includes a set of the coefficients of spherical harmonics (Stokes' coefficient) C_{nm} and S_{nm} with degree n and order m complete to 60. We used the degree-one components (C_{10} , C_{11} , and S_{11}), which reflect the geocenter motion, estimated by combining GRACE and ocean model [Swenson et al., 2008] because GRACE alone cannot measure them. In order to interpret gravity changes in terms of surface mass variations, we need to calculate equivalent σ water thickness (EWT) using the relationship [Wahr et al., 1998]. We assumed that the GRACE gravity changes reflect those of the surface load, and converted them into EWT. Chao (2005) showed that the inverse solution is unique in this case.

Because the GRACE data suffer from correlated errors and short-wavelength noises, spatial filtering is indispensable. Without spatial filtering, strong north-south stripes remain in the data due to correlated errors [Swenson and Wahr, 2006]. Such north-south stripes, however, diminish as the latitude becomes higher, because GRACE operates in the polar orbits and the spatial density of the GRACE measurements increase toward higher latitudes. Hence, GRACE achieves higher precision in the polar region including the Arctic Islands. In fact, we can recognize geophysical signatures there, such as GIA and mass losses in ice sheets and mountain glaciers, even in the GRACE data without any spatial filtering.

Here we apply only “ weak ” spatial filters, i.e. the anisotropic fan filter with averaging radius of 150 km to reduce short wavelength noises [Zhang et al., 2009] and the de-correlation filter using polynomials of degree 3 for coefficients with orders 14 or higher to reduce longitudinal stripes [Swenson and Wahr, 2006]. The choice for the De-correlation filter is important because signals of glacial mass changes could be weakened or moved away from the actual location depending on the combination of polynomial fitting or applied order of coefficients. Here we set up the optimal filter by trial-and-error based on visual inspection.

In addition, we should remove the effects of ongoing GIA in North America, Scandinavia, and their vicinity from the GRACE data. Gravity increases associated with GIA would partly cancel the gravity decreases by ice losses, causing the underestimation of the actual mass losses. We corrected for such contributions using the model of Peltier (2004). The uncertainty of GIA correction will be discussed in Section 4.4.1.

4.2.2 Ice loss in small glacier systems of the Arctic Islands from GRACE

Following the methods described in the previous section, we plotted the time-series of EWT at five points in small glacier systems of the Arctic Islands, i.e. Iceland (64°N, 16°W), Svalbard (78°N, 22°E), Novaya Zemlya (75°N, 59°E), Franz Josef Land (80°N, 60°E), and Severnaya Zemlya (79°N, 98°E), in Figure 4.2c. The obtained time-series were modeled with linear, quadratic and seasonal changes by least-squares adjustment. In the adjustments, the GRACE system errors σ_{err} were used as the weights. The observed EWT time-series all showed negative trends (red line), suggesting that ice losses do occur there. Their EWT linear trends are -4.0 ± 0.3 cm/yr in Iceland, -1.4 ± 0.4 cm/yr in Svalbard, -2.3 ± 0.4 cm/yr in Novaya Zemlya, -0.8 ± 0.3 cm/yr in Franz Josef Land, and -0.8 ± 0.3 cm/yr in Severnaya Zemlya. The errors are one-sigma uncertainties of the linear terms.

It is notable that the time-series of EWT in Svalbard, Novaya Zemlya and Franz Josef Land, show significant temporal variability. They decrease before 2008 and increase around 2009-2010. The linear trends before 2008 (green lines in Figure 4.2c) are often larger in some regions, i.e. -3.6 ± 0.7 cm/yr for Iceland, -2.4 ± 1.1 cm/yr for Svalbard, -4.3 ± 1.4 cm/yr for Novaya Zemlya, -1.7 ± 0.9 cm/yr for Franz Josef Land, and $+0.2 \pm 0.9$ cm/yr for Severnaya Zemlya. We map such linear trends in EWT from February 2004 to January 2012 (hereafter 2004.02-2012.01) and February 2004 to January 2008 (hereafter 2004.02-2008.01) in Figures 4.2a and 4.2b, respectively. We can see stronger negative trends in the three glaciers, i.e. Svalbard, Novaya Zemlya and Franz Josef Land, for the period 2004.02-2008.01 in comparison

with 2004.02-2012.01. Origin of such temporal variability will be discussed in the next chapter and Section 4.4.2.

4.3 Estimation of ice loss

4.3.1 Method for estimation

Based on the linear trend maps obtained in the previous section, we estimated the total ice loss rates of the individual glacier systems of the Arctic Islands. Here we employed the technique of point-mass modeling [Baur and Sneeuw, 2011], a method suitable to derive mass changes at particular surface points from time-variable gravity fields from GRACE. The basic idea behind this method is to solve an inverse problem from the observed gravity changes to the actual mass variations by least-squares adjustment assuming that the mass variation occurs in these specific locations. The gravitational force acting on orbiting satellite from mass variation is determined by Newton's law of universal gravitation. So, the changes in distributed point-mass on the Earth's surface can be inverted from the Green's function expressed in the Newton's equation and the gravity changes observed by GRACE. In this method, Tikhonov-regularized least-squares method is employed to stabilize the inverse problem [Tikhonov, 1963; Koch 1999].

Here we assumed that mass changes occur only on ice covered areas (white dots in Figure 4.1), and performed point-mass modeling using the linear trend maps of the EWT from GRACE. By distributing the point-mass only on ice covered areas, we can somewhat reduce the signal leakage from outside (e.g. non-ice covered area like oceanic area). The optimum regularization parameters, expressed as λ in eq.

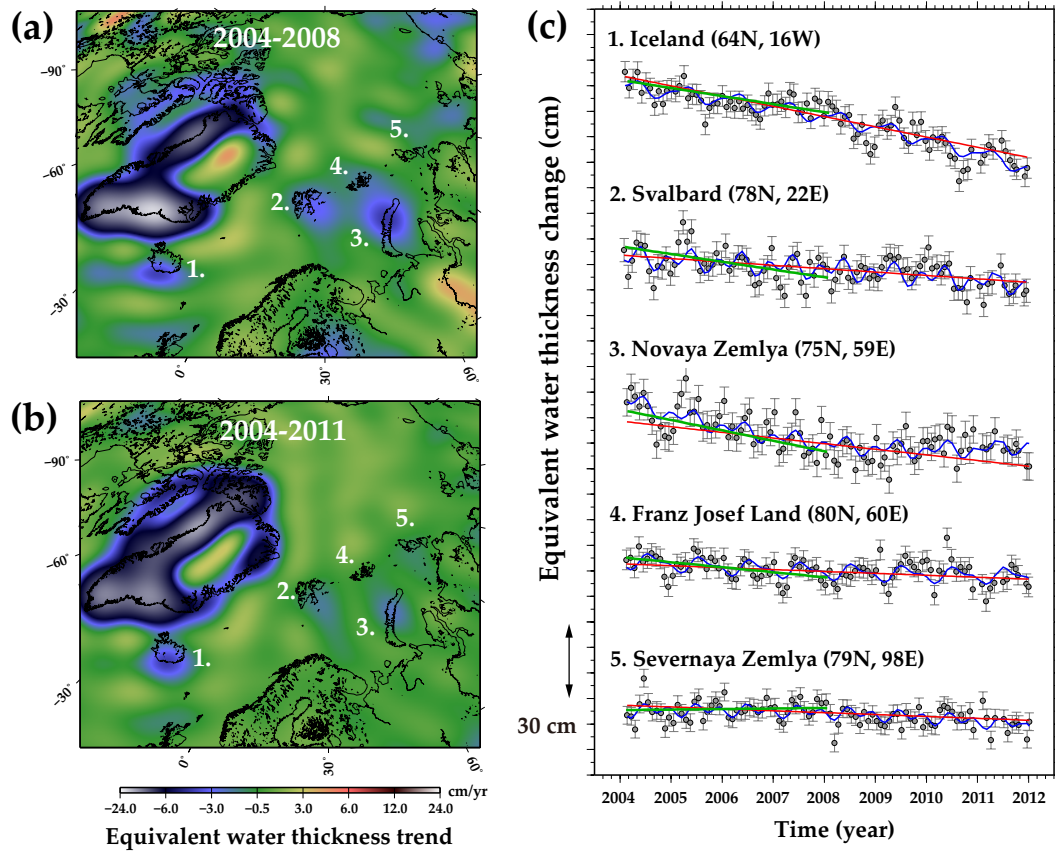


Figure 4.2: (a) Map of the linear trends of the GRACE EWT in NH during 2004.02-2012.01. (b) That during 2004.02-2008.01. (c) Time-series of the GRACE EWT at points in 1. Iceland (64°N , 16°W), 2. Svalbard (78°N , 22°E), 3. Novaya Zemlya (75°N , 59°E), 4. Franz Josef Land (80°N , 60°E), and 5. Severnaya Zemlya (79°N , 98°E). The smooth curves with blue color indicate best-fit models by least-squares method assuming linear, quadratic and seasonal changes. The red and green lines show the linear components during 2004.02-2012.01 and 2004.02-2008.01. The errors bars are the GRACE standard errors expressed in EWT.

(10) of Baur and Sneeuw (2011), were inferred by grid-search to match the GRACE data best.

4.3.2 Iceland

Figure 4.3 shows the results for Iceland. Iceland is so close to Greenland in terms of GRACE resolution that the observed mass changes around Iceland would include the ice loss signals from Greenland. To alleviate this problem, we performed joint inversion of mass changes in Iceland together with those in Greenland. The synthesized ice loss rates by point-mass modeling around Iceland suggest that ice loss mainly occurs in the southeastern glaciers, corresponding to the Vatnajokull Ice Cap, the largest glacial reservoir in Iceland. The majority of glaciers in Iceland are located in the southeast Iceland where precipitations are high under the strong influence of the polar easterly. The total ice covered area in Iceland is $\sim 10,900 \text{ km}^2$, $\sim 80\%$ of which is within Vatnajokull [Dyurgerov and Meier, 2005].

We integrated the synthesized ice loss rates at grid points in Iceland (Figure 4.3b), and obtained the total ice loss rates as $10.9 \pm 2.1 \text{ Gt/yr}$ for the period 2004.02-2012.01 and $10.6 \pm 3.4 \text{ Gt/yr}$ for the period 2004.02-2008.01. The errors were estimated by combining one-sigma errors in the linear regression, uncertainties in the GIA models, and changes in the land hydrology. The detail of error estimation will be described in the Section 4.4.1. The residuals between the observed and the synthesized mass changes (Figures 4.3d, h) are well below the estimated error level. It appears that the glaciers in Iceland are significantly and constantly melting during the studied period. Our estimates agree well with the previous estimates [Wouters et al., 2008; Jacob et al., 2012].

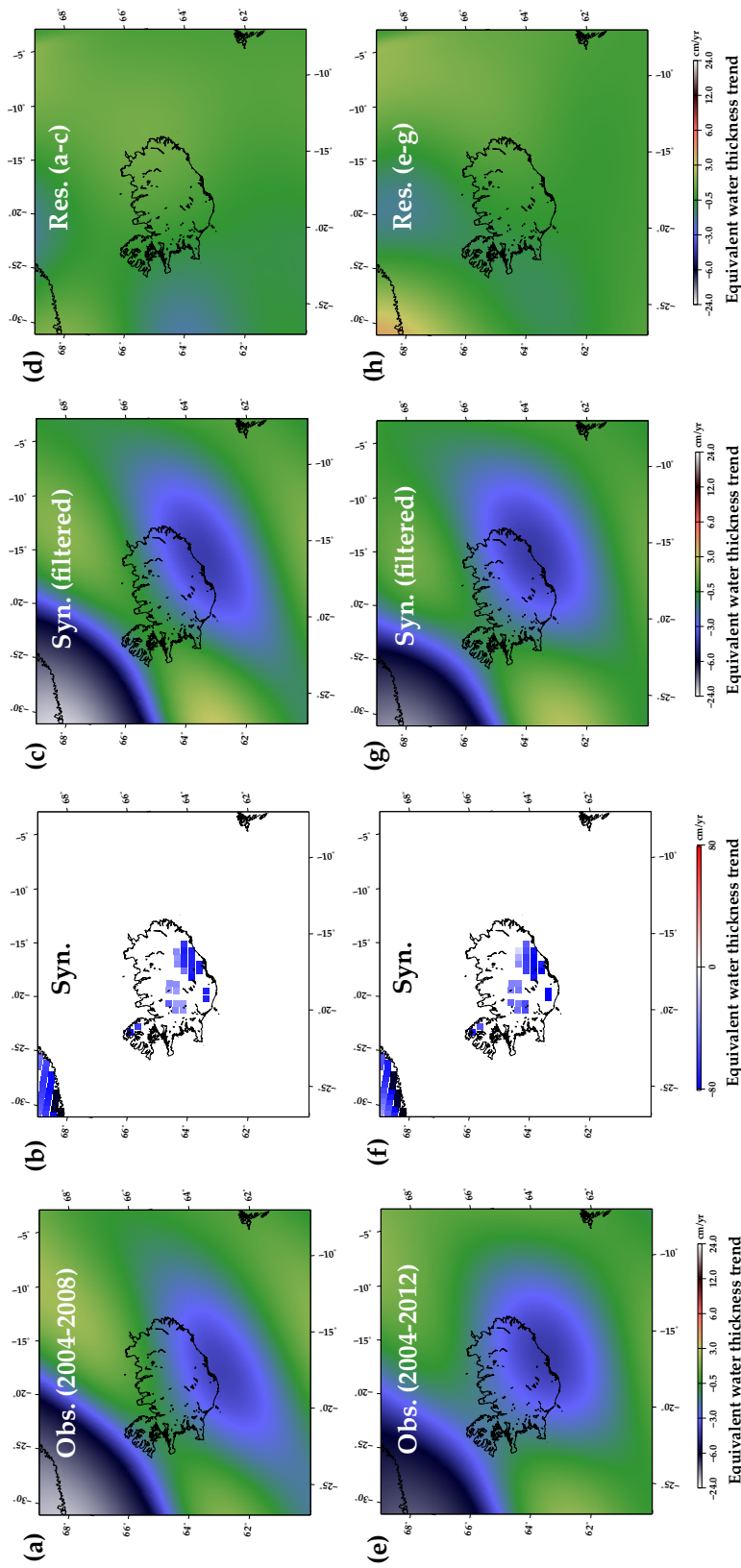


Figure 4.3: Distributions of the EWT linear trends in Iceland. (a)-(d) are for the period 2004.02-2012.01 and (e)-(h) are for the period 2004.02-2012.01. (a) and (e) are the linear trend observed by GRACE, (b) and (f) are synthesized linear trend obtained by point-mass modeling, (c) and (g) are synthesized linear trend after applying the same filter as GRACE, and (d) and (h) are the residual between the observed (a,e) and the synthesized (c,g), respectively.

4.3.3 Svalbard

Figure 4.4 shows the results for Svalbard. The ice covered area of $\sim 21,800 \text{ km}^2$ is located in its main island Spitsbergen, $\sim 11,300 \text{ km}^2$ in the northwestern island Nordaustlandet, $\sim 2,130 \text{ km}^2$ in the southern island Edgeoya, and $\sim 1,400 \text{ km}^2$ in other small islands. The total ice covered area is $\sim 36,600 \text{ km}^2$ [Dyurgerov and Meier, 2005]. These glaciers are fed by precipitation from the polar easterly and retain a bulk of water ice in southeastern Svalbard. The ice loss estimated using GRACE suggests that ice loss mainly occurs in the glaciers of Edgeoya and southeastern Spitsbergen. It is notable that the ice loss rate significantly varies in time. The obtained ice loss rate is $3.6 \pm 2.9 \text{ Gt/yr}$ for the period 2004.02-2012.01 and $6.9 \pm 3.6 \text{ Gt/yr}$ for the period 2004.02-2008.01.

Past GRACE studies in this region suggested the rate as $8.8 \pm 3 \text{ Gt/yr}$ [Wouters et al., 2008], $9.1 \pm 1.1 \text{ Gt/yr}$ [Mémmin et al., 2011], and $3 \pm 2 \text{ Gt/yr}$ [Jacob et al., 2012]. The latest estimate by Jacob et al. (2012) is considerably smaller than the two earlier estimates. This difference would reflect the inclusion of the GRACE data after 2009, i.e. Jacob et al. (2012) included the data up to 2010.12 while Wouters et al. (2008) and Mémmin et al. (2011) used those up to 2008.01 and 2009.01, respectively. As described before, Svalbard shows significant mass increase around the 2009/2010 winter. We speculate that such mass increase is due to the strong negative phase of the Arctic Oscillation (AO) occurred in the 2009/2010 winter.

Unprecedentedly strong negative AO occurred in that winter brought unusual coldness and heavy precipitation in various regions of NH [e.g. Cohen et al., 2010; Seager et al., 2010]. AO is a seesaw like fluctuation in the sea-level pressure between

polar and middle latitude regions of NH, and its index characterizes the dominant pattern of atmospheric circulation in NH [Thompson and Wallace, 1998]. Here we regard that AO is synonymous with the North Atlantic Oscillation [Walker and Bliss, 1932].

The GRACE observations suggested that the extreme negative AO in the 2009/2010 winter enhanced the precipitations in middle latitude regions of Eurasia, southeastern US, and southern Greenland [Chapter 3; Matsuo and Heki, 2012]. The polarity of AO largely controls wintertime mass balance in Svalbard. Field studies of mass balance showed larger decrease during the period 1990-1996, when positive AO prevailed, than in the period 1997-2004 [Rasmussen and Kohler, 2007]. This tendency is consistent with the case in the 2009/2010 winter, a case opposite to 1990-1996. The detail discussion on the relationship between the wintertime AO and mass balance in each glacier system will be described in the Section 4.4.2.

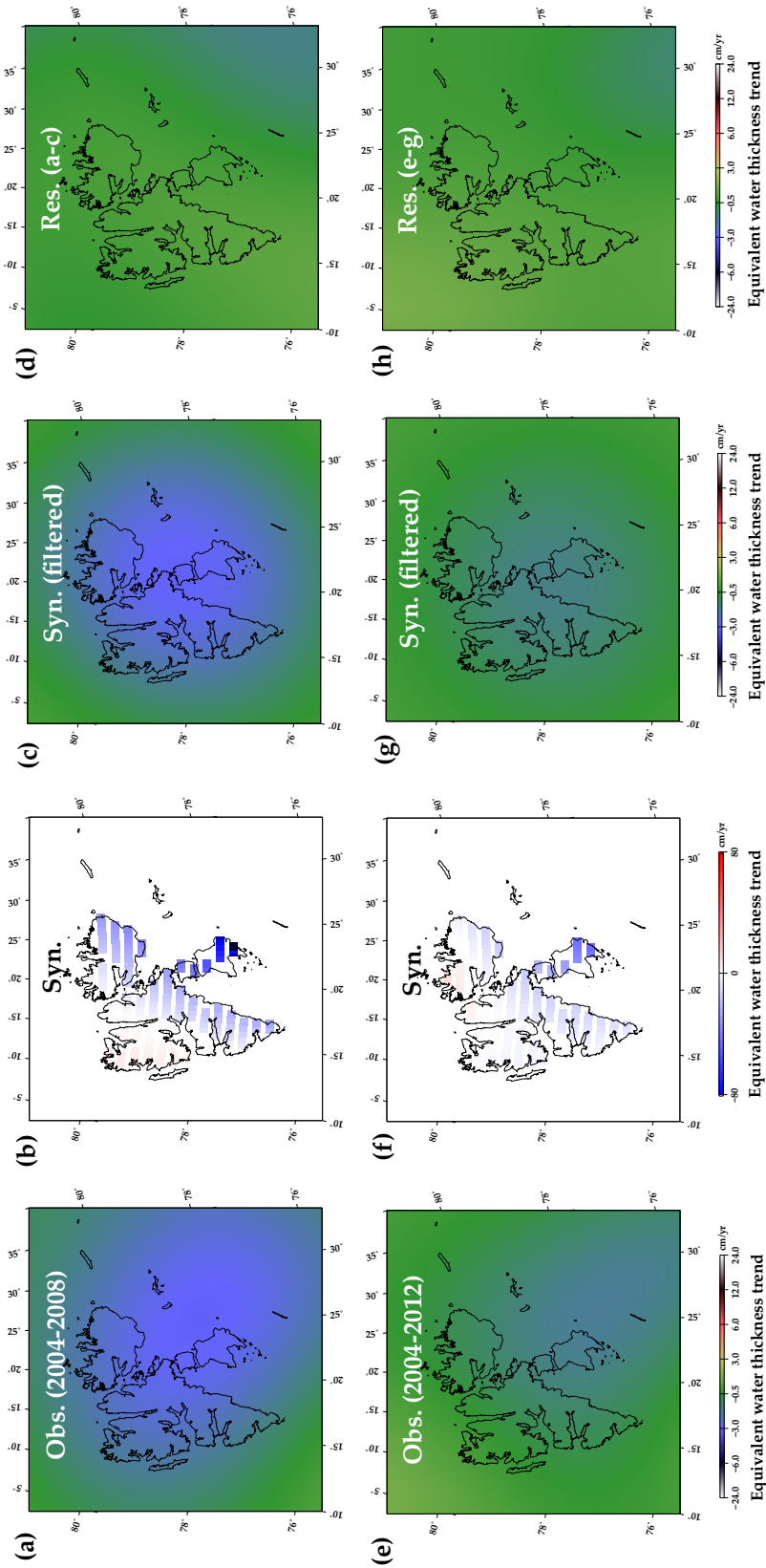


Figure 4.4: Distributions of the EWT linear trend in Svalbard. See Figure 4.3 for detail.

4.3.4 Russian High Arctic

Figure 4.4 shows the results for the Russian High Arctic, where ice covers area of $\sim 23,600 \text{ km}^2$ in the Novaya Zemlya, $\sim 13,500 \text{ km}^2$ in the Franz Josef Land, and $\sim 18,300 \text{ km}^2$ in the Severnaya Zemlya. The total ice covered area amounts to $\sim 55,400 \text{ km}^2$ [Dyrgerov and Meier, 2005]. We jointly inverted mass changes in these three glacier systems to reduce the signal leakages from neighboring glacier systems. The synthesized result for the Novaya Zemlya suggests that the observed mass trend there can be well explained by the ice loss in the northern glaciers. The obtained ice loss rate there is $5.2 \pm 3.9 \text{ Gt/yr}$ for the period 2004.02-2012.01 and $11.2 \pm 5.5 \text{ Gt/yr}$ for the period 2004.02-2012.01, i.e. a significant difference exists between the periods. From the time-series of EWT shown in Fig. 4.2c, we can see the large positive EWT deviation in the 2009/2010 winter. This is coincident with the occurrence of the strongest negative AO during the studied period. Like in Svalbard, the mass balance there seems to have some relationship with AO.

The obtained ice loss rate in the Franz Josef Land is $0.8 \pm 1.3 \text{ Gt/yr}$ for the period 2004.02-2012.01 and $3.5 \pm 1.9 \text{ Gt/yr}$ for the period 2004.02-2008.01. This glacier system also shows gravity decrease (mass loss) with a time-variable rate. However, the rate is relatively small and it might be difficult to discriminate the fluctuation signature from the leakage of the mass changes in the Novaya Zemlya. Further accumulation of the GRACE data would be necessary to investigate temporal variability of mass balance there.

The obtained ice loss rate in the Severnaya Zemlya is $0.9 \pm 2.2 \text{ Gt/yr}$ for the period 2004.02-2012.01 and $0.8 \pm 1.3 \text{ Gt/yr}$ for the period 2004.02-2008.01. The

variability in trend is relatively small. Glaciers in the Severnaya Zemlya might be in a relatively stable state because this region is less influenced by low atmospheric pressure from the Barents Sea and has relatively small catchment and ablation of the glaciers [Koryakin, 1986].

Finally, we got the total ice loss rate in the Russian High Arctic as 6.9 ± 7.4 Gt/yr for the period 2004.02-2012.01 and 15.4 ± 11.9 Gt/yr for the period 2004.02-2008.01. Moholdt et al. (2012) recently estimated regional mass budget of these glacier systems using ICESat laser altimetry, and reported the total ice loss rate of 9.8 ± 1.9 Gt/yr for the period 2004.01-2009.10. Their estimate is consistent with the average of our estimates over the two periods 2004.02-2012.01 and 2004.02-2008.01.

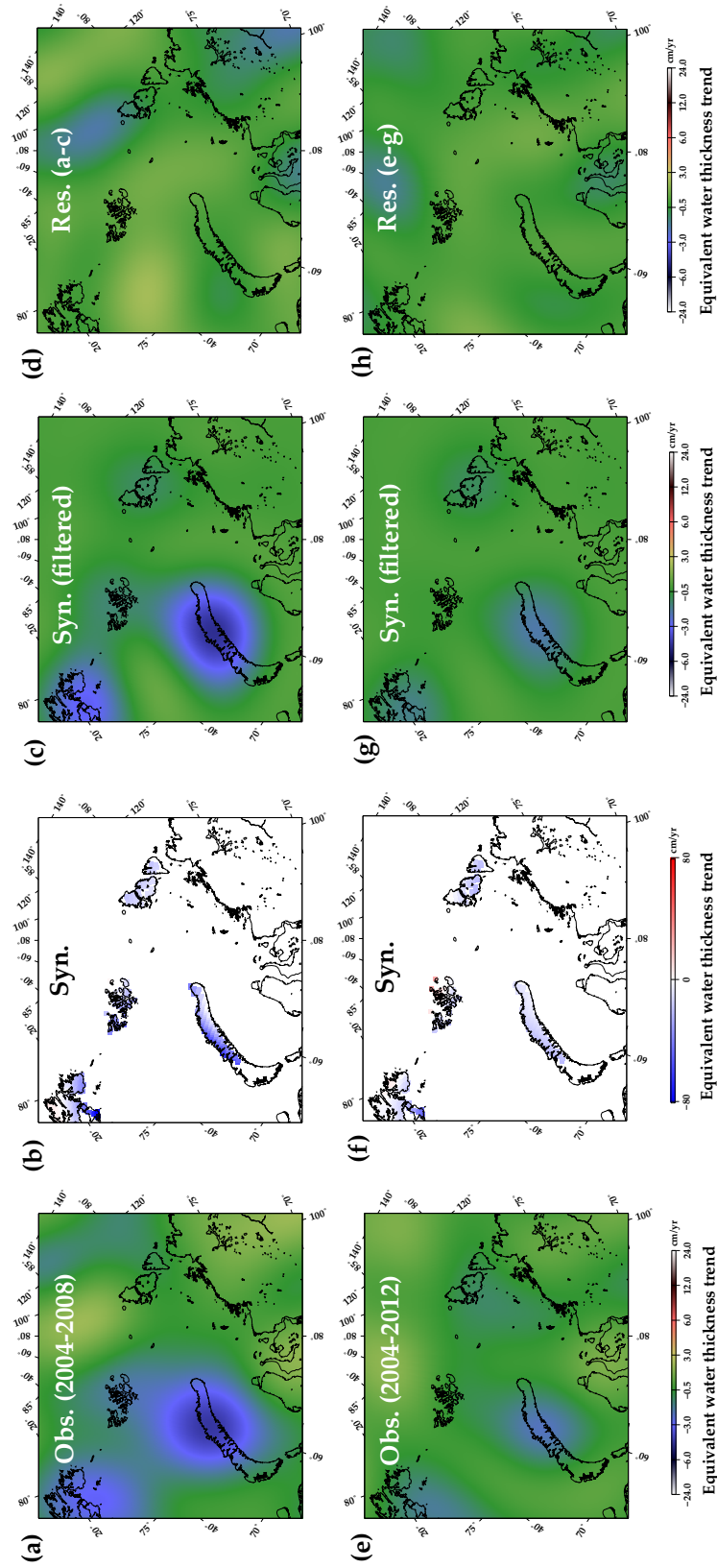


Figure 4.5: Distributions of the EWT linear trend in the Russian High Arctic. See Figure 4.3 for detail.

4.4 Discussion

4.4.1 Sources of errors for the ice loss rate

We considered three possible sources of estimation errors; error in the linear regression for the GRACE EWT time-series, uncertainty in the GIA models, and mass changes in terrestrial water storage.

Figure 4.6 shows the distributions of one-sigma uncertainty of the trends for the period 2004.02-2012.01 and 2004.02-2008.01. These were obtained *a posteriori* by bringing the chi-square of the post-fit residuals to unity. The error in the period 2004-2008 would be larger than that in 2004-2012 because of the shorter time span of the data. The contributions of this type of error to the estimated ice loss rate were evaluated from the changes in the inversion results of point-mass modeling by including these errors. They are shown in Table 4.1.

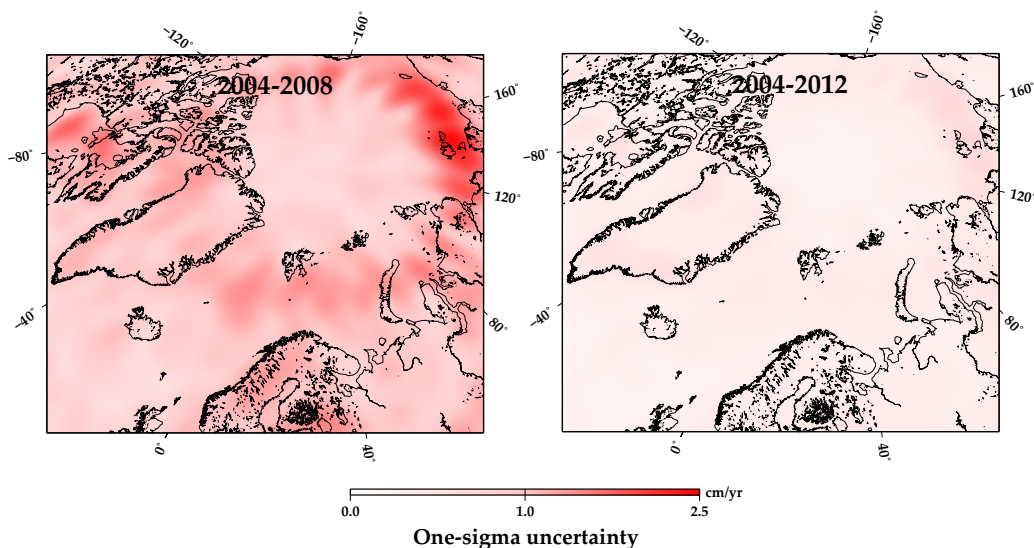


Figure 4.6: Distribution map of the one-sigma uncertainty of GRACE linear fitting for the period 2004.02-2008.01 (left) and 2004.02-2012.01 (right).

The GIA correction is important to correctly estimate actual glacial mass changes. As for the region studied here, significant GIA signatures can be found around the Barents Sea and Kara Sea, and they largely affect the estimation of glacial mass changes in Svalbard and Russian High Arctic. In order to assess the uncertainty of GIA models, we used four GIA models proposed by Peltier (2004), Paulson et al. (2007), Schotman et al. (<ftp://dutlru2.lr.tudelft.nl/pub/wouter/pgs/>), and Spada and Stocchi (<ftp://dutlru2.lr.tudelft.nl/pub/wouter/pgs/>) (Figure 4.7). The first two models are based on the ICE-5G ice loading history model (Peltier, 2004), and the last two models are based on the ICE-3G model [Tushingham and Peltier, 1991]. The details and differences of these GIA models are discussed in Guo et al. (2012). We investigated the differences of the estimated mass changes by using these four GIA models for each glacier system following the method described in Section 4.3. The results are shown in Table 4.1. Significant variations are found especially in Svalbard, Novaya Zemlya, and Severnaya Zemlya. They are all located around the Barents Sea, where the GIA contributions are large and not well constrained [e.g. Svendsen et al., 2004].

Natural changes in terrestrial water storage may obscure ice loss signals. We assessed their mass changes using the Global Land Data Assimilation System (GLDAS) Noah model [Rodell et al., 2004]. Figures 4.8a, b represent predicted linear mass changes in land hydrology from GLDAS in the period 2004.02-2008.01 and 2004.02-2012.01. Their total mass changes were also estimated in the same manner as Section 4.3, and the results are shown in Table 4.1. Here we did not correct the ice loss rate with these values but included them in the estimation errors because the reliability of long-term trend in the GLDAS model is not well known.

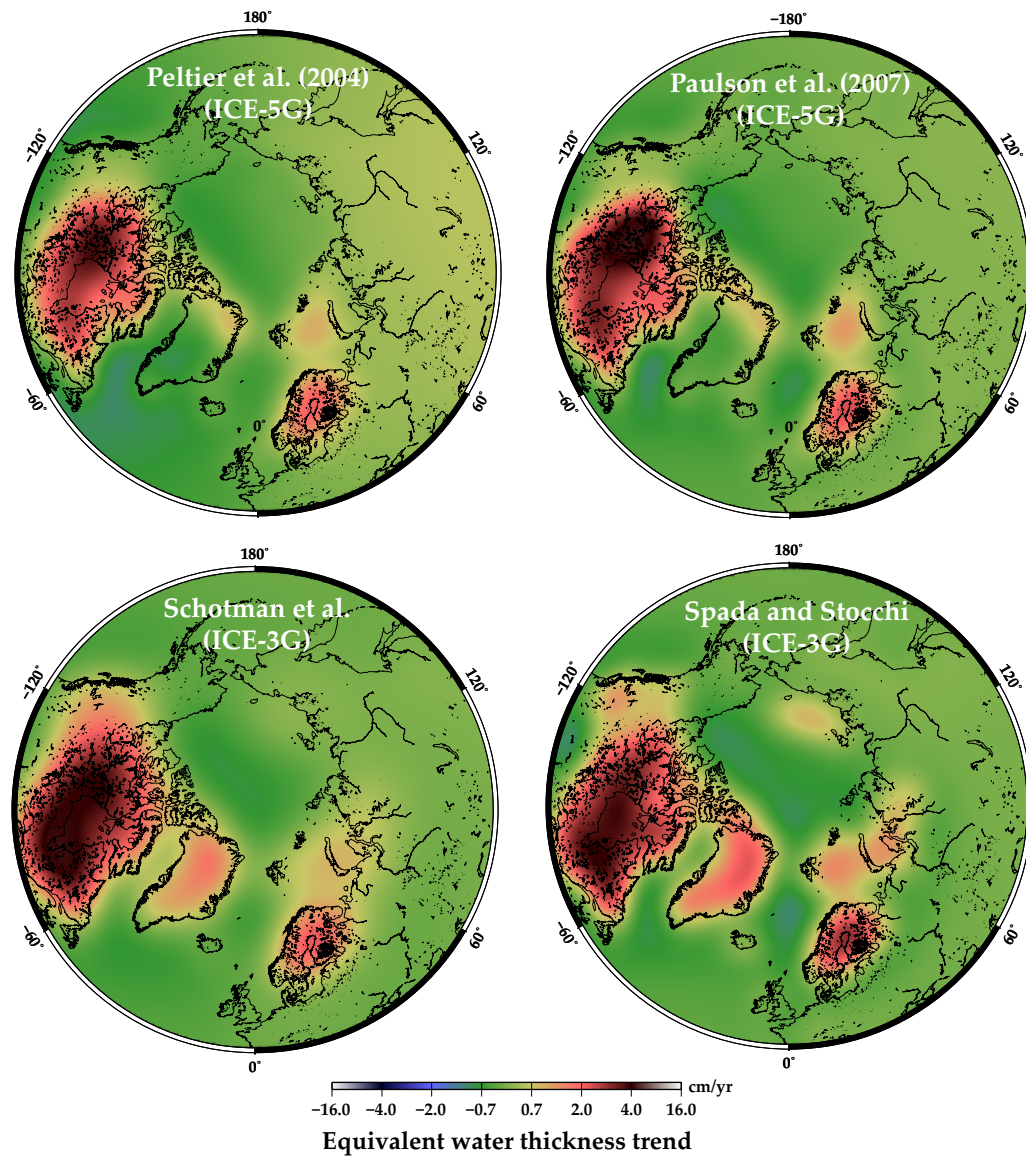


Figure 4.7: Linear mass trends predicted by four different GIA models, Peltier (2004), Paulson et al. (2007), Schotman et al., and Spada and Stocchi. The 150 km Fan filter and the P3M14 De-correlation filter are applied. All GIA models are downloaded from their webpage.

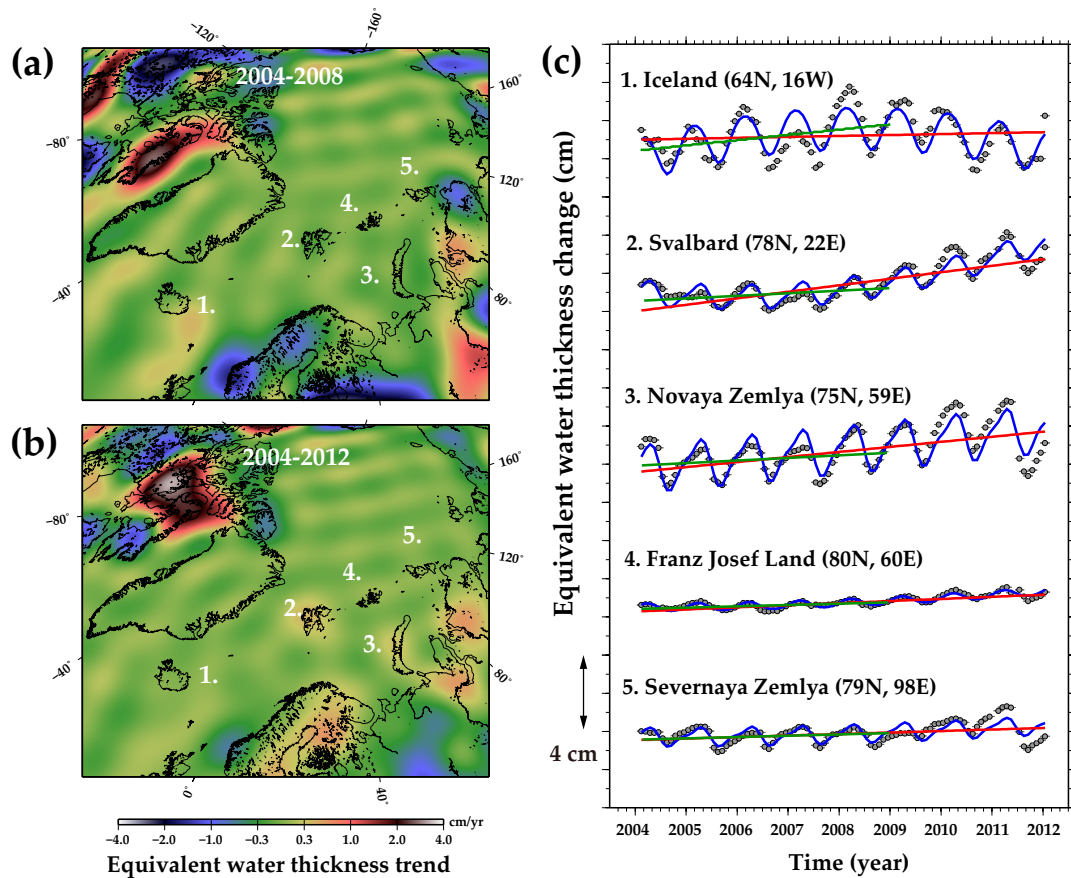


Figure 4.8: (a) Map of the linear trends of the GLDAS EWT in NH during 2004.02-2012.01. (b) That during 2004.02-2008.01. The same filters as GRACE were applied. We excluded Greenland because of relatively poor reliability there. (c) Time-series of the GLDAS EWT at each glacier system. The smooth curves with blue color indicate best-fit models by least-squares method assuming linear, quadratic and seasonal changes. The red and green lines show the linear components during 2004.02-2012.01 and 2004.02-2008.01.

4.4.2 AO and the temporal variability of the ice loss rates

As described in Section 4.4.3 and 4.4.4, the observed temporal variability of the ice loss in Svalbard and Novaya Zemlya might reflect AO. To evaluate the relationship between the observed mass changes and AO, we analyzed their statistical correlation using the AO index (AOI). AOI are derived as the first leading mode of empirical orthogonal function of monthly mean sea-level pressure anomaly field in the north of 20N, which represents the scale and phase of AO.

We followed the method of Chapter 3 to evaluate the relationship between GRACE mass changes and AO; removing linear, quadratic, and seasonal components from the EWT time-series of GRACE by least-squares method (here we refer to the residual as the EWT deviation), calculating averages of the three winter months (JFM; January, February, and March), and computing correlation coefficients between the wintertime EWT deviation and AOI. The results for each glacier system are shown in Figure 4.9. High correlations are found in Svalbard (-0.75), Novaya Zemlya (-0.62), and Franz Josef Land (-0.64). This suggests that the mass balances of these glacier systems are significantly influenced by AO.

In fact, the EWT time-series of the land hydrology inferred from the GLDAS model (Figure 4.8c) showed the positive and negative deviation from the model curves in Svalbard and Novaya Zemlya in the winter of 2009/2010 and 2006/2007, characterized by the strong negative and positive AOI. Positive/negative precipitation anomalies are considered to be caused by negative/positive AO in these two glacier systems. As for the EWT in Franz Josef Land, it would be difficult to discuss its relationship with AO due to small signals and the leakage from Novaya Zemlya.

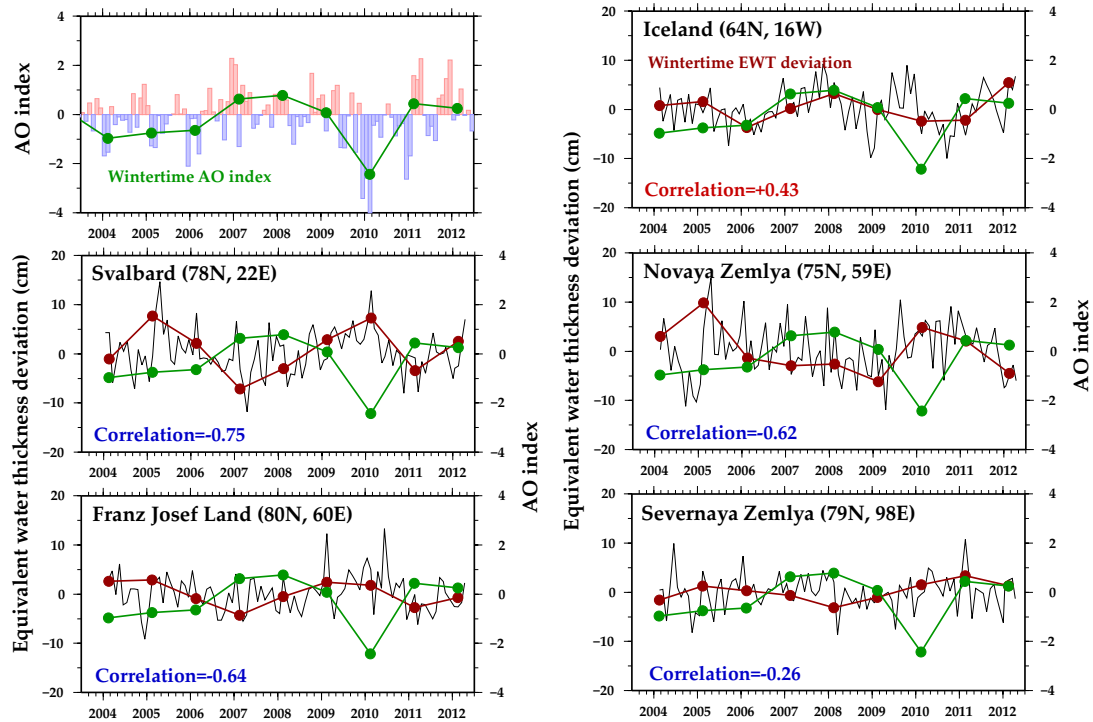


Figure 4.9: Time-series of AO index and GRACE EWT deviation in each glacier system, which are calculated by removing linear, quadratic, and seasonal components from the EWT time-series by least-squares method. AO index are provided by National Oceanic and Atmospheric Administration (http://www.cpc.ncep.noaa.gov/products/precip/CWlink/daily_ao_index/ao.shtml). Grey lines are monthly values of EWT deviation. Red curves are the three month (January, February, and March) averages of the EWDs. Green curves show winter AO index. The correlation coefficient between EWDs and AO index are given in the lower left corners (red and blue characters show positive and negative correlations, respectively).

Glacial system	Mass loss (Gt yr ⁻¹)	Fitting error (Gt yr ⁻¹)	GIA (Gt yr ⁻¹)	Hydrology (Gt yr ⁻¹)
<i>2004-2008</i>				
Iceland	10.6 ± 3.4	2.3	0.8	0.6
Svalbard	6.9 ± 3.6	1.6	1.9	0.1
Novaya Zemlya	11.2 ± 5.5	3.7	1.7	0.2
Severnaya Zemlya	0.7 ± 3.2	1.5	1.7	0.0
Franz Josef Land	3.5 ± 3.2	2.3	0.9	0.0
Total		32.9 ± 18.9		
<i>2004-2012</i>				
Iceland	10.9 ± 3.4	1.2	0.8	0.2
Svalbard	3.6 ± 3.6	0.5	1.9	1.0
Novaya Zemlya	5.2 ± 3.9	2.0	1.7	0.3
Severnaya Zemlya	0.9 ± 2.2	0.4	1.7	0.2
Franz Josef Land	0.8 ± 1.3	0.3	0.9	0.1
Total		21.4 ± 12.4		

Table 4.1: Glacial mass losses in the Arctic glacial system.

4.5 Conclusion

Most ice sheets and glaciers worldwide have experienced substantial amount of ice loss over the last decade. Small glacier systems in the Arctic Islands also follow this trend. GRACE observation during 2004-2012 suggested the average ice loss rates of 10.9 ± 2.1 Gt/yr in Iceland, 3.6 ± 2.9 Gt/yr in Svalbard, and 6.9 ± 7.4 Gt/yr in the Russian High Arctic. The total ice loss rate is 21.4 ± 12.4 Gt/yr, equivalent to 0.06 ± 0.03 mm/yr sea level rise. The observed mass changes by GRACE can be well explained by point-mass changes distributed over these glaciers.

We should note that mass balance of particular glacial regions is influenced by climatic fluctuations like AO, and regional differences in the responses to such fluctuations. For example, the mass in Iceland shows steady negative trend in the studied period, but those in Svalbard and the Russian High Arctic (especially Novaya Zemlya) behave differently: significant decrease prior to 2008 and increase around the 2009/2010 winter. The transition coincides with the occurrence time of the strong negative AO. The extreme AO in the winter of 2009/2010 brought the significant increase of surface temperature in and around Svalbard and the Russian High Arctic [Cohen et al., 2010]. The observed surface temperature there in January-March 2010 was $\sim 2.5^\circ\text{C}$ higher than that of 30 year (1971-2001) mean. This increased surface temperature would have produced the increased atmospheric moisture and regionally enhanced the winter precipitation in these islands and temporary positive trends in the mass of these glaciers.

In fact, the EWT time-series of GLDAS, which is based on meteorological data including snow accumulation, showed positive mass anomaly in Svalbard and

Novaya Zemlya in the 2009/2010 winter, suggesting that the strong negative AO brought anomalous precipitation there. It is known that the April ice extent in the Nordic Seas has a strong negative correlation with the winter AOI (Vinje, 2001), suggesting that AO largely control the climate in this region. The average ice loss rates during 2004-2008 (i.e. excluding the 2009/2010 winter) are 10.6 ± 3.4 Gt/yr in Iceland, 6.9 ± 3.6 Gt/yr in Svalbard, 15.4 ± 11.9 Gt/yr in the Russian High Arctic. The total ice loss rate is 32.9 ± 18.9 Gt/yr, 1.5 times as large as the 2004-2012 rate.

According to the field observation during 1961-2003, the average ice loss rates were 2.4 ± 2.2 Gt/yr in Iceland, 6.1 ± 1.3 Gt/yr in Svalbard, 4.0 ± 1.8 Gt/yr in the Russian High Arctic, respectively. The total ice loss rate was 12.5 ± 5.3 Gt/yr [Dyurgerov and Meier, 2005]), about one half of the GRACE results in 2004-2012. However, these *in situ* results are highly uncertain since they rely on extrapolation of a handful of measurements [e.g. Dyurgerov, 2010]. Though the spatial resolution is limited, GRACE can directly measure such mass changes over extensive glacier systems. Our GRACE estimates suggest that the ice loss rate in the Arctic Islands, as a whole, seems to have doubled in the last decade.

This apparent acceleration matches with the global tendency of the increasing glacial loss in Alaska, Patagonia, and the Asian High Mountain Ranges in comparison with the period 1961-2003 [Matsuo and Heki, 2010]. Our study has revealed that the recent global warming enhanced ice melting also in small glacier systems in the Arctic Islands. However, as described above, the ice loss in this region is fairly variable in time. Thus the assessment of their mass balance should be repeated in various time windows in order to correctly understand their long-term behavior. GRACE and future satellite gravimetry missions will remain a powerful tool to enable quantitative

assessment of such time-variable mass changes in glaciers and ice sheets all over the world especially where *in situ* observations are limited, e.g. polar and high mountain regions.

Chapter 5

Ice mass variations in Greenland from low-degree gravity field by Satellite Laser Ranging during 1991-2011

Paper will be submitted soon

Matsuo, K., B. F. Chao, T. Otsubo, and K. Heki : Ice mass variations in Greenland from low-degree gravity field by Satellite Laser Ranging during 1991-2011, *in preparation.*

5.1 Introduction

Ongoing increase in the Earth's atmospheric temperature brings about the enhanced loss of water ice in polar region and high mountain area, contributing to the global sea-level-rise. The Greenland Ice Sheet (GrIS) is the second largest reservoirs of fresh water on the Earth after the Antarctic ice sheet. Its total volume is around 3 million km³, and account for about 10% of total global fresh water. Hence the GrIS has a high potential for the contribution to the global sea-level-rise. Some researchers warned that if the annual average temperature in Greenland increases by more than about 3°C, the GrIS could raise the global sea-level by 7 meters during the next 1000 years or more [Gregory et al., 2004]. Therefore, long-term and quantitative assessment of the GrIS mass balance is one of the most important challenges in Earth Science.

The mass balance of the GrIS has been monitored and estimated by various geodetic observations over the last two decades. From 1990s through the early 2000s, the GrIS mass balance has been mainly estimated by geometric measurement using airborne laser and satellite radar altimetry. Airborne laser altimetry in 1993-2004 showed moderate mass loss from -60 Gt/yr (1993-1998) to -90 Gt/yr (1998-2004) [e.g. Krabill et al., 2004; Thomas et al., 2006], while satellite radar altimetry by ERS-1,2 in 1992-2006 suggested a near-balance rate of -11 to +7 Gt/yr (1992-2002) [Zwally et al., 2005; Zwally et al., 2011] and a small mass loss of -20 Gt/yr (1995-2006) [Li and Davis, 2008]. Mass balance estimations by combining Interferometric Synthesized Aperture Radar (InSAR) and meteorological models were significantly negative from -90 to -260 Gt/yr during 1996-2007 [Rignot et al., 2005; Rignot et al.,

2008].

Since 2002, satellite mission GRACE has started to measure the GrIS mass balance by gravimetry. GRACE enables direct measurements of the GrIS mass balance, but earlier estimates have also differed widely: the mass loss of 101 Gt/yr between July 2003 and July 2005 [Luthcke et al., 2006], 239 Gt/yr between April 2002 and April 2006 [Velicogna and Wahr., 2006a]. This is partly because of their difference in observational time window, reflecting the strong inter-annual variability of the GrIS mass balance in this period [e.g. Chen et al., 2011]. Recent GRACE estimates during 2002 - 2010 are being settled to the similar mass loss of ~200 Gt/yr [e.g. Shcrama et al., 2011]. This agrees well with geometric estimate by ICESat laser altimetry and InSAR in the same period [e.g. Sasgen et al., 2012]. The GrIS mass balance estimated by space geodetic techniques in the last two decades is summarized in Figure 5.1.

Temporal variations in the Earth's low-degree gravity field have been determined from Satellite Laser Ranging (SLR) data, which measure the distance from the ground-based stations to an artificial satellite (SLR satellite) orbiting the Earth with laser retroreflectors. Over time the SLR data after appropriate data processing provide precise information on temporal changes in satellite's orbital elements, and hence the temporal variations in the Earth's gravity field, signifying global-scale mass redistribution in the Earth system [e.g. Chao, 1994]. The first study to detect temporal variations in the Earth's gravity field using SLR data is the secular decrease in the zonal gravitational harmonic coefficient (Stokes' coefficient) of degree 2: J_2 ($= -\sqrt{5}C_{20}$), which represents physically the Earth's dynamic oblateness, due to the viscous rebound of the solid Earth by GIA and the Earth's secular spin-down by the

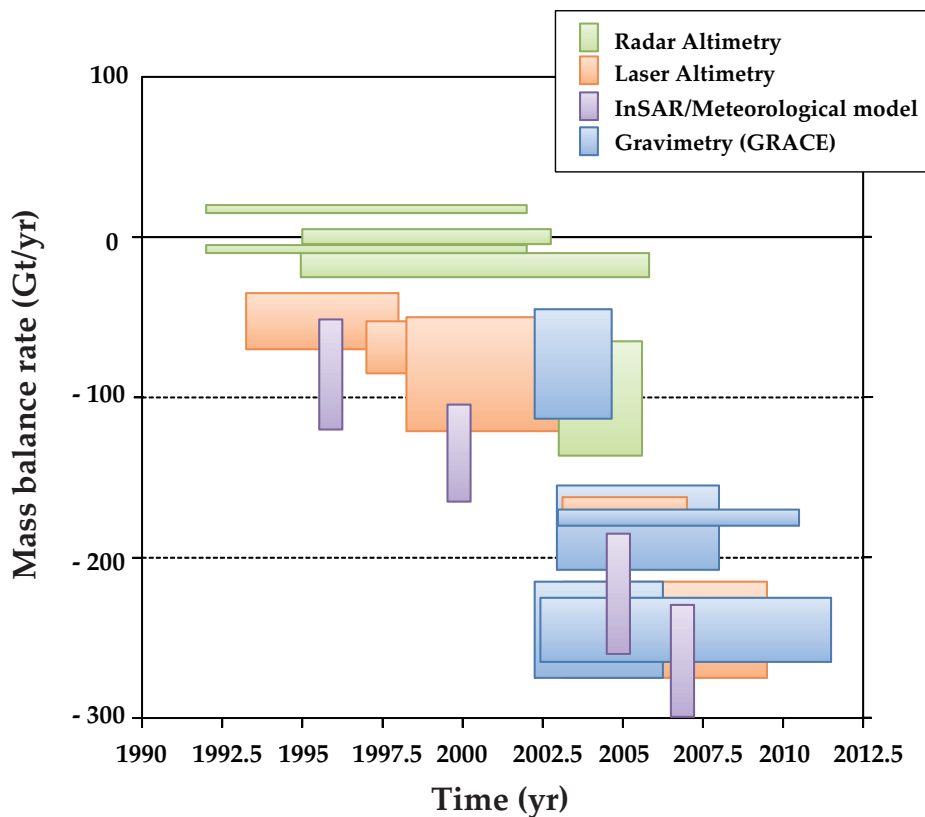


Figure 5.1: Greenland mass balance estimated by space geodetic techniques in the last two decades: satellite radar altimetry (green), satellite laser altimetry (orange), InSAR/metrological model (purple), and satellite gravimetry (blue). Vertical width of rectangular represents estimation error, and horizontal length represents time span of observation.

friction of external tidal forces (tidal breaking) [Yoder et al., 1983; Rubincam 1984]. Cox and Chao (2002) found sudden shift in the J_2 trend from decrease to increase around 1998. Its cause still remains unclear even now. Seasonal variations of the J_2 term or higher degrees were also detected by SLR, which reflects the changes in atmospheric mass and water storage on land by precipitation [Nerem et al., 1993; Cheng and Tapley., 1998]. Although limited in spatial resolution, the SLR data have been available for a longer time span over 30 years. Nerem and Wahr (2011) analyzed the changes in a 34-year time-series of the J_2 term from SLR, and reported

that, apart from Glacial Isostatic Adjustment (GIA), ice loss from Greenland and Antarctica has become the dominant contributor to the current J_2 trend since 2002.

In this study, we investigate temporal variations of Greenland's ice mass using low-degree Stokes' coefficients with degree and order up to 4 inferred from SLR data for the 21-year period 1991-2011. The Stokes' coefficients with degree and order up to 60 observed by GRACE are analyzed for the validation of our SLR gravity solutions. This is the first study to quantitatively assess the mass balance of GrIS from satellite gravimetry before 2002, i.e. the launch of GRACE. We compare our SLR estimate with earlier geometric estimates by laser and radar altimetry, and evaluate the validity of our estimate. Additionally, in order to further validate our SLR result back to 1990s, we examine the vertical displacement measured by the Global Positioning System (GPS) which manifests ice mass variations in the GrIS. Lastly, we discuss the relationship between the observed GrIS mass balance and recent climate changes.

5.2 Data and Method

The Hitotsubashi University and National Institute of Information and Communications Technology of Japan are developing an analysis software package named 'C5++' to consistently process various data acquired by space geodetic techniques [Hobiger et al., 2011]. Using this software, which implements up-to-date geophysical model centered on IERS conventions (2010), we determined the low-degree Stokes' coefficients of the Earth's gravity field by incorporating the laser tracking data of five SLR satellites: LAGEOS 1 & 2, Starlette, Ajisai, and Stella, obtaining

monthly data series (henceforth the HIT-U solution) of the Stokes' coefficients of degree and order up to 4 between 1991 January and 2011 December. Only three SLR satellites (Starlette, LAGEOS 1, and Ajisai) were available prior to 1992, while the other two satellites (LAGEOS 2 and Stella) were added after 1992 November and 1993 October, respectively. The changes in the atmospheric mass and subsequent oceanic mass have been removed from HIT-U solution using the AOD1B product of GRACE [Flechtner et al., 2008]. In addition, the contribution of hydrological mass changes in continental areas except for Greenland and Antarctica has been corrected using the GLDAS Noah model [Rodell et al., 2004].

In order to validate our SLR solution, we also use SLR gravity solutions provided by Cheng and Ries (2011) at University of Texas Center for Space Research (UT/CSR). Their SLR solutions are also determined from laser tracking of five SLR satellites, and consists of the Stokes' coefficients of degree and order up to 5 spanning November 1994 through May 2011 (Henceforth, we refer to their SLR solutions as UT/CSR solution). Because the UT/CSR solution is given in weekly, we converted it to monthly in order to directly compare with our HIT-U solution.

We use a monthly GRACE data set (CSR Level-2 RL05) with degree and order up to 60 from 2003 January to 2011 December. The degree-1 components (C_{10} , C_{11} , and S_{11}), reflecting the Earth's geocenter motion, were derived by combining GRACE and ocean model [Swenson and Wahr, 2008]. We apply the anisotropic Fan filter with averaging radius of 150 km to reduce short wavelength noises [Zhang et al., 2009], together with the de-correlation filter using polynomials of degree 3 for coefficients with orders 15 or higher to alleviate longitudinal stripes [Swenson and Wahr, 2006]. Here we adopt relatively "weak" spatial filters because of higher preci-

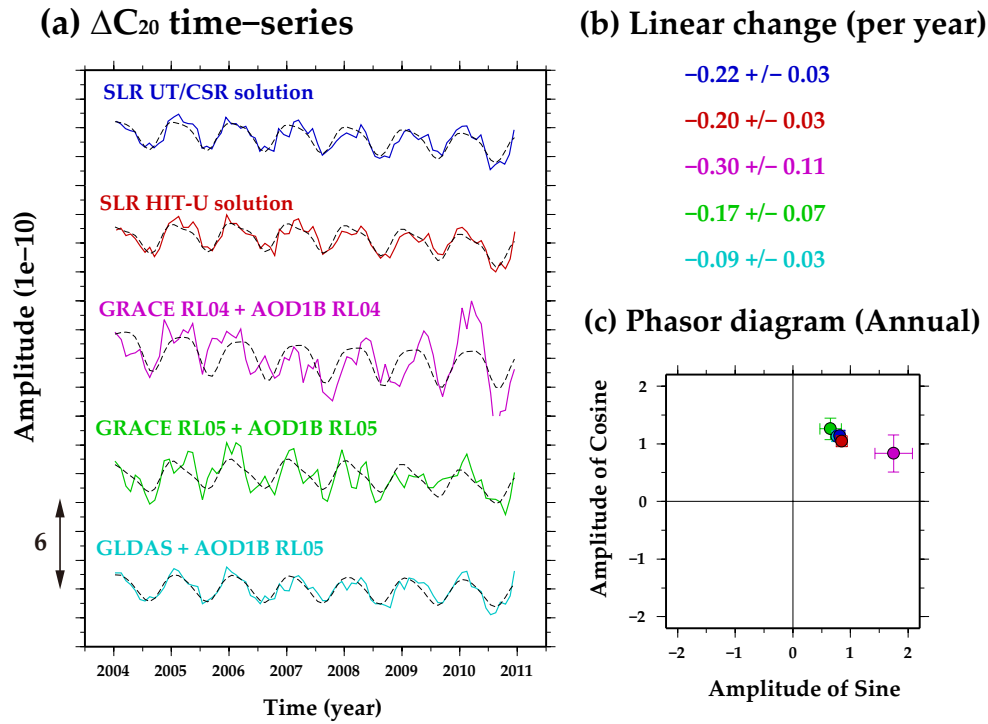


Figure 5.2: Comparison of ΔC_{20} time-series from SLR (HIT-U and UT/CSR solutions, and GRACE (RL04 and RL05), and GLDAS land hydrology model. (a) Time-series of ΔC_{20} of each solution. The broken lines represent the modeled curve with linear, quadratic, and seasonal changes by least-squares method. (b) Amplitude of linear changes of each solution. (c) Phasor diagram of annual changes of each solution.

sion of GRACE data in the polar region including Greenland, owing to the increasing spatial density of the GRACE measurements toward higher latitudes [Chapter 4 of this thesis]. Conventionally, the GRACE's J_2 terms are replaced with that by SLR because GRACE's determination of J_2 is known to be rather poor. Here we do not do so in order to keep data independency between GRACE and SLR. This hardly influences our final conclusion, as the accuracy of J_2 terms has been greatly improved in the GRACE RL05 data. In fact, The J_2 value from the GRACE RL05 became much closer to that from SLR as compared to that from the GRACE RL04 both in linear and annual and term (Figure 5.2).

We convert the Stokes' coefficients of SLR and GRACE to changes in gravity anomaly expressed in equivalent water depth using the equation (2.2) of Chapter 2. Here we assume that the SLR and GRACE gravity changes reflect variations in surface mass loads, thereof inverse solution is unique (Chao, 2005). Secular mass changes by ongoing GIA in North America, Scandinavia, and their vicinity must be removed from SLR and GRACE data because they obscures the signals of ice mass variations in the polar ice reservoirs, causing the underestimation or overestimation of the actual mass changes. Here we corrected the contributions of GIA using the model of Paulson et al. (2007).

Our interest of this study is the mass changes in the GrIS. So, we use only the components of the Stokes' coefficient that reflects the GrIS mass change. Figure 5.3 shows the linear trend of global mass change caused by GIA and the ice loss (or gain) in the GrIS and Antarctica during 2003-2011. The GIA mass changes are derived from the model of Paulson et al. (2007), and the ice mass changes from GRACE after subtracting GIA contribution. Figure 5.4 represents power spectrum of these three mass changes in the Stokes' coefficient. Concerning cosine term, the amplitudes of the Stokes' coefficients with order 2 or higher are almost zero value for Greenland. On the other hand, as for sine term, those with order 3 or higher are well small. These components will contaminate the estimation of the GrIS mass change because of low signal-to-noise ratio. Thus, we use the Stokes' coefficient with order up to 1 for cosine term and up to 2 for sine term.

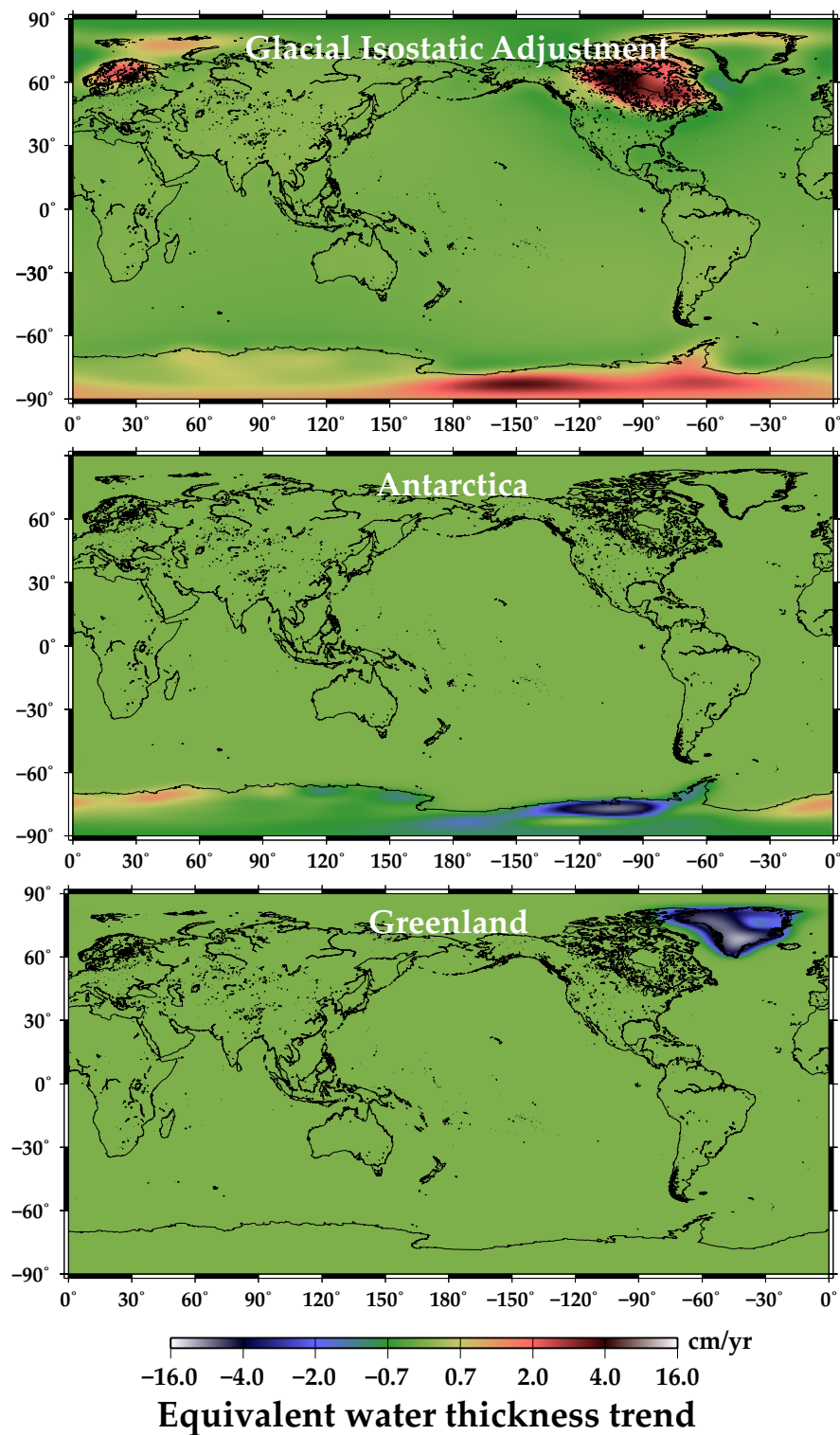


Figure 5.3: Linear mass trend maps of the mass changes by GIA and the ice mass changes in the GrIS and Antarctica. The GIA mass changes are derived from the model of Paulson et al. (2007). The ice mass changes are from GRACE after the subtraction of GIA effect.

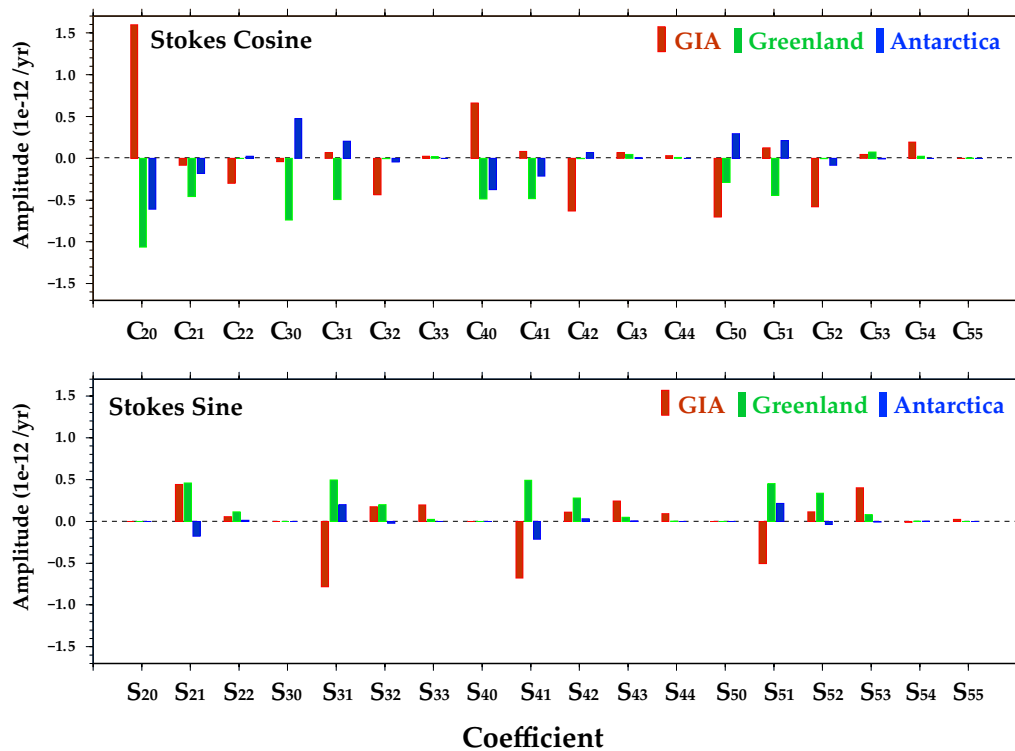


Figure 5.4: Power spectrum of three major mass changes (GIA, Ice mass variations in Antarctica and Greenland) in the Earth as expressed in the Stokes' coefficient.

5.3 Results

5.3.1 GRACE estimates of the GrIS mass balance in the period

2003-2011

Using GRACE data, we delineate linear trend maps of mass changes in the GrIS at five epochs, 2003.5, 2005.5, 2007.5, 2009.5, and 2011.5 (Figure 5.5). We fit the time-series of mass variations from GRACE at each grid point with linear, quadratic and seasonal components by least-squares method, and extract the linear component. The five epochs all show significant negative trend, suggesting that ice

loss does occur there. The ice loss is the sum of melting, carving, and sublimation. It is noteworthy that the ice loss rates are accelerating and propagating northwestward as time passes. Figure 5.6 shows the time-series of mass changes at three points of the GrIS, northwestern Greenland (77°N , -65°E), central western Greenland (72°N , -55°E), and southeastern Greenland (66°N , -40°E). One can find the characteristic mass variations depending on space. The GrIS in southeastern area is decreasing with relatively constant rate over time. That in central western area shows slight increasing trend from 2003 to 2005 and shifts to decreasing trend afterwards. That in northwestern area shows small mass loss from 2003 to 2005 and significant mass loss afterwards. Such mass changes in northwestern part and central western part appear as quadratic component of the fitted curves. The same accelerating mass loss is found in the glacier system of the Baffin Island of the Canadian Arctic Archipelago that lies just near the northwestern and central western Greenland [Gardner et al., 2011].

Based on the linear trend over the nine-year interval from 2003 to 2011, we estimate the total mass balance of the GrIS by means of point-mass modeling proposed by Baur and Sneeuw (2011). The basic idea behind this method is to solve an inverse problem from the observed gravity changes to the actual mass variations by least-squares adjustment assuming that the mass variation occurs in these specific locations. We distribute the assumed point masses to the geographical location of ice sheet and performed inversion of the GrIS mass balance. The optimum regularization parameters, expressed as λ in eq. (10) of Baur and Sneeuw (2011), are inferred by grid-search to match the GRACE data best. Figure 5.7 shows the result of the inversion. The synthesized mass trend (Figure 5.7b) signifies the significant ice loss along southeastern coastal area and north-central western coastal area, agreeing well

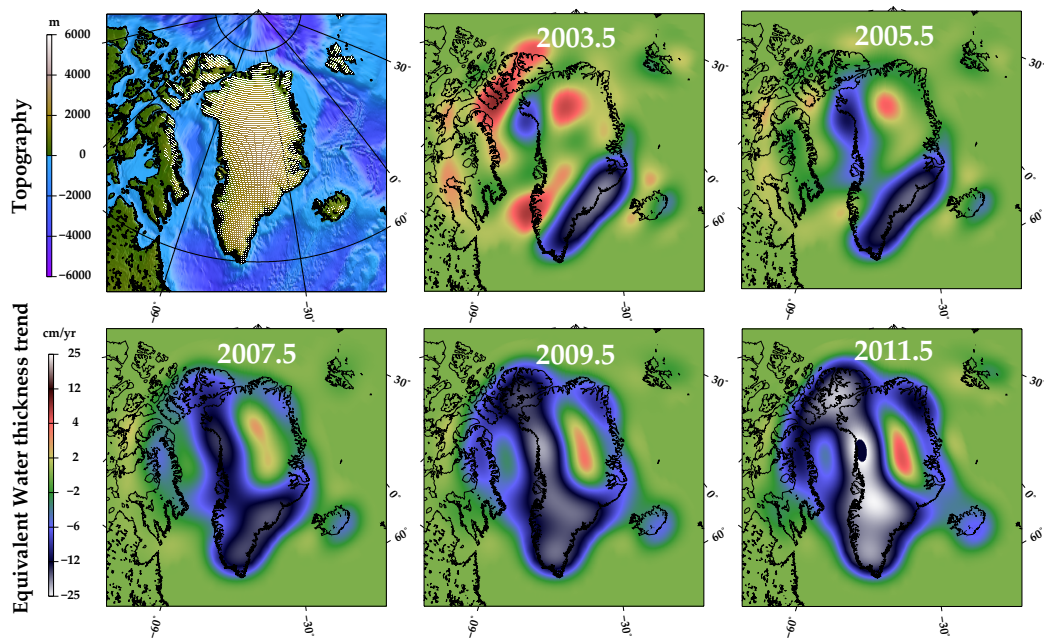


Figure 5.5: Linear trend of mass changes in the GrIS observed by GRACE at five epochs, 2003.5, 2005.5, 2007.5, 2009.5, and 2011.5. The contribution of GIA has been removed using the model of Paulson et al. (2007).

with the ice thickness trend of the GrIS from ICESat altimetry [e.g. Zwally et al., 2011]. We apply the same filters as GRACE data processing (150 km Fan filter and P3M15 de-stripping filter) for the synthesized result (Figure 5.7c), and confirm the good agreement with the observed. Finally, we got the average ice loss rate of -221.7 ± 7.6 Gt/yr over the GrIS in the period 2003-2011. Our result is almost the same as the previous GRACE results [e.g. Shcrama et al., 2011].

5.3.2 SLR estimates of the GrIS mass balance in the period 1991-2002 and 2003-2011

Following the method described in the section 5.2 and 5.3.1, we compute the linear trend maps of mass changes from SLR gravity data of HIT-U solution. Figure

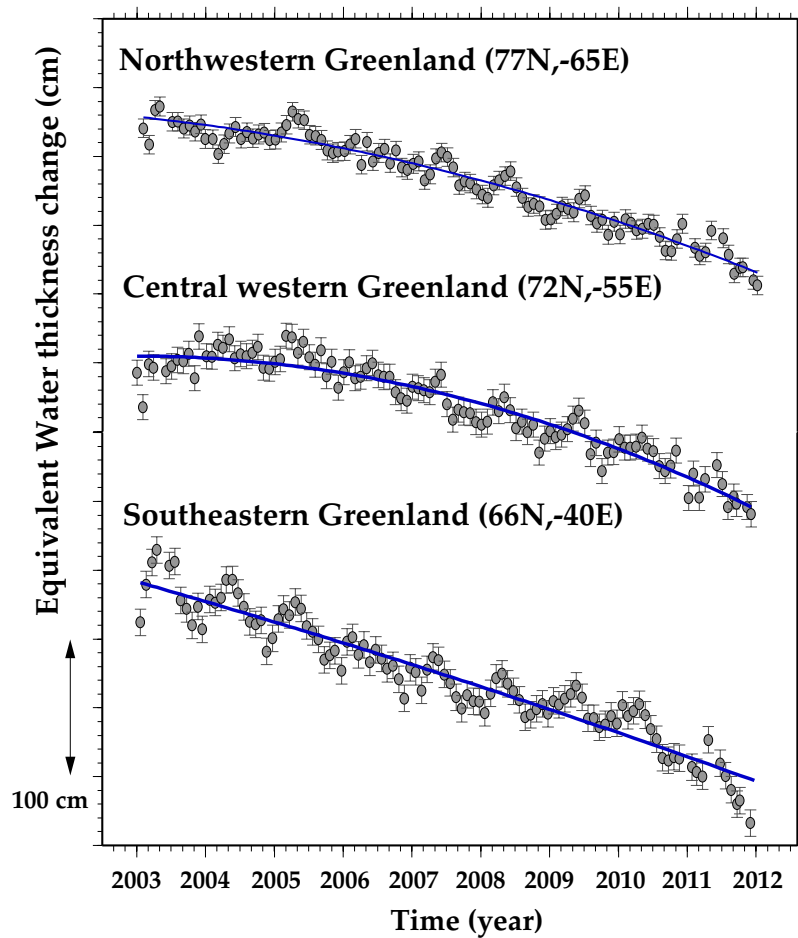


Figure 5.6: Time series of mass changes at three points of the GrIS observed by GRACE, northwestern Greenland (77°N , -65°E), central western Greenland (72°N , -55°E), and southeastern Greenland (66°N , -40°E). The blue curves are regression curves with linear and quadratic terms by least-squares method.

5.8a presents nine snapshots of linear mass trend around Greenland from SLR every other year during 1994-2010. First three epochs (1994-1998) indicates slight positive trend around the southern area, the next two (2000-2002) near-balance over the entire area, and the last four (2004-2010) significant negative trend around the southeastern area. Thus, SLR HIT-U solution indicates that the ice mass of the GrIS was near-balance in the 1990s and started to decrease in the 2000s. Figure 5.8b shows the corresponding linear trend from GRACE at four epochs from 2004 to 2010. They

agree well with SLR both in spatial pattern and amplitude, which demonstrates that SLR HIT-U solution is of sufficient good quality and properly reflects ice mass variations of the GrIS although its center of changes seems to somewhat dislocate from that of GRACE.

To further validate our SLR result, we calculate the time-series of mass changes around the GrIS using SLR gravity data from UT/CSR solution during 1994-2011. Figure 5.9 represents the time-series of mass changes at central western Greenland (72°N , -55°E) from SLR UT/CSR solution, SLR HIT-U solution, and GRACE RL05 data with same resolution as SLR. The two SLR mass changes show small positive trend or near balance in the 1990s and the large negative trend in the 2000s, agreeing well with each other.

In order to investigate the uncertainties in the GIA corrections and their influences, we experimented with four different GIA models that assumes different ice deglaciation history and different inner structure of the Earth. The results are

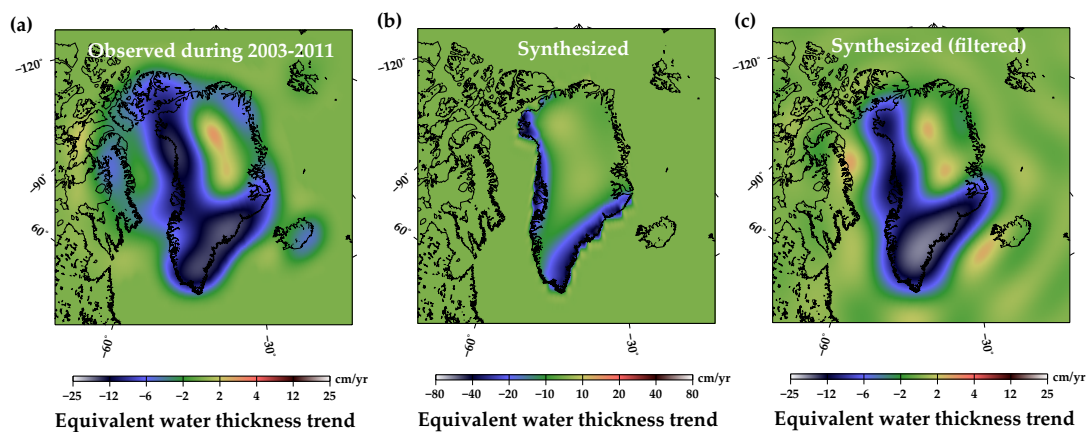


Figure 5.7: (a) The observed mass trend by GRACE during 2003-2011. (b) The Synthesized mass trend by Point-mass modeling (c) Applying the same filters as GRACE for the synthesized result.

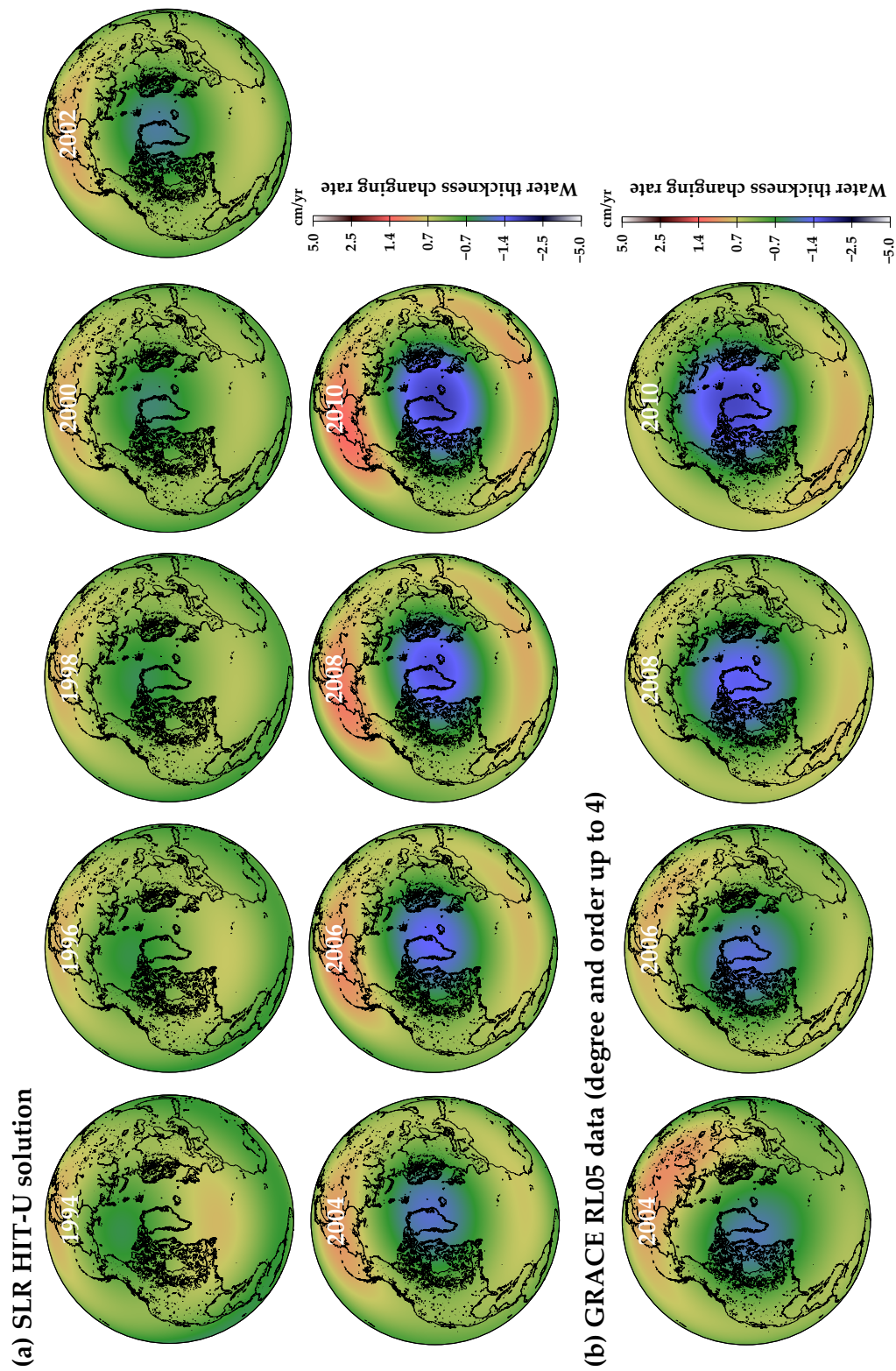


Figure 5.8: Linear trend of mass changes around the GrIS observed by (a) SLR and (b) GRACE. The contribution of GIA has been removed using the model of Paulson et al. (2007).

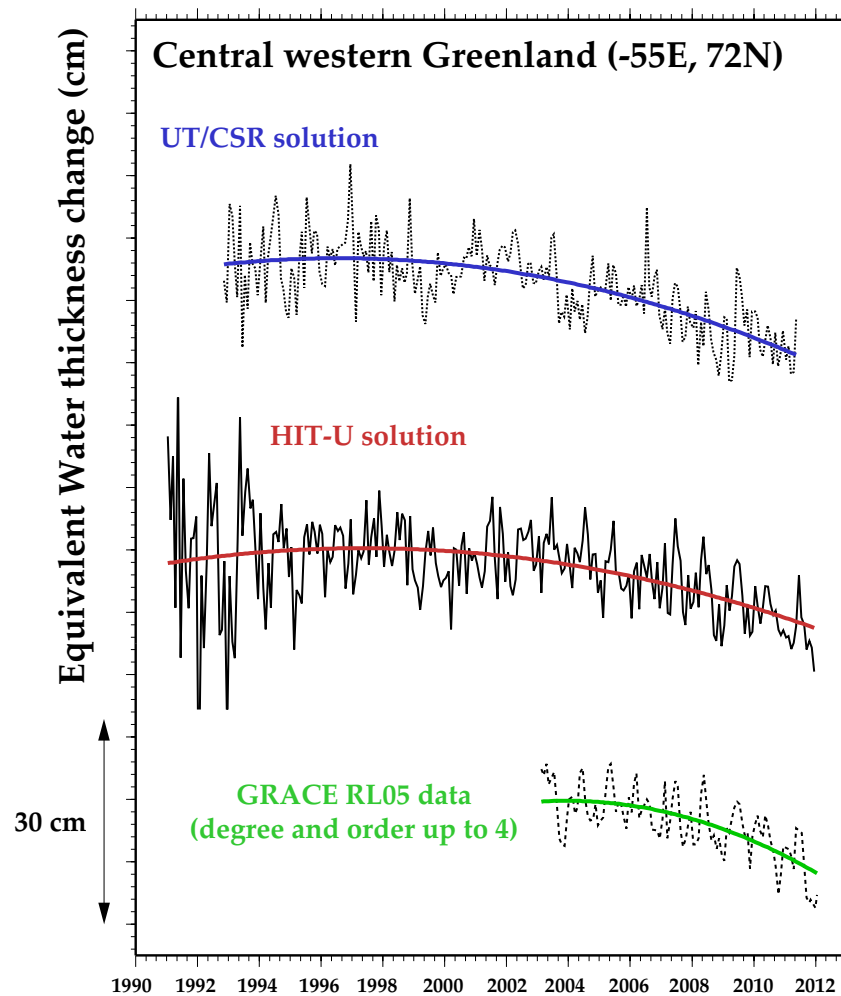


Figure 5.9: Time series of mass changes at central western Greenland (72°N , -55°E) from SLR UT/CSR solution, HIT-U solution, and GRACE RL05 with degree and order up to 4.

shown in the auxiliary material. Although giving rise to differences in the amplitude of mass variations (Fig. 5.10), they do not change the general scenario mentioned above about the GrIS mass balance during the studies period.

We perform inversion of the GrIS mass balance based on the linear mass changes by SLR HIT-U solution for the period 1991-2002 and 2003-2011 in the same manner as the section 5.3.1. The estimated mass balance rate of the GrIS in the period

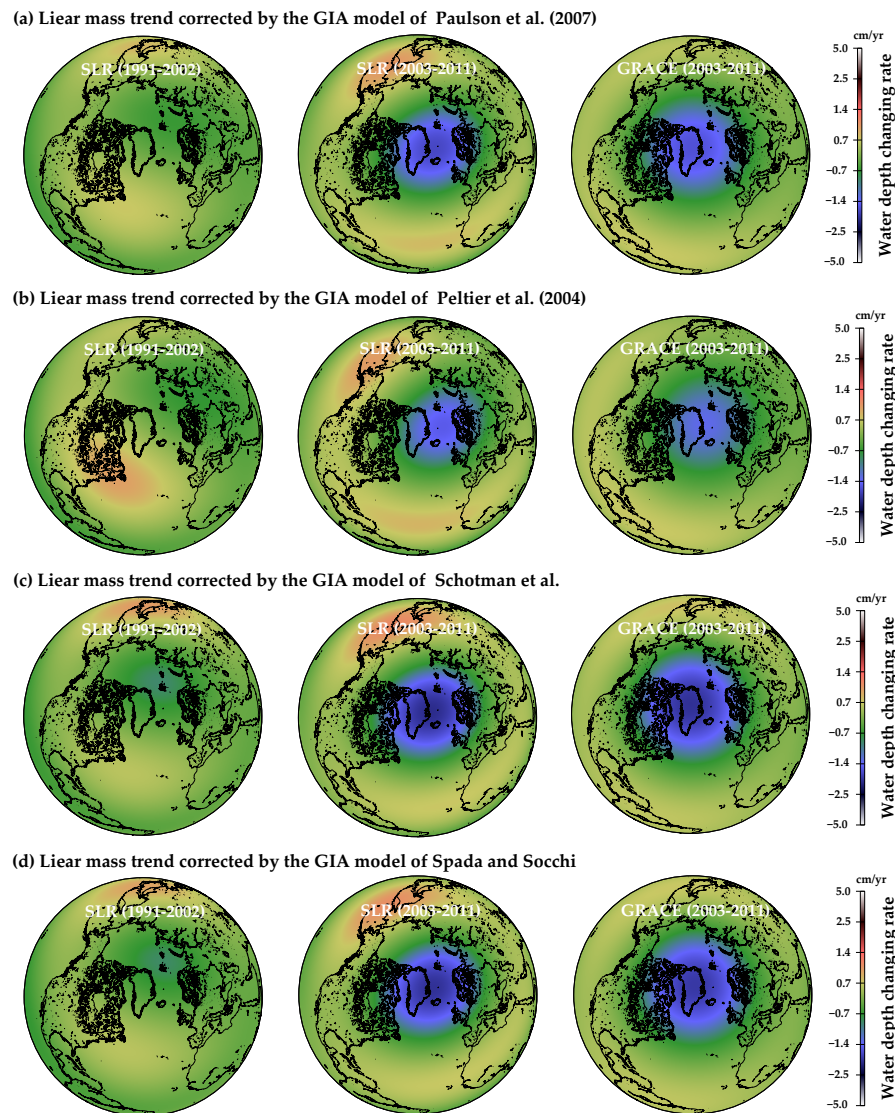


Figure 5.10: Linear mass trend maps after correcting four GIA models of (a) Paulson et al. (2007) which is constructed by assuming ICE-5G deglaciation history and the Earth's inner structure with upper mantle viscosity in 0.9×10^{21} Pa s, and lower mantle viscosity in 3.6×10^{21} Pa s, and lithosphere thickness in 98 km, (b) Peltier et al. (2004) which is constructed by assuming ICE-5G deglaciation history and the Earth's inner structure with upper mantle viscosity in $0.4-1.5 \times 10^{21}$ Pa s, and lower mantle viscosity in $1.4-3.9 \times 10^{21}$ Pa s, and lithosphere thickness in 90 km, (c) Schotman et al. which is constructed by assuming ICE-3G deglaciation history and the Earth's inner structure with upper mantle viscosity in 0.5×10^{21} Pa s, and lower mantle viscosity in 5.0×10^{21} Pa s, and lithosphere thickness in 115 km, (d) Spada and Stocchi which is constructed by assuming ICE-3G deglaciation history and the Earth's inner structure with upper mantle viscosity in 1.0×10^{21} Pa s, and lower mantle viscosity in 2.0×10^{21} Pa s, and lithosphere thickness in 100 km. All GIA data are available from <ftp://dutlr2.lr.tudelft.nl/pub/wouter/pgs.tar>.

2003-2011 was negative trend of 220.6 ± 17.8 Gt/yr, almost the same as GRACE and ICESat estimates (Figure 5.11d-f). In the period 1991-2002, the estimated mass balance rate was positive trend of 18.2 ± 25.0 Gt/yr, which is close to the ERS-1,2 estimates (Figure 5.11a-c). The spatial pattern of mass change in this period can be characterized by ice loss in northern area and ice gain in central-southern area. Such pattern is also in accordance with the changes in the ice thickness from the ERS-1,2 altimetry. The ERS-1,2 altimetry suggested the decreasing trend of mass in coastal area and the increasing trend in in land area, especially southern area (Figure 5.12). Our synthesized result also shows the increasing trend of mass in southern area. So, it can be said that our SLR estimate properly detected the signal of the GrIS mass balance both in the period 1991-2002 and 2003-2011. SLR observation seems to support the result by the ERS-1,2 altimetry rather than the Airborne laser altimetry and InSAR measurement.

5.3.3 Ice mass changes from GPS vertical displacement

Ice mass load causes crustal deformation especially in vertical direction. As a result of the Earth's elastic response to the redistribution of surface load, an ice gain (increase of surface load) depresses the crust whereas an ice loss (decrease of surface load) uplifts the crust. Thus, vertical crustal displacement can be an indicator of surface mass variation. It has been revealed that the vertical displacement of GPS stations installed on the rocky margins of Greenland nicely manifests the ice mass variations of the GrIS [e.g. Jiang et al., 2010; Bevis et al., 2012]. As of 2012, there are about sixty GPS stations in Greenland. Among them, GPS points in THU1,2,3 (Thule Airbase; 77°N, -69°E), KELY (Kellyville; 67°N, -51°E), and

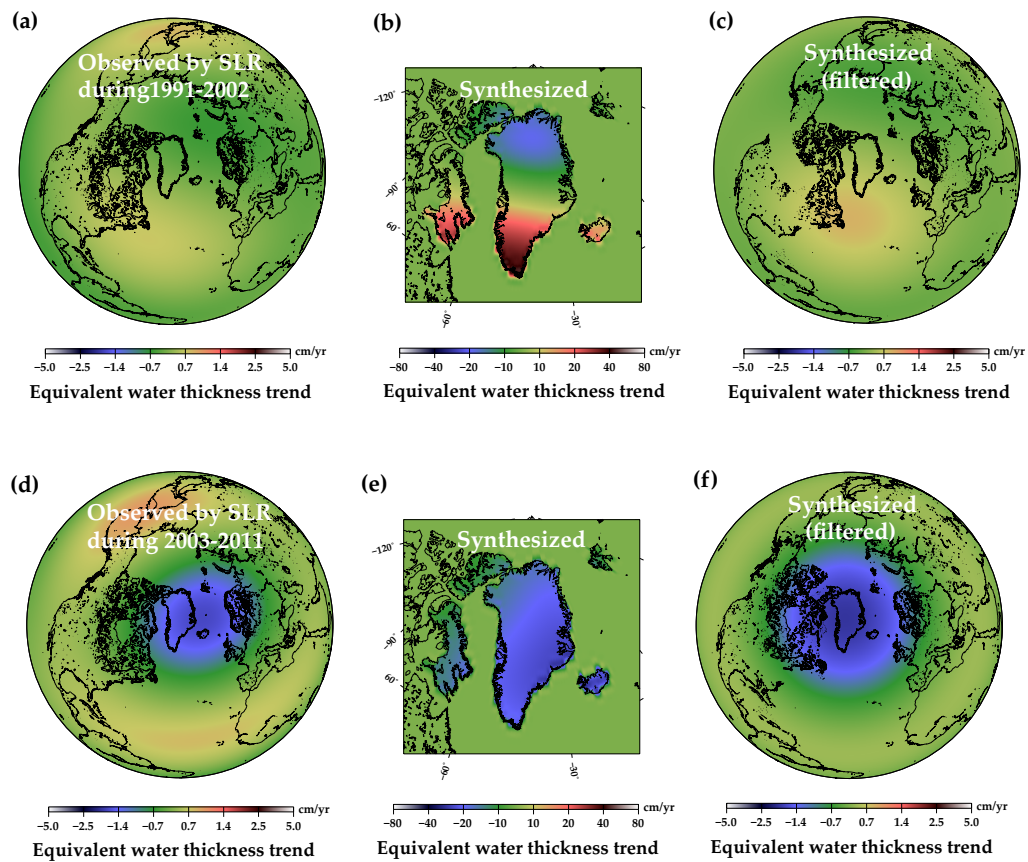


Figure 5.11: (a) The observed mass trend by SLR (HIT-U solution) during 1991-2002. (b) The Synthesized mass trend by Point-mass modeling (c) Converting the synthesized result to the same resolution as SLR (d) The observed mass trend by SLR (HIT-U solution) during 2003-2011. (e) The Synthesized mass trend by Point-mass modeling (f) Converting the synthesized result to the same resolution as SLR.

KULU (Kulusuk; 66°N , -37°E), have continued to measure the bedrock displacement in Greenland since 1995 and 1997. Here we utilize the data of vertical displacement of these three GPS stations to validate the SLR result shown in Section 5.3.2. We use the processed GPS data provided by the Scripps Orbit and Permanent Array Center (SOPAC) of University of California, San Diego. In the same manner as GRACE and SLR, we model the time-series of GPS vertical displacement with linear, quadratic, and seasonal changes. To eliminate data outlier, we remove the data deviating from

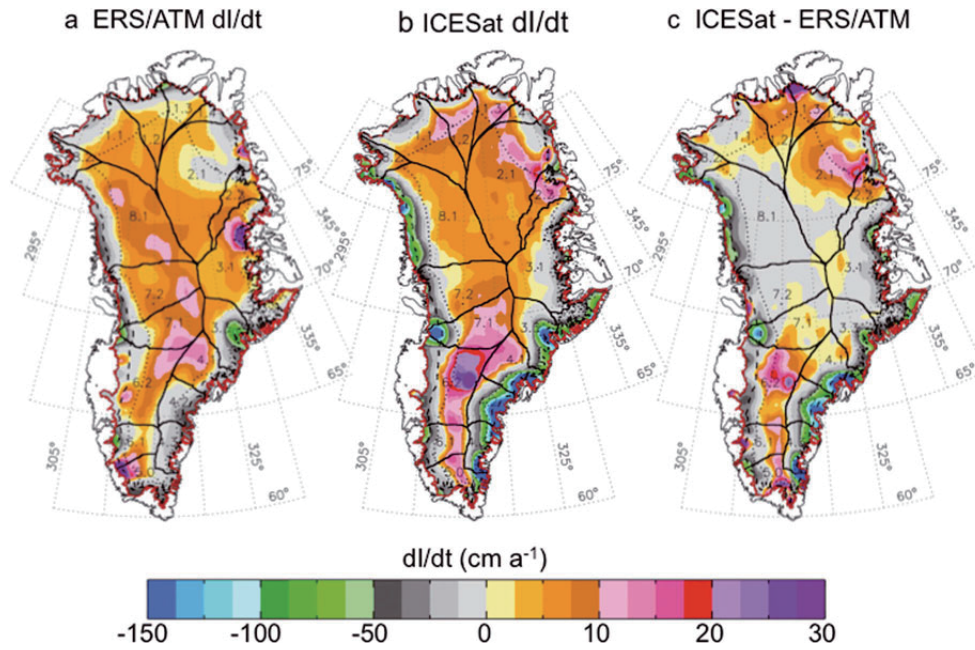


Figure 5.12: Linear trend of ice thickness from ERS-1,2 radar altimetry during 1991-2002 and ICESat laser altimetry during 2003-2011 [Zwally et al., 2011].

modeled curve by 3-sigma formal errors or larger.

In order to compare the GPS vertical displacement with the GRACE and SLR gravity change in the same unit, we convert the SLR gravity change to equivalent vertical load deformation through elastic loading theory on the spherical earth using the load Love numbers [e.g. Farrell, 1972; van Dam et al., 2007].

$$\Delta U(\phi, \lambda) = \frac{GM}{gR} \sum_{n=2}^{n_{max}} h_n \sum_{m=0}^n [\Delta C_{nm} \cos m\lambda + \Delta S_{nm} \sin m\lambda] P_{nm}(\sin \phi) \quad (5.1)$$

where G is the universal gravity constant, and M is the Earth's mass. g is the standard gravity of the Earth. h_n is the load Love number at degree n .

Figure 5.13 shows the time-series of vertical displacement measured by GPS

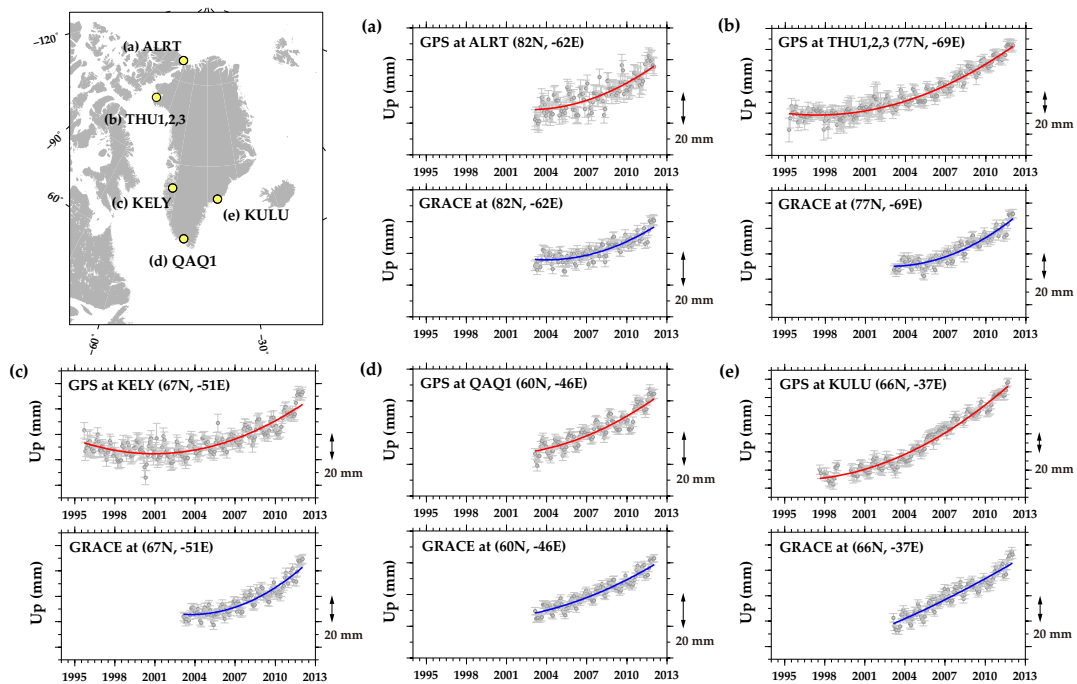


Figure 5.13: Time-series of vertical displacement of GPS stations installed on the bedrock at (a) the Cornwallis Island (82°N , -62°E), (b) Thule Airbase (77°N , -69°E), (c) Kellyville (67°N , -51°E), (d) Qaqortoq (60°N , -46°E), and (e) Kulusuk (66°N , -37°E). Red curves show the regression curves of linear and quadratic components of GPS vertical displacement. Blue are those of GRACE vertical displacement.

stations and calculated by GRACE with degree and order complete to 60. We can confirm good agreement with each other, suggesting that the GPS vertical displacement correctly reflects mass changes in the GrIS.

The GPS stations THU1,2,3 (Thule Airbase) at northwestern Greenland and KELY (Kellyville) at central western Greenland are most noteworthy because they have data in the 1990s. GPS station at THU1-3 shows slow uplift at a rate of $+1.92 \pm 0.20$ mm/yr between 1995 and 2002, and quicken the uplift rate to $+6.23 \pm 0.28$ mm/yr between 2003 and 2011. This indicates that the ice loss occurred around this region over the period, but its uplifting rate in the first period becomes three times as fast as that in the last period. GPS station at KELY shows the slow subsidence with

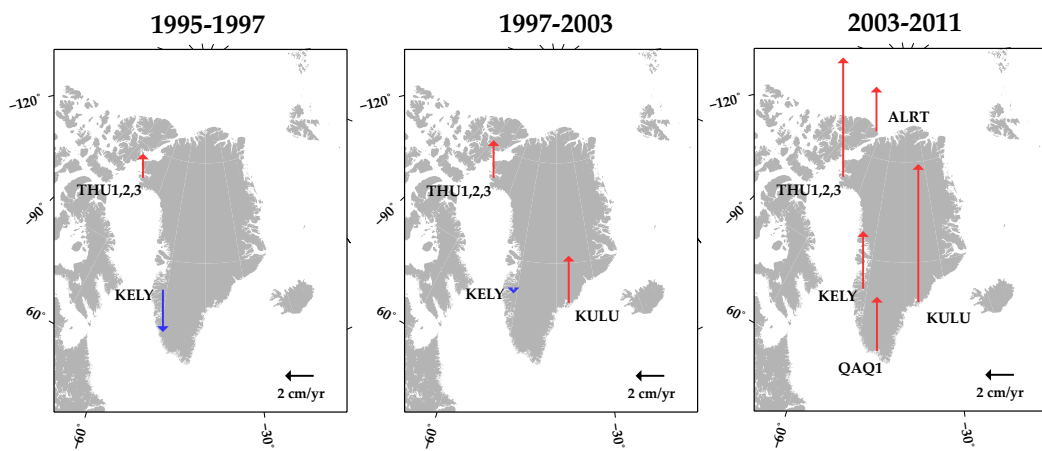


Figure 5.14: Linear trend of GPS vertical displacement during 1995-1997, 1997-2003, and 2003-2011.

a rate of -1.23 ± 0.12 mm/yr between 1995 and 2002, and reverts to the fast uplift with a rate of $+4.87 \pm 0.29$ mm/yr between 2003 and 2011. Figure 5.14 shows the transition of the trend of vertical displacement in the three time span, 1995-1997, 1997-2003, and 2003-2011.

Figure 5.15 represents the time-series of average vertical displacement of the three GPS stations (THU1-3, KELY, KULU) and that computed from the SLR HIT-U solution. They show quite similar behaviors – slightly depressing during 1995-1999, near-balance during 2000-2002, and significantly uplifting after 2003. One notices the large difference in the amplitude between SLR calculation and GPS observation. Their linear and quadratic components are $+0.60 \pm 0.09$ mm/yr and $+0.07 \pm 0.02$ mm/yr² for SLR, $+3.61 \pm 0.39$ mm/yr and $+0.41 \pm 0.09$ mm/yr² for GPS, respectively. Such difference in amplitude can be attributed to the low spatial resolution of SLR gravimetry. Because SLR gravimetry detects mass variations averaging over a large distance of ~ 5000 km, they are less sensitive to local mass variations, in contrast to GPS which captures deformations due to local as well as global mass variations.

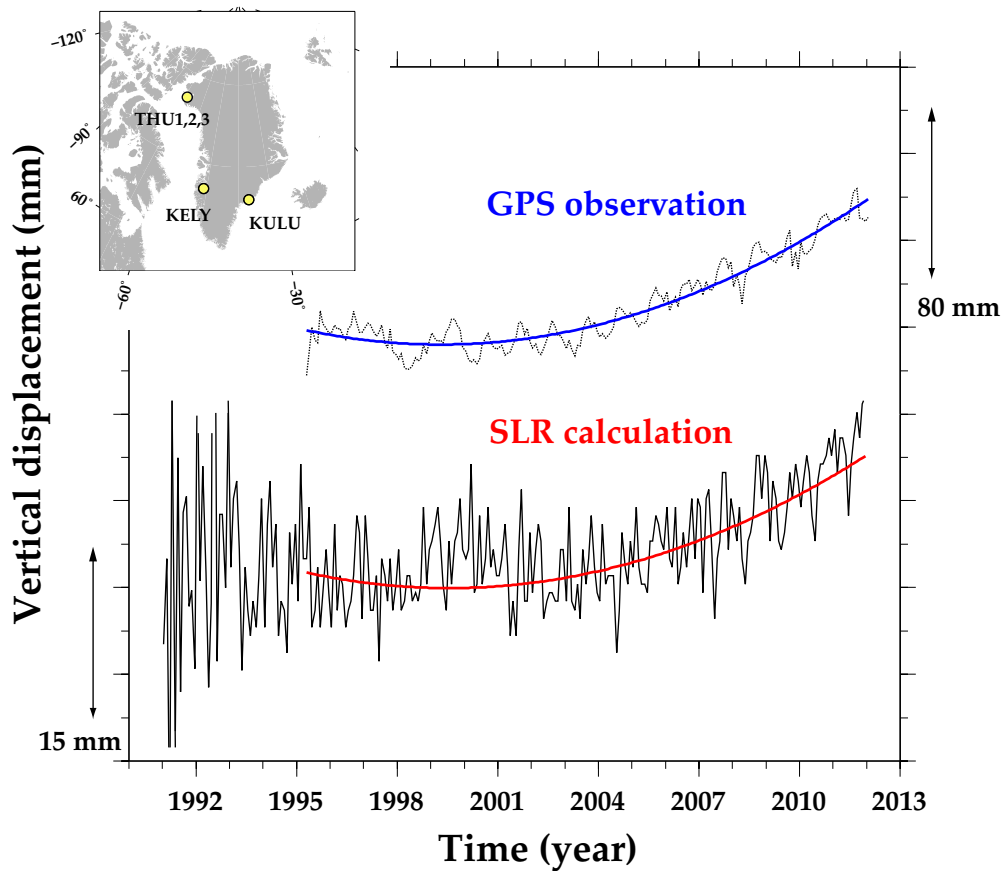


Figure 5.15: Time-series of average vertical displacement of the three GPS stations (THU1,2,3, KELY, and KULU) and that computed from SLR HIT-U solution. The contribution of GIA has been removed using the model of Paulson et al. (2007). The blue and red lines are regression curves with linear and quadratic terms for GPS and SLR.

This results in the different-amplitude estimations between GPS and GRACE as previously reported [Khan et al., 2010], herein a scaling factor of 6.0 can be adopted to adjust the amplitude of the SLR estimation.

5.4 Discussion

5.4.1 Relationship between the GrIS mass balance and climatic changes

SLR gravity solutions revealed that the GrIS mass balance was weak or near balance between 1991 and 2002 and switched to strong negative trend afterwards. This agrees well with ERS-1,2 radar altimetry. Such mass trend can be attributed to global warming to a large extent. It is known that warming in Northern Hemisphere started in 1970s, and warming in Greenland did in 1990s (Figure 5.16). The increased temperature causes the loss of ice through melting and calving. On the other hands, it also brings about enhancement of precipitation because of the increase in water vapor in the atmosphere produced from ocean [Hanna et al., 2008]. Satellite altimetry of the GrIS in the last two decades showed the ice thinning along coastal area and the ice thickening in inland area [e.g. Zwally et al., 2011]. We consider that our SLR results detected the shift of their balancing, i.e. the former was dominant before 2002 and the latter became dominant afterwards.

Matsuo and Heki (2012) [Chapter 3] found that the Arctic Oscillation (AO), one of a major atmospheric climate pattern in Northern Hemisphere [Thompson and Wallace, 1998], modulated the mass balance of the GrIS through precipitation anomaly using GRACE data. It appears that positive AO brings higher precipitation in winter in northern part of Greenland, and negative AO brings it in southern part. Its boundary lies along the latitude of $\sim 75^{\circ}\text{N}$. This would contribute to the inter-annual variation in the GrIS mass balance.

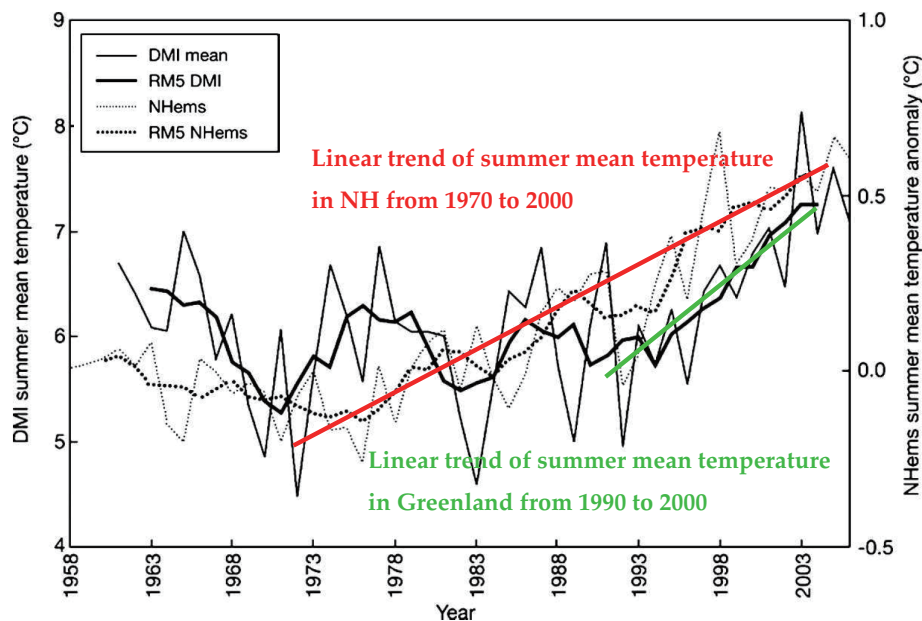


Figure 5.16: Time-series of summer mean temperature in Northern Hemisphere and Greenland in the last 50 years [Hanna et al., 2008].

5.4.2 EOF analysis of non-seasonal mass changes from GRACE

The mass changes associated with global warming and AO should be included in GRACE gravity data as one package. We can retrieve their mass changes by EOF analysis. EOF analysis, also known as the Principal Component Analysis, enables us to extract principal changing mode in time-series of the dataset and to separate spatial variability (spatial function) from temporal variability (temporal function). We performed EOF analysis of non-seasonal mass changes in Greenland from GRACE in the period 2002-2012. Figure 5.17 shows the spatial and temporal function of the first and second mode. The temporal function of first model can be characterized by long-term and linear mass trend. The spatial function is in accordance with the ice thinning distribution observed by ICESat altimetry. So, this mode is considered

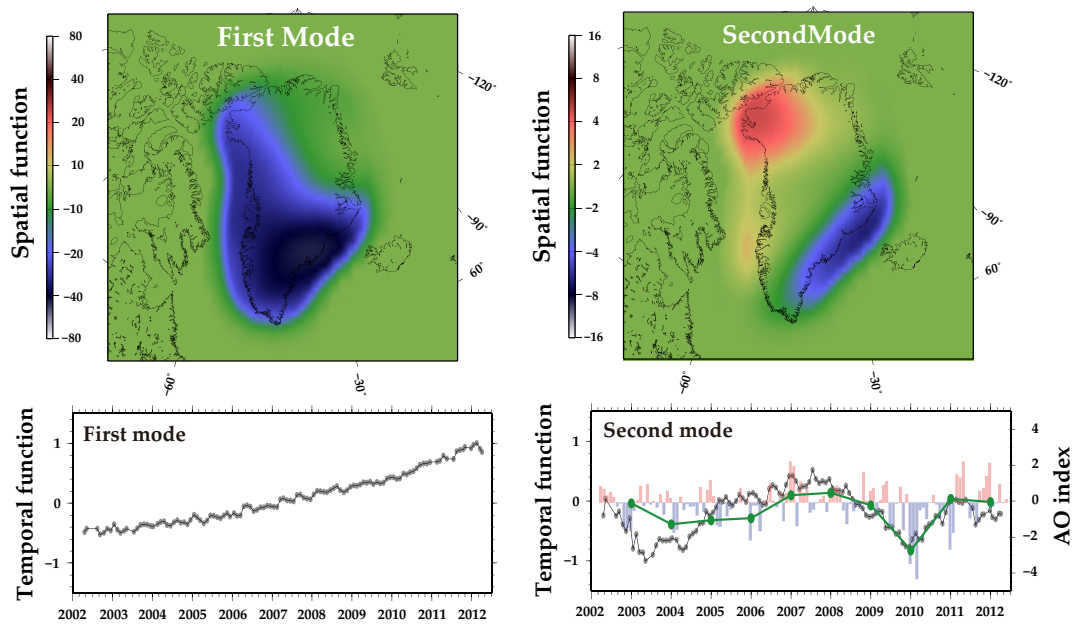


Figure 5.17: First mode and second mode of non-seasonal mass changes derived from EOF analysis of GRACE data during 2002-2012.

to reflect mass loss associated with global warming. The contribution ratio of this mode is about 97%. The temporal function of second mode is very similar to the time-series of wintertime AO index. The spatial function also corresponds to the distribution of precipitation anomaly by AO [Chapter 3]. This mode would reflect mass variation associated with AO. The contribution ratio of this mode is about 2%. Namely, 99% of mass change in the GrIS could be explained by global warming and AO.

5.5 Conclusion

A 21-year, monthly time-series of low-degree gravity field coefficients up to degree and order 4 has been derived from SLR data of multiple satellites. Here we have utilized the SLR HIT-U gravity solutions to examine the ice mass variations in the GrIS, finding that the GrIS ice mass trend was slightly positive or near balance in the 1990s, near-balance during 2000-2002, and becoming significantly negative afterwards. We confirmed that these mass variations match well with both GRACE gravimetry since 2003 and local GPS positioning since 1995. On the other hand, it appears that SLR gravimetry during 1991-2002 suggests a better agreement with the satellite radar altimetry by ERS-1,2 (-11 to +7 Gt/yr) than airborne laser altimetry (-60 Gt/yr) and InSAR/meteorological results (-90 Gt/yr) in the same period.

The temporal variation in the GrIS mass trend can be attributed to a large extent to global warming, which causes increased melting, and acceleration of outlet glaciers. At the same time, certain places may gain ice mass through enhancement of precipitation due to the increase in atmospheric water vapor source from ocean. According to satellite altimetry in the last two decades, the GrIS is experiencing ice thinning especially in the coastal margins of southeastern and northwestern area, and ice thickening in the high inland plateaus of southern area. In a sense our SLR solutions witness the shift of the power balance between these two regions, i.e. the coastal ice loss overtook ice gain during the last two decades.

The main conclusion of the present study is that retrospective SLR data allow to "observe" the mass variations of the GrIS prior to the GRACE observation since 2002. It is possible to further extend the SLR data back into the 1980s, the quality

of which, however, is poorer. For the future, the GRACE mission shall come to an end within the coming few years while GRACE follow-on mission is scheduled for launch no sooner than 2017. Gravimetry by multiple SLR satellites could be expected to play a role in bridging possible data gap.

Chapter 6

Coseismic gravity changes of the 2011 Tohoku-Oki great Earthquake from satellite gravimetry

Paper was published in *Geophysical Reserch Letter*

Matsuo, K. and K. Heki, 2011: Coseismic gravity changes of the 2011 Tohoku-Oki Earthquake from satellite gravimetry, *Geophys. Res. Lett.*, 38, L00G12, doi:10.1029/2011GL049018.

6.1 Introduction

The 2011 off the pacific coast of Tohoku earthquake (hereafter Tohoku-Oki Earthquake) is a gigantic interplate thrust earthquake which occurred at 05:46 UT, 11 March, 2011, at the Japan Trench in the east of northeastern (NE) Japan. Japan Meteorological Agency (JMA) estimated the ruptured area of this earthquake to be as large as $500 \text{ km} \times 200 \text{ km}$ and the moment magnitude (M_w) to be 9.0 [Ammon et al., 2011; Ozawa et al., 2011]. This is the largest earthquake in Japan and the fifth in the world over the course of recorded history. This region resides in the boundary between the North American (Okhotsk) plate and the Pacific Plate, subducting at the rate of $\sim 9.0 \text{ mm/yr}$ [DeMets et al., 1994] and is known as one of the most active seismic zones in Japan. Therefore, the intensive investigations have been performed with state-of-the-art geodetic and seismic observation in both land and sea floor there [e.g. Heki et al., 1997; Yamanaka and Kikuchi, 2004]. In Japan, the dense GPS array, GEONET (GPS Earth Observation Network), has been developed over the Japanese Island by Geospatial Information Authority of Japan (GSI) for the purpose of continuous measurement of crustal deformation. The number of sites attains ~ 1200 and their data sets can be obtained freely from GSI's web site (<ftp://terras.gsi.go.jp>). The largest deformation observed in this earthquake is $\sim 5 \text{ m}$ toward ESE and $\sim 1 \text{ m}$ down at a GPS station of Oshika Peninsula in NE Japan [Ozawa et al., 2011]. In addition to GPS measurement on land, seafloor positioning using GPS/acoustic ranging techniques has been performed by Japan Coast Guard off Miyagi prefecture which is just near the epicenter [Fujita et al., 2006]. From this measurement, the eastward movement of $\sim 24 \text{ m}$ and the uplift of $\sim 3 \text{ m}$ were observed near the epicenter, ~ 130

km off the coast of Oshika Peninsula [Sato et al., 2011]. This, together with the ~31 m displacement toward ESE measured by the Tohoku University groups at a submarine benchmark ~175 km offshore, would be the world record of the coseismic displacement ever measured.

Earthquakes changes the Earth's gravity field by the two processes, i.e. deformation of layer boundaries with density contrasts (e.g. sea floor and Moho) and density changes of rocks around fault due to volumetric strains. Such coseismic gravity changes have been first detected by superconducting gravimetry after the 2003 Tokachi-Oki earthquake (M_w 8.0) [Imanishi et al., 2004]. Gravity Recovery and Climate Experiment (GRACE) satellites, launched in 2002 to study time-variable gravity field, revealed two-dimensional distributions of coseismic gravity changes of the 2004 Sumatra-Andaman earthquake (M_w 9.0-9.3) [Han et al., 2006], and the 2010 Central Chile (Maule) earthquake (M_w 8.8) [Han et al., 2010; Heki and Matsuo, 2010]. The magnitude of Tohoku-Oki Earthquake (M_w 9.0) is just between these two earthquakes, and will provide another good example of the detection of coseismic gravity changes by GRACE gravimetry.

6.2 GRACE observation of gravity changes

GRACE can measure the Earth's gravity field accurate to several μGal with spatial and temporal resolutions of a few hundred kilometers (km) and a month, respectively. A GRACE data set consists of coefficients of spherical harmonics (Stokes's coefficient) with degree and order complete to 60. Here we used 105 data sets of monthly solutions (Level-2 data, Release 04) by Center for Space Research,

Univ. Texas, from April 2002 to May 2011. We replaced the Earth's oblateness values (C_{20}) with those from Satellite Laser Ranging [Cheng and Tapley, 2004] because of their poor accuracy. We applied the anisotropic Fan filter with averaging radius of 300 km to reduce short wavelength noises [Zhang et al., 2009], together with the De-correlation filter using polynomials of degree 3 for coefficients with orders 15 or higher to alleviate longitudinal stripes [Swenson and Wahr, 2006]. The movement of geocenter, expressed with the degree-one components (C_{10} , C_{11} , and S_{11}), was not taken into account because they contribute little to local gravity changes studied here.

Gravity may change by various geophysical processes other than earthquakes. The largest of those would be seasonal and inter-annual hydrological changes on land [e.g. Tapley et al., 2004; Morishita and Heki, 2008]. Although the width of the Japanese Islands is smaller than the spatial resolution of GRACE, fairly large seasonal mass changes due mainly to winter snow [Heki, 2004] may influence the GRACE data. Actually, GRACE showed such changes of amplitude of $\sim 2 \mu\text{Gal}$, with the peak in winter [Heki, 2010]. To remove such hydrological signals, it has been effective to use the Global Land Data Assimilation System (GLDAS) hydrological model [Rodell et al., 2004], which considers soil moisture, snow, and canopy water. Following Heki and Matsuo [2010], we removed the land hydrological contributions by subtracting the GLDAS Noah models.

Figure 6.1 shows the time-series of monthly gravity changes at (38.0°N , 138.0°E), ~ 350 km west of epicenter. We can see a significant gravity decrease of $\sim 5.0 \mu\text{Gal}$ in 2011 March and the decrease reached $\sim 7.0 \mu\text{Gal}$ in April suggesting that coseismic gravity changes did occur there. Note that the gravity jump between February and March, 2011, underestimates the true coseismic change because the March data

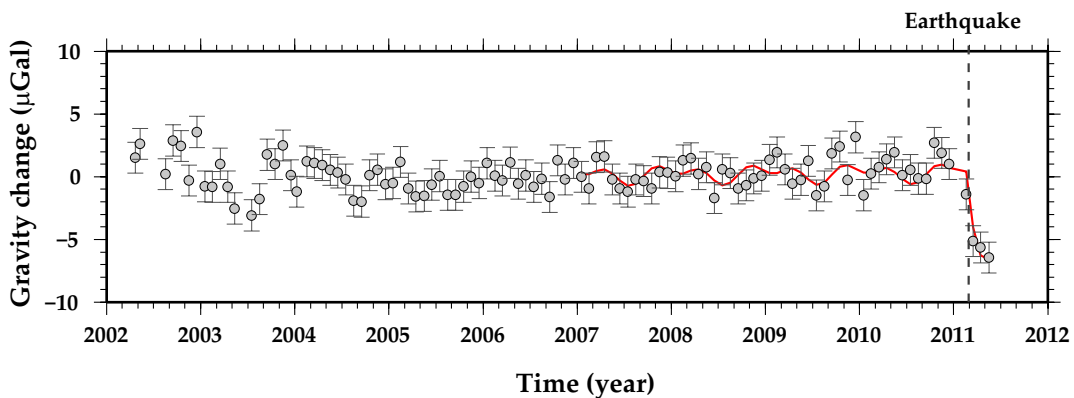


Figure 6.1: Time series of the monthly gravity values at 38.0°N , 138.0°E (open circle in Figure 2a) recovered by GRACE. The Fan filter of averaging radius 300 km [Zhang et al., 2009] and the De-stripping filter P3M15 [Swenson and Wahr, 2006] have been applied. Hydrological contributions (GLDAS/Noah) have been subtracted from GRACE time series. Data after 2007.0 have been modeled (thick red curves) assuming linear and seasonal (annual and semiannual) changes and a coseismic jump by the least-squares fitting ($2/3$ of the total jump is assumed to occur for the 2011 March data because the earthquake occurred on March 11). Error bars show one-sigma formal errors inferred *a posteriori* by bringing the chi-square of the post-fit residual to unity.

include ~ 10 days before the earthquake. Therefore, we estimated the true coseismic gravity changes using least-squares method assuming that $2/3$ of coseismic jump occurred between February and March and $1/3$ of the jump occurred between March and April.

We show the two-dimensional distribution of the coseismic gravity changes in Figure 6.2a. The observed gravity changes are dominated by the negative changes in the back-arc region, with the largest decrease of $\sim 7.0 \mu\text{Gal}$ 300-400 km landward from the focal region. One-sigma formal errors of the coseismic gravity changes are typically $1 \mu\text{Gal}$ or less.

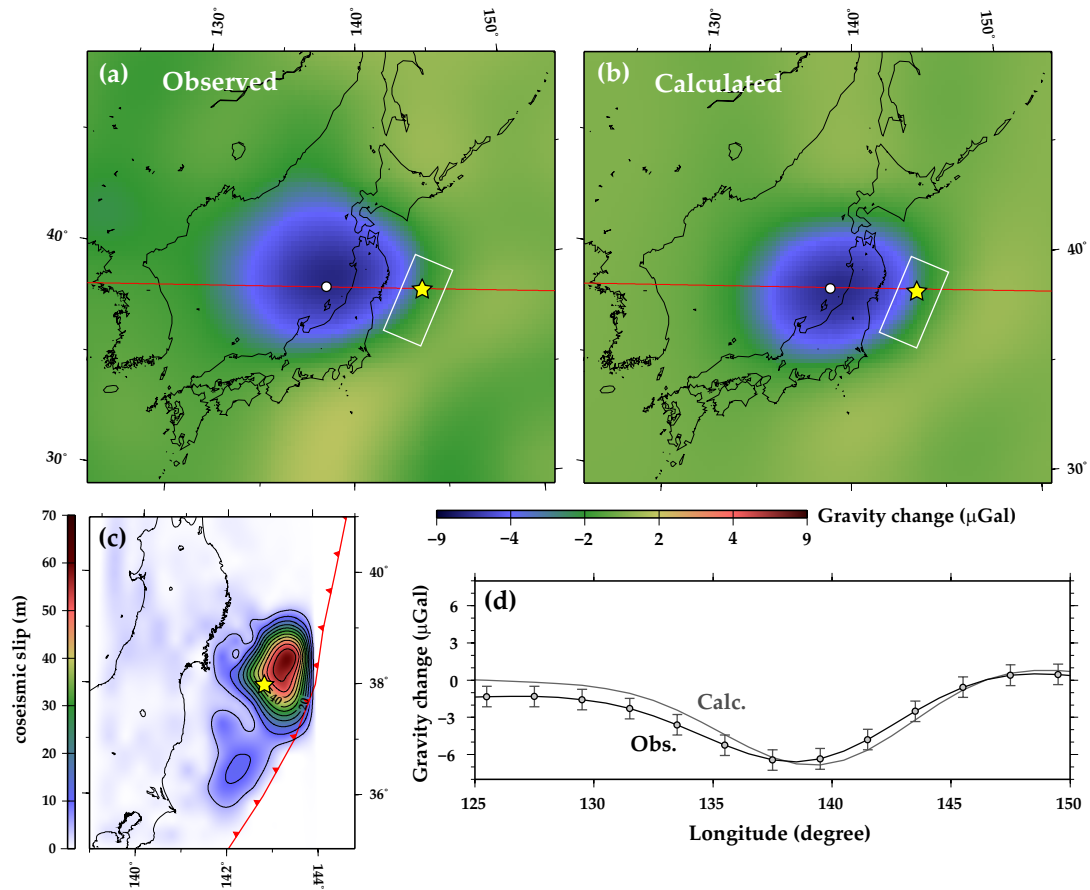


Figure 6.2: Geographical distribution of coseismic gravity changes observed by GRACE (a), and calculated according to Sun et al. [2009] (b) using the coseismic slip distribution by GSI [2011] (c). Yellow stars in a, b and c denote the epicenter (38.1°N , 142.9°E). The contours of coseismic slips in (c) are drawn every 20 m (thick contour) and 5 m (thin contour). The red line with triangles denotes the Japan Trench. GRACE data have been corrected with the GLDAS/Noah land hydrological models. In (d), we compare profiles at latitude 38.0°N (red curves in a and b). For the observed profile, one-sigma formal errors are shown every two degrees.

6.3 Model calculation of gravity changes

Coseismic slip distribution on the fault plane of plate boundary has been estimated by Geospatial Information Authority of Japan (GSI) [GSI, 2011] by combining Global Positioning System (GPS) data from terrestrial stations [Ozawa et al., 2011] and ocean bottom stations [Sato et al., 2011]. Figure 6.2c shows the slip distribution projected onto the Earth's surface. The maximum slip of ~ 60 m is located ~ 50 km northeast of the epicenter. The dip angles of the fault are fixed to 10° .

Using these fault parameters, we calculated coseismic gravity changes following the method of Sun et al. [2009]. The calculated gravity changes show significant short-wavelength gravity changes with the maximum change of ~ 2 mGal near the epicenter. They mainly reflect surface deformations of the ocean floor. In order to compare them with GRACE results (Figure 6.2a), we removed the components with degree/order of 60 or higher and applied the same spatial filters (Fan filter and De-striping filter).

Because the software assumes dry earth (no sea water), we corrected for the contribution of sea water that replaces crustal rocks as the seafloor moves vertically [Heki and Matsuo, 2010]. Figure 6.2 compares the observed and the calculated gravity changes. They are quite similar to each other both in spatial pattern and amplitude. Their profiles along the latitude 38° coincide with each other within observational uncertainties (Figure 6.2d). Such long-wavelength negative gravity changes are considered to reflect, to a large extent, dilatation of rocks occurred above the down-dip end of the fault.

6.4 Discussion

Coseismic gravity changes of the 2011 Tohoku-Oki Earthquake has been detected by GRACE. This becomes the third detection of coseismic gravity changes by GRACE. Besides them, several earthquakes exceeding $M_w 8$ have occurred since the launch of GRACE. The largest of those are the 2005 March Nias earthquake in Indonesia ($M_w 8.7$) [Briggs et al., 2006], the 2007 September Bengkulu earthquake in Indonesia ($M_w 8.5$) [Gusman et al., 2010], and the 2006 November earthquake in the Kuril Islands ($M_w 8.3$) [Fujii and Satake, 2008].

For the 2005 Nias earthquake, Einarsson et al. [2010] concluded it difficult to isolate its coseismic gravity changes because it is too close to the 2004 Sumatra-Andaman earthquake both in space and time. However, we could detect small but significant coseismic gravity changes of the Nias earthquake. The maximum coseismic gravity decrease was $\sim 2 \mu\text{Gal}$ 300-400 km northeast of the epicenter (Figure 6.3). For the other two earthquakes, we did not find significant coseismic gravity changes. All the cases are interplate shallow-angle thrust faulting, and show similar spatial pattern of coseismic gravity changes, i.e. those dominated by negative changes at the back-arc side of the rupture area. In Figure 6.4, we compare seismic moments and maximum gravity decreases observed by GRACE. It appears that the gravity change roughly scales with the moment, and the threshold of their detection with GRACE seems to lie somewhere around $M_w 8.6-8.7$.

Large mass redistribution by earthquake would also excite the earth's polar motion [Chao and Gross, 1987]. Its amount can be inferred from the changes in the degree-2 tesseral components of the gravity change (ΔC_{21} and ΔS_{21}) [Chen and

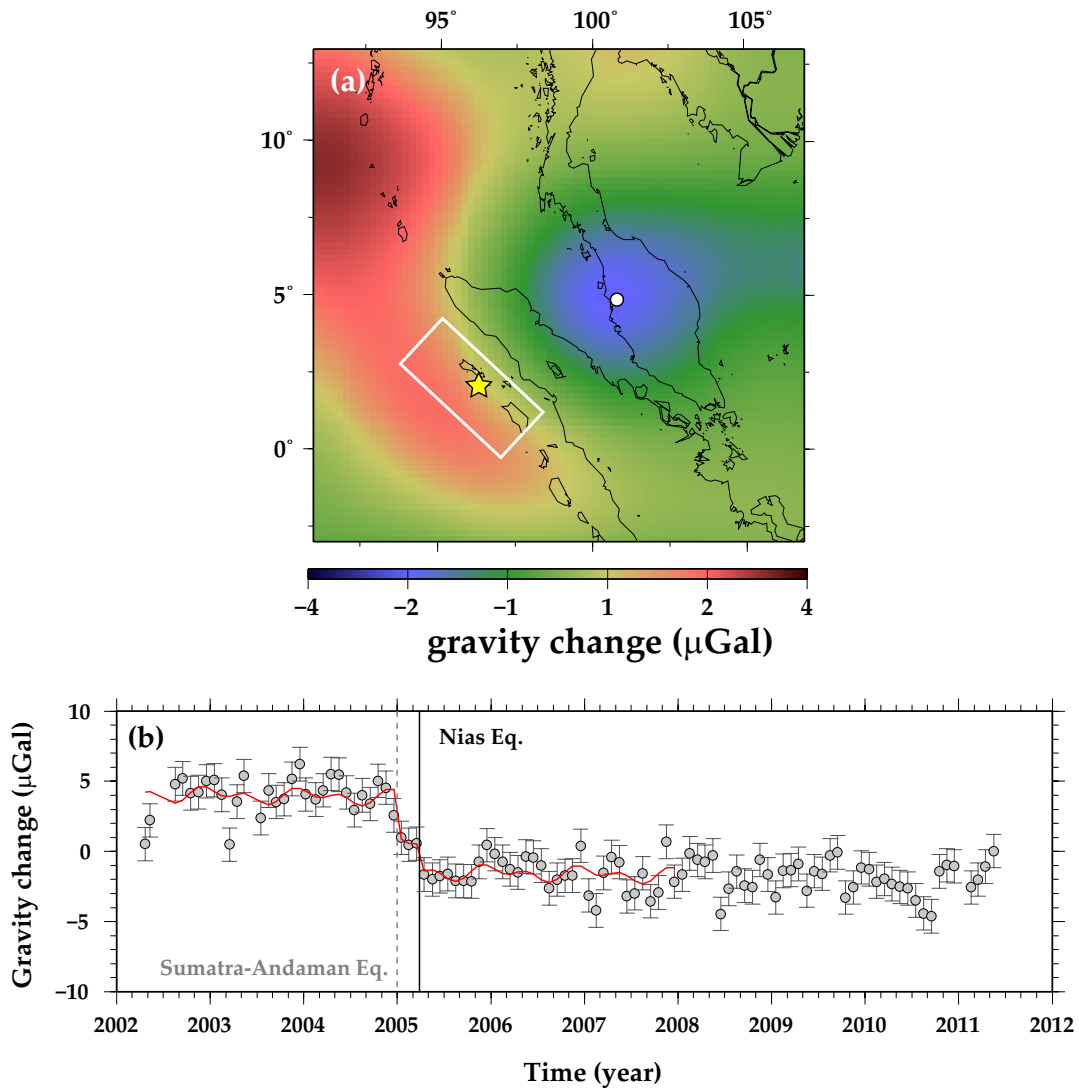


Figure 6.3: (a) Time series of the monthly gravity values at 5.0°N , 101.0°E (open circle in b) recovered by GRACE. Hydrological contributions (GLDAS/Noah) have been subtracted from GRACE time series. Data before 2008.0 have been modeled (thick red curves) assuming linear and seasonal changes and the two coseismic jumps for the 2004 Sumatra-Andaman and the 2005 Nias earthquakes. Error bars show one-sigma formal errors inferred *a posteriori* by bringing the chi-square of the post-fit residual to unity. (b) Geographical distribution of coseismic gravity changes of the 2005 Nias earthquake recovered by GRACE. A yellow star in b denotes the epicenter (2.1°N , 97.0°E). A white rectangular in b is the fault plane of this earthquake, which has $400\text{ km} \times 200\text{ km}$ area striking 325° and dipping 10° [Briggs et al., 2006]. Positive gravity changes seen in northeast of the focal region are the leakage of the postseismic gravity changes of the 2004 Sumatra-Andaman earthquake.

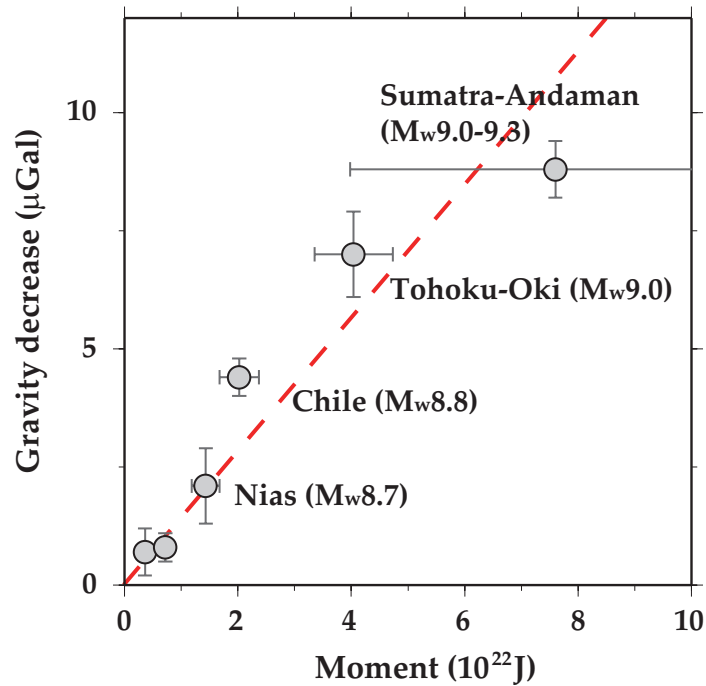


Figure 6.4: Coseismic gravity decreases observed by GRACE for recent earthquakes larger than M_w 8 as a function of seismic moment. The bottom-left two, without significant coseismic changes, are the 2006 Kuril Islands earthquake (M_w 8.3) and the 2007 Bengkulu earthquake (M_w 8.5). We can see simple linear relationship between the two quantities (red broken line).

Wilson, 2008]. We converted the coseismic changes of C_{21} and S_{21} associated with the 2011 Tohoku-Oki earthquake observed by GRACE to the motion of the north pole. It was ~ 14 cm toward 136° E, and this is close to the value (~ 15 cm) calculated using a simple fault parameter by the Paris Observatory (<http://hpiers.obspm.fr/eop-pc/>). Its direction is similar to that of the 2010 Chile earthquake (~ 8.7 cm), and their combined effect could be detected in the future as the difference of the average excitation pole positions between the periods before 2010 February and after 2011 March.

Postseismic recovery of gravity decrease with a time constant of ~ 0.6 year was found after the 2004 Sumatra-Andaman earthquake [Ogawa and Heki, 2007]. On the

other hand, the 2010 Chile earthquake has not shown appreciable postseismic gravity changes so far. The mechanisms for postseismic gravity changes are still controversial. It is interpreted as the flow of supercritical water around the down-dip end of the fault [Ogawa and Heki, 2007], Burgers rheology of the low viscosity material in shallow mantle [Panet et al., 2007], and afterslip [Hasegawa et al., submitted]. The 2011 Tohoku-Oki earthquake would be a good test field to investigate how gravity changes after a great earthquake, because we can constrain their mechanisms with crustal movements observed by the dense GPS network over the Japanese Islands.

Chapter 7

Conclusion

Recent climate changes like global warming cause the mass redistributions on the Earth through ice loss/gain and precipitation anomalies. An earthquake alters surface topography and modifies the distribution of subsurface rock density in and around the focal area by fault dislocation. If they are large enough, they could leave a “ gravity change ” signature detectable by satellite gravity measurements. In this thesis, I investigated such large-scale mass transportations using the data from satellite gravimetry by GRACE and SLR. The studies conducted here are summarized as follow;

Chapter 3: “ Precipitation anomaly brought about by Arctic Oscillation ”

- (1) Characteristic spatial patterns of anomalous precipitation by Arctic Oscillation, AO for short, have been revealed by GRACE gravimetry.

-
- (2) Positive/negative AO episodes are considered to enhance wintertime precipitations in the high/middle latitude regions in the Northern Hemisphere, respectively.
 - (3) Positive/negative AO episodes seem to enhance wintertime precipitations in the northern/southern part of Greenland, respectively.
 - (4) AO signatures can be seen from other geodetic data such as surface displacements observed by GPS and the polar motion excitation observed by VLBI.

Chapter 4: “ Ongoing ice loss in glaciers of Iceland, Svalbard, and Russian High Arctic ”

- (1) Ice loss signatures in small glacier systems of the Arctic Islands have been detected with the newly released GRACE gravity solution (RL05).
- (2) Newly developed inversion method “ point-mass modeling ” has been employed to estimate actual mass changes with a high accuracy.
- (3) These glaciers showed significant ice loss, which is a manifestation of the global warming tendency as seen in polar ice sheets and mountain glaciers.
- (4) Significant inter-annual variability has been found in some glaciers, i.e. Svalbard and Russian High Arctic. This would be related to the occurrence of strong AO.

Chapter 5: “ Application of the SLR gravity solution for the monitoring of the Greenland Ice Sheet mass changes ”

- (1) Mass balance of the Greenland Ice Sheet during 1991-2011 has been estimated using the low-degree global gravity fields determined by SLR.
- (2) Our SLR gravity solution has enough quality to detect the mass changes in Greenland.
- (3) The SLR gravity solution suggests that mass balance of Greenland was slightly positive or nearly balanced during the 1990s, and became significantly negative in the 2000s. This agrees well with surface displacement by GPS and previous studies by satellite radar altimetry.
- (4) Recent mass changes in Greenland can be explained as a combination of the two climatic changes, i.e. global warming and AO, to a large extent.

Chapter6: “ Coseismic gravity changes caused by the 2011 Tohoku-Oki great Earthquake ”

- (1) Coseismic gravity changes of the 2011 Tohoku-Oki Earthquake have been detected by GRACE.
- (2) This is the third case that GRACE detected coseismic gravity changes.
- (3) The observed gravity change mostly reflects crustal dilatation on the upper side of the down-dip end of the fault.
- (4) It appears that the gravity change roughly scales with the moment, and the threshold of their detection with GRACE seems to lie somewhere around M_w 8.6-8.7.

The GRACE satellites have paved a fresh avenue in studying geophysical phenomena accompanied by large-scale mass movements. Gravimetry is the only way that allows quantitative assessment of the Earth's mass variations although we cannot discriminate the material responsible for the variation, i.e. rock, ice, or water. Combination with other geodetic tools such as GPS positioning or radar/laser altimetry would compensate the drawback of gravimetry. The satellite gravity mission (including SLR) will continue in the future. In fact, a new SLR satellite named " LARES " has been launched by Italian Space Agency in February 2012, which could further improve the quality of SLR gravity solution. The GRACE follow-on mission is scheduled for launch in 2017. These gravity data will surely provide new insights into the changing surface and interior of the Earth.

Bibliography

- [1] Adam, D., 2002. Gravity measurement - Amazing GRACE (Gravity Recovery and Climate Experiment) Nature 416, 10-11.
- [2] Amante, C. and B. W. Eakins, 2009: ETOPO1 1 Arc-Minute Global Relief Model: Procedures, Data Sources and Analysis. NOAA Technical Memorandum NESDIS NGDC-24, 19 pp.
- [3] Ambaum, M. H. P., B. J. Hoskins, and D. B. Stephenson, 2001: Arctic Oscillation or North Atlantic Oscillation?, J. Climate, 14, 3495-3507, doi:10.1175/1520-0442(2001)014<3495:AOONAO>2.0.CO;2.
- [4] Ball, S., 2011. Exceptional rainfall in Gibraltar during winter 2009/2010, Weather, vol. 66, issue 1, pp. 22-25, doi:10.1002/wea.733.
- [5] Baur, O., and N. Sneeuw., 2011: Assessing Greenland ice mass loss by mean of point-mass modeling: a viable methodology, J. Geod., 85, 607-615, doi:10.1007/s00190-011-0463-1.
- [6] Bevis, M., Wahr, J., Shfaqat A. Khan, Finn Bo Madsen, Abel Brown, Michael Willis, Eric Kendrick, Per Knudsen, Jason E. Box, Tonie van Dam, Dana J. Caccamise II, Bjorn Johns, Thomas Nylen, Robin Abbott, Seth White, Jeremy

-
- Miner, Rene Forsberg, Hao Zhou, Jian Wang, Terry Wilson, David Bromwich, and Olivier Francis, 2012: Bedrock displacements in Greenland manifest ice mass variations, climate cycles and climate change, *PNAS*, 109, 11944-11948, doi: 10.1073/pnas.1204664109.
- [7] Briggs, R. W., Sieh, K., Meltzner, A. J., Natawidjaja, D., Galezka, J., Suwargadi, B., Hsu, Y., Simons, M., Hananto, N., Suprihanto, I., Prayudi, D., Avouac., J.-P., Prawirodirdjo, L., Bock, Y., 2006: Deformation and slip along the Sunda Megathrust in the great 2005 Nias-Simeulue earthquake, *Science*, 311, 1897, doi:10.1126/science.1122602.
- [8] Chambers, D. P., Wahr, J., Nerem, R. S., 2004: Preliminary observations of global ocean mass variations with GRACE. *Geophys. Res. Lett.*, 31, L13310. doi:10.1029/2004GL020461.
- [9] Chao, B. F. and R. S. Gross, 1987: Changes in the Earth's rotation and low-degree gravitational field induced by earthquakes, *Geophys. J. Int.*, vol. 91, issue 3, pp. 569-596.
- [10] Chao, B. F., 1988: Excitation of the earth's polar motion due to mass variations in major hydrological reservoirs, *J. Geophys. Res.*, 93, B11, P13811-13819, doi:10.1029/JB093iB11p13811.
- [11] Chao, B. F., 1994: The Geoid and Earth Rotation, in *Geophysical Interpretations of Geoid*, ed. P. Vanicek and N. Christou, CRC Press, Boca Raton.

-
- [12] Chao, B. F., 2005: On inversion for mass distribution from global (time-variable) gravity field. *J. Geodyn.*, 39, 223-230, doi:10.1016/j.jog.2004.11.001.
- [13] Chen, J. L. and C. R. Wilson, 2008: Low degree gravity changes from GRACE, Earth rotation, geophysical models, and satellite laser ranging, *J. Geophys. Res.*, 113, B06402, doi:10.1029/2007JB005397.
- [14] Chen, J.L., Tapley, B.D. and Wilson, C.R., 2006: Alaskan mountain Glacial melting observed by Satellite gravimetry, *Earth planet. Sci. Lett.*, 248, 368-378, doi:10.1016/j.epsl.2006.05.039.
- [15] Chen, J. L., Wilson, C. R., Tapley, B. D., Blankenship, D., Ivins, E. R., 2007: Patagonia Icefield melting observed by Gravity Recovery and Climate Experiment (GRACE). *Geophys. Res. Lett.*, 34, L22501, doi:10.1029/2007GL031871.
- [16] Chen, J. L., Wilson, C. R., Blankenship, D., and B. D., Tapley. 2009: Accelerated Antarctic ice loss from satellite gravity measurements, *Nature geosci.*, Vol.2 , 859-862, doi:10.1038/NGEOnature694.
- [17] Chen, J. L., C. R. Wilson, and B. D. Tapley, 2011: Interannual variability of Greenland ice losses from satellite gravimetry, *J. Geophys. Res.*, 116, B07406, doi:10.1029/2010JB007789.
- [18] Cheng, M. K., and B. D. Tapley, 1999: Seasonal variations in low degree zonal harmonics of the Earth's gravity field from satellite laser ranging observations, *J. Geophys. Res.*, 104, 2667-2681.

-
- [19] Cheng, M. and B. D. Tapley, 2004: Variations in the Earth's oblateness during the past 28 years, *J. Geophys. Res.*, 109, B09402, doi:10.1029/2004JB003028.
- [20] Cheng, M., J. C. Ries, and B. D. Tapley, 2011: Variations of the Earth's Figure Axis from Satellite Laser Ranging and GRACE, *J. Geophys. Res.*, 116, B01409, 2011, DOI:10.1029/2010JB000850.
- [21] Cohen, J., Foster, J., Barlow, M., Saito, K., and J. Jone, 2010: Winter 2009-2010: A case study of an extreme Arctic Oscillation event, *Geophys. Res. Lett.*, 37, L17707, doi:10.1029/2010GL044256.
- [22] Cox, C. M., and B. F. Chao (2002), Detection of a large-scale mass redistribution in the terrestrial system since 1998, *Science*, 297, 831-833, 2002.
- [23] Dyurgerov, M. B. and Meier M. F., 2005: *Glaciers and the Changing Earth System: A 2004 Snapshot.*, Occasional Paper 58, Institute of Arctic and Alpine Research, University of Colorado, Boulder, 118pp.
- [24] Dyurgerov, M. B. 2010: *Reanalysis of Glacier Changes: From the IGY to the IPY, 1960?2008*, Data of Glaciological Studies, Publication 108, Moscow, October 2010, (in English), 116 pp.
- [25] Einarsson, I., A. Hoehner, R. Wang, and J. Kusche, 2010: Gravity changes due to the Sumatra Andaman and Nias earthquakes as detected by the GRACE satellites: A reexamination, *Geophys. J. Int.*, 183, 733-747, doi:10.1111/j.1365-246X.2010.04756.x.
- [26] Farrell, W. E., 1972. Deformation of the Earth by Surface Loads, *Reviews of Geophysics and Space Physics*, Vol. 10, No.3, pp.761-797.

-
- [27] Fenoglio-Marc, L., Kusche, J., Becker, M., 2006: Mass variation in the Mediterranean Sea from GRACE and its validation by altimetry, steric and hydrologic fields, *Geophys. Res. Lett.*, 33, L19606, doi:10.1029/2006GL026851.
- [28] Fujii, Y., and K. Satake, 2008b: Tsunami sources of the November 2006 and January 2007 great Kuril earthquakes, *Bull. Seismol. Soc. Am.*, 98, 1559-1571, doi:10.1785/0120070221.
- [29] Gardner, A. S., Moholdt, G., Wouters, B., Wolken, G. J., Burgess, D. O., Sharp, M. J., Cogley, J. G., Braun, C., and Labine, C., 2011: Sharply increased mass loss from glaciers and ice caps in the Canadian Arctic Archipelago, *Nature*, 473, 357-360, doi:10.1038/nature10089.
- [30] Geospatial Information Authority of Japan, 2011: Coseismic slip distribution model on the plane of plate boundary based on GPS land and sea-floor positioning, <http://www.gsi.go.jp/common/000060854.pdf>.
- [31] Gregory, J. M. and S. C. B. Raper, 2004: Climatology: Threatened loss of the Greenland ice-sheet. *Nature*, 428, 616. doi:10.1038/428616a.
- [32] Guo, J. Y., Huang, Z. W., Shum, C. K., van der Wal, W. 2012: Comparisons among contemporary glacial isostatic adjustment models, *J. of Geodyn.*, doi:10.1016/j.jog.2012.03.011.
- [33] Gusman, A. R., Y. Tanioka, T. Kobayashi, H. Latief, and W. Pandoe, 2010: Slip distribution of the 2007 Bengkulu earthquake inferred from

-
- tsunami waveforms and InSAR data, *J. Geophys. Res.*, 115, B12316, doi:10.1029/2010JB007567.
- [34] Han, S.C., Shum, C.K., Bevis, M., Ji, C., Kuo, C.Y., 2006: Crustal dilatation observed by GRACE after the 2004 Sumatra-Andaman earthquake, *Science*, 313, 658-666, doi:10.1126/science.1128661.
- [35] Han, S-C., J. Sauber, and S. Luthcke, 2010: Regional gravity decrease after the 2010 Maule (Chile) earthquake indicates large-scale mass redistribution, *Geophys. Res. Lett.*, 37, L23307, doi:10.1029/2010GL045449.
- [36] Heki, K., 2004: Dense GPS array as a sensor of for seasonal changes of surface loads, in *State of the Planet: Frontiers and Challenges in Geophysics*, edited by R. S. J. Sparks and C.J. Hawkesworth, *Geophysical Monograph Series 150*, 177-196, American Geophys. Union, Washington.
- [37] Heki, K., 2010: Can GRACE detect winter snows in Japan?, paper presented at the EGU General Assembly 2010.
- [38] Heki, K. and K. Matsuo, 2010: Coseismic gravity changes of the 2010 earthquake in Central Chile from satellite gravimetry, *Geophys. Res. Lett.*, 37, L24306, doi:10.1029/2010GL045335.
- [39] Hobiger T., Gotoh, T., Otsubo, T., Kubooka, T., Sekido, M., Takiguchi, H., Takeuchi H., 2011: c5++ - Multi-technique Analysis Software for Next Generation Geodetic Instruments, *IVS 2010 General Meeting Proceedings*, 212-216.

-
- [40] Hurrell, J. M., 1995: Decadal trends in the North Atlantic Oscillation: regional temperature and precipitation, *Science*, 269, 676-679, doi:10.1126/science.269.5224.676.
- [41] Hurrell, J. M., Kushnir, Y., Ottersen, G., and M. Visbeck, 2003: An overview of the North Atlantic Oscillation, in *The North Atlantic Oscillation: Climatic Significance and Environmental Impact*, Geophys. Monogr. Ser., vol. 134, edited by J. Hurrell et al., pp.1-35, AGU, Washington, D.C.
- [42] Imanishi, Y., T. Sato, T. Higashi, W. Sun, and S. Okubo, 2004: A network of superconducting gravimeters detects submicrogal coseismic gravity changes, *Science*, 306, 476-478.
- [43] Jacob, T., Wahr, J., Pfeffer, W. T., and Swenson, S., 2012: Recent contributions of glaciers and ice caps to sea level rise, *Nature*, 482, 514-518, doi:10.1038/nature10847.
- [44] Koch, K-R., 1999: Parameter estimation and hypothesis testing in linear models, Springer, Berlin.
- [45] Koryakin, V. S., 1986: Decrease in glacier cover on the inlands of the Eurasian arctic during the 20th century, *Polar Geography and Geology*, 10, 157-165, doi:10.1080/10889378609377283.
- [46] Kozai, Y., 1959: The Motion of a Close Earth Satellite, *Astronomical Journal*. 64(1274): 367-377.
- [47] Krabill, W., W. Abdalati, E. Frederick, S. Manizade, C. Martin, J. Sonntag, R. Swift, R. Thomas, W. Wright, J. Yungel, 2000: Greenland Ice Sheet:

-
- High-Elevation Balance and Peripheral Thinning, *Science*, 289, 428-430, doi: 10.1126/science.289.5478.428.
- [48] Krabill, W., E. Hanna, P. Huybrechts, W. Abdalati, J. Cappelen, B. Csatho, E. Frederick, S. Manizade, C. Martin, J. Sonntag, R. Swift, R. Thomas, and J. Yungel, 2004: Greenland Ice Sheet: Increased coastal thinning, *Geophys. Res. Lett.*, 31 L24403, doi:10.1029/2004GL021533.
- [49] Li, Y., and C. H. Davis, 2008: Decadal Mass Balance of the Greenland and Antarctic Ice Sheets from High Resolution Elevation Change Analysis of ERS-2 and Envisat Radar Altimetry Measurements, *Geoscience and Remote Sensing Symposium*, 2008. IGARSS 2008. IEEE International, 4, 339-342, doi:10.1109/IGARSS.2008.4779727.
- [50] Luthcke, S. B., H. J. Zwally, W. Abdalati, D. D. Rowlands, R. D. Ray, R. S. Nerem, F. G. Lemoine, J. J. McCarthy, D. S. Chinn, 2006: Recent Greenland Ice Mass Loss by Drainage System from Satellite Gravity Observations, *Science*, 314, 1286-1289, doi:10.1126/science.1130776.
- [51] Luthcke, S. B., Arendt A. A., Rowlands, D.D., McCarthy J. J., Larsen, C.F., 2008: Recent glacier mass changes in the Gulf of Alaska region from GRACE mascon solutions, *J. Glaciol.*, 54(188), 767-777, doi: 10.3189/002214308787779933.
- [52] L'Heureux, M., Butler, A., Jha, B., Kumar, A., and W. Wang, 2010: Unusual extremes in the negative phase of the Arctic Oscillation during 2009, *Geophys. Res. Lett.*, 37, L10704, doi:10.1029/2010GL043338.

-
- [53] Matsuo, K. and K. Heki, 2010: Time-variable ice loss in Asian high mountains from satellite gravimetry, *Earth planet. Sci. Lett.*, 290, 30-36, doi:10.1016/j.epsl.2009.11.053.
- [54] Matsuo, K. and K. Heki, 2011: Coseismic gravity changes of the 2011 Tohoku-Oki Earthquake from satellite gravimetry, *Geophys. Res. Lett.*, 38, L00G12, doi:10.1029/2011GL049018, 2011.
- [55] Matsuo, K. and K. Heki, 2012: Anomalous precipitation signatures of the Arctic Oscillation in the time-variable gravity field by GRACE, *Geophys. J. Int.*, 130, 1495-1506, doi:10.1111/j.1365-246X.2012.05588.x.
- [56] Moholdt, G., Wouters, B. and A. S. Gardner, 2012: Recent mass changes of glaciers in the Russian High Arctic, *Geophys. Res. Lett.*, 39, L10502, doi:10.1029/2012GL051466.
- [57] Morishita, Y. and K. Heki, 2008: Characteristic precipitation patterns of El Nino/La Nina in time-variable gravity fields by GRACE, *Earth planet. Sci. Lett.*, 272, 677-682, doi:10.1016/j.epsl.2008.06.003.
- [58] Mémin, A., Rogister, Y., Hinderer, J., Omang, O. C., and B. Luck, 2011: Secular gravity variation at Svalbard (Norway) from ground observations and GRACE satellite data, *Geophys. J. Int.*, 184, 1119-1130, doi: 10.1111/j.1365-246X.2010.04922.x.
- [59] Nerem, R. S., Chao, B. F., Au, A. Y., Chan, J. C., Klosko, S. M., Pavlis, N. K., Williamson, R. G., 1993: Temporal variations of the Earth's gravitational field from satellite laser ranging to Lageos. *Geophys. Res. Lett.*, 20, 595-598.

-
- [60] Nerem, R. S. and J. Wahr, 2011: Recent changes in the Earth's oblateness driven by Greenland and Antarctic ice mass loss, *Geophys. Res. Lett.*, 38, L13501, doi:10.1029/2011GL047879.
- [61] Ogawa, R., B. F. Chao, and K. Heki, 2011: Acceleration signal in GRACE time-variable gravity in relation to interannual hydrological changes, *Geophys. J. Int.*, 184, 673-679, doi:10.1111/j.1365-246X.2010.04843.x.
- [62] Ozawa, S., T. Nishimura, H. Suito, T. Kobayashi, M. Tobita, and T. Imakiire, 2011: Coseismic and postseismic slip of the 2011 magnitude-9 Tohoku-Oki earthquake, *Nature*, doi:10.1038/nature10227.
- [63] Paulson, A., Zhong, S., and J. Wahr, 2007: Inference of mantle viscosity from GRACE and relative sea level data, *Geophys. J. Int.*, 171, 497-508, doi: 10.1111/j.1365-246X.2007.03556.x.
- [64] Panet, I., F. Pollitz, V. Mikhailov, M. Diament, P. Banerjee, and K. Grijalva, 2010: Upper mantle rheology from GRACE and GPS postseismic deformation after the 2004 Sumatra Andaman earthquake, *Geochem. Geophys. Geosyst.*, 11, Q06008, doi:10.1029/2009GC002905.
- [65] Peltier, W.R., 2004: Global glacial isostasy and the surface of the ice-age earth: the ICE-5G (VM2) model and GRACE, *Annual Review of Earth and Planetary Sciences* 32, 111-149, DOI: 10.1146/annurev.earth.32.082503.144359.

-
- [66] Quadrelli, R., V. Pavan, F. Molteni, 2001: Wintertime variability of Mediterranean precipitation and its link with large-scale circulation anomalies, *Climate Dynamics*, 17, 457-466.
- [67] Rasmussen, L. A. and J. Kohler, 2007: Mass balance of three Svalbard glaciers reconstructed back to 1948, *Polar Research*, 26, 168-174, doi:10.1111/j.1751-8369.2007.00023.x.
- [68] Rodell, M. and Houser, P. R., Jambor, U., Gottschalck, J., Mitchell, K., Meng, C.J., Arsenault, K., Cosgrove, B., Radakovich, J., Bosilovich, M., Entin, J.K., Walker, J.P., Lohmann, D., Toll, D., 2004: The Global Land Data Assimilation System. *Bull. Am. Meteorol. Soc.* 85, 381-394.
- [69] Rignot, E. and K. Pannir, 2006: Changes in the Velocity Structure of the Greenland Ice Sheet, *Science*, 311, 986, doi:10.1126/science.1121381.
- [70] Ropelewski, C. F., Halpert, M. S., 1987: Global and regional scale precipitation patterns associated with the El Niño/southern oscillation. *Monthly Weather Rev.* 115, 1606-1626.
- [71] Rubincam, D.P., 1984: Postglacial rebound observed by Lageos and the effective viscosity of the lower mantle, *J. Geophys. Res.*, 89, 1077-1087.
- [72] Sasgen, I., van den Broeke, M., Bamber, J. L., Rignot, E., Sørensen, L. S., Wouters, B., Martinec, Z., Velicogna, I., Simonsen, S. B., 2012: Timing and origin of recent regional ice-mass loss in Greenland, *Earth planet. Sci. Lett.*, 333-334, 293-303, doi: 10.1016/j.epsl.2012.03.033.

-
- [73] Sato, M., T. Ishikawa, N. Ujihara, S. Yoshida, M. Fujita, M. Mochizuki, A. Asada, 2011: Displacement Above the Hypocenter of the 2011 Tohoku-Oki Earthquake, *Science*, 332, 1395, doi:10.1126/science.1207401.
- [74] Sun, W., S. Okubo, G. Fu, and A. Araya, 2009: General formulations of global and co-seismic deformations caused by an arbitrary dislocation in a spherically symmetric earth model ? applicable to deformed earth surface and space-fixed point, *Geophys. J. Int.*, 177, 817-833.
- [75] Schmidt, R., Petrovic, S., Guntner, A., Barthelmes, F., Wunsch, J., Kusche, J., 2008. Periodic components of water storage changes from GRACE and global hydrology models, *J. Geophys. Res.*, 113, B08419, doi:10.1029/2007JB005363.
- [76] Schrama E., B. Wouters, B. Vermeersen, 2011: Present Day Regional Mass Loss of Greenland Observed with Satellite Gravimetry, *Surv. Geophys.*, 32, 377-385, doi:10.1007/s10712-011-9113-7.
- [77] Seager, R., Kushnir, Y., Nakamura, J., Ting, M., and N. Naik, 2010: Northern hemisphere winter snow anomalies: ENSO, NAO and the winter of 2009/10, *Geophys. Res. Lett.*, 37, L14703, doi:10.1029/2010GL043830.
- [78] Steffen, H., Gitlein, O., Denker, H., Müller, J., Timmen, L., 2009. Present rate of uplift in Fennoscandia from GRACE and absolute gravimetry, *Tectonophysics*, 474, 69-77, doi:10.1016/j.tecto.2009.01.012474.
- [79] Svendsen, . I., Gataullin, V., Mangerud, J., and L. Polyak, 2004: The glacial history of the Barents and Kara sea region, in *Quaternary Glaciations: Extent*

and Chronology-Part 1: Europe, *Dev. Quat. Sci.*, vol. 2, edited by J. Ehlers and P. Gibbard, pp. 369-378, Elsevier, Amsterdam.

- [80] Swenson, S. and J. Wahr, 2006: Post-processing removal of correlated errors in GRACE data, *Geophys. Res. Lett.*, 33, L08402, doi:10.1029/2005GL025285.
- [81] Swenson, S., D. Chambers, and J. Wahr, 2008: Estimating Geocenter Variations from a Combination of GRACE and Ocean Model Output, *J. Geophys. Res.*, 113, B08410, doi:10.1029/2007JB005338.
- [82] Syed, T. H., Famiglietti, J. S., Rodell, M., Chen, J. and C. R. Wilson, 2008: Analysis of terrestrial water storage changes from GRACE and GLDAS, *Water Resour. Res.*, 44, W02433, doi:10.1029/2006WR005779.
- [83] Tamisiea, M.E., Leuliette, E.W., Davis, J.L., Mitrovica, J.X., 2005: Constraining hydrological and cryospheric mass flux in southeastern Alaska using space-based gravity measurements. *Geophys. Res. Lett.* 32, L20501. doi:10.1029/2005GL023961.
- [84] Tamisiea, M. E., Mitrovica, J. X. and J. L. Davis, 2007: GRACE gravity data constrain ancient ice geometries and continental dynamics over Laurentia, *Science*, 316, 881-883, doi:10.1126/science.1137157.
- [85] Tapley, B.D., Bettadpur, S., Ries, J.C., Thompson, P.F., Watkins, M.M., 2004: GRACE measurements of mass variability in the earth system. *Science* 305, 503-505. doi: 10.1126/science.1099192.

-
- [86] Thompson, D. W. J. and J. M. Wallace, 1998: The Arctic Oscillation signature in the wintertime geopotential height and temperature fields, *Geophys. Res. Lett.*, 25, 1297-1300, doi:10.1029/98GL00950.
- [87] Thompson, D. W. J. and J. M. Wallace, 2000: Annular modes in the extratropical circulation, Part I: Month-to-Month variation, *J. Clim.*, 13, 1000-1016, doi:10.1175/1520-0442(2000)013;1000:AMITEC;2.0.CO;2.
- [88] Thompson, D. W. J. and J. M. Wallace, 2001: Regional climate impacts of the Northern Hemisphere Annular Mode and associated climate trends, *Science*, 293, 85-89, doi:10.1126/science.1058958.
- [89] Tikhonov, A. N., 1963: Regularization of incorrectly posed problems, *Sov Mat Dokl* 4:1035-1038.
- [90] Tushingham, A.M., Peltier, W.R., 1991: ICE-3G: A new global model of late pleistocene deglaciation based upon geophysical predictions of post-glacial relative sea level change, *J. Geophys. Res.* 96, 4497-4523, doi: 10.1029/90JB01583.
- [91] van Dam, T., Wahr, J. and D. Lavallée, 2007: A comparison of annual vertical crustal displacements from GPS and Gravity Recovery and Climate Experiment (GRACE) over Europe. *J. Geophys. Res.*, 112, B03404, doi:10.1029/2006JB004335.
- [92] Velicogna, I. and J. Wahr, 2006a: Measurements of time-variable gravity show mass loss in Antarctica. *Science*, 311(5768), 1754-1756. doi: DOI 10.1126/science.1123785.

-
- [93] Velicogna, I. and J. Wahr, 2006b: Acceleration of Greenland ice mass loss in spring 2004, *Nature*, 443, 329-331, doi:10.1038/nature05168.
- [94] Velicogna, I., 2009: Increasing rates of ice mass loss from the Greenland and Antarctic ice sheets revealed by GRACE, *Geophys. Res. Lett.* 36, L19503, doi:10.1029/2009GL040222.
- [95] Vinje, T., 2001: Anomalies and Trends of Sea-Ice Extent and Atmospheric Circulation in the Nordic Seas during the Period 1864-1998, *J. Clim.*, 14, 255-267, doi: 10.1175/1520-0442(2001)014<0255:AATOSI;2.0.CO;2.
- [96] Wahr, J., M. Molenaar, and F. Bryan, 1998: Time variability of the Earth's gravity field: Hydrological and oceanic effects and their possible detection using GRACE, *J. Geophys. Res.*, 103, 30205-30229, doi:10.1029/98JB02844.
- [97] Walker, G. T., Bliss E. W., 1932: World weather V, *Memoirs of the Royal Meteorological Society* 4, 53-83.
- [98] Wallace, J. M. and D.S. Gutzler, 1981: Teleconnection in the geopotential height field during the Northern Hemisphere winter, *Mon. Wea. Rev.*, 109, 784-812.
- [99] Wallace, J. M., 2000. North Atlantic Oscillation/annular mode: Two paradigms-one phenomenon, *Quart. J. Roy. Meteor. Soc.*, 126, 791-805.
- [100] Wang, C., Liu, H., Lee, S., 2010: The record-breaking cold temperatures during the winter of 2009/2010 in the Northern Hemisphere, *Atmos. Sci. Lett.*, 11, 161-168, doi: 10.1002/asl.278.

-
- [101] Wouters, B., Chamber, D., and E. J. O. Schrama, 2008: GRACE observes small-scale mass loss in Greenland, *Geophys. Res. Lett.*, 35, L20501, doi:10.1029/2008GL034816.
- [102] Yoder, C.F., Williams, J.G., Dickey, J.O., Schutz, B.E., Eanes, R.J. and B.D. Tapley, 1983: Secular variation of Earth's gravitational harmonic J coefficient from Lageos and non-tidal acceleration of Earth rotation, *Nature*, 303, 757-762.
- [103] Zhang, Z., B. F. Chao, Y. Lu, and H. T. Hsu, 2009: An effective filtering for GRACE time-variable gravity: Fan filter, *Geophys. Res. Lett.*, 36, L17311, doi: 10.1029/2009GL039459.
- [104] Zwally, H. J., J. Li, A. C. Brenner, M. Beckley, H. G. Cornejo, J. Dimarzio, M. B. Giovinetto, T. A. Neumann, J. Robbins, J. L Saba, Y. Donghui, W. Wang, 2011: Greenland ice sheet mass balance: distribution of increased mass loss with climate warming; 2003-07 versus 199-?2002, *J. Glaciol.*, 57(201), 88-102, doi:10.3189/002214311795306682.
- [105] Zwally, H. J., M. B. Giovinetto, J. Li, H. G. Cornejo, M. A. Beckley, A. C. Brenner, J. L. Saba, D. Yi, 2005: Mass changes of the Greenland and Antarctic ice sheets and shelves and contributions to sea-level rise: 1992-2002, *J. Glaciol.*, 51(175), 509?527, doi:10.3189/172756505781829007.